

Editor-in-Chief B.E.Paton

Editorial board:

Yu.S.Borisov	V.F.Khorunov
A.Ya.Ishchenko	I.V.Krivtsun
B.V.Khitrovskaya	L.M.Lobanov
V.I.Kyrián	A.A.Mazur
S.I.Kuchuk	Yatsenko
Yu.N.Lankin	I.K.Pokhodnya
V.N.Lipodaev	V.D.Poznyakov
V.I.Makhnenko	K.A.Yushchenko
O.K.Nazarenko	A.T.Zelnichenko
I.A.Ryabtsev	

International editorial council:

N.P.Alyoshin	(Russia)
U.Diltay	(Germany)
Guan Qiao	(China)
D. von Hofe	(Germany)
V.I.Lysak	(Russia)
N.I.Nikiforov	(Russia)
B.E.Paton	(Ukraine)
Ya.Pilarczyk	(Poland)
G.A.Turichin	(Russia)
Zhang Yanmin	(China)
A.S.Zubchenko	(Russia)

Promotion group:

V.N.Lipodaev, V.I.Lokteva
A.T.Zelnichenko (exec. director)

Translators:

A.A.Fomin, O.S.Kurochko,
I.N.Kutianova, T.K.Vasilenko

Editor:

N.A.Dmitrieva

Electron galley:

D.I.Sereda, T.Yu.Snegiryova

Address:

E.O. Paton Electric Welding Institute,
International Association «Welding»,
11, Bozhenko str., 03680, Kyiv, Ukraine
Tel.: (38044) 200 67 57, 200 82 77
Fax: (38044) 200 04 86, 200 82 77
E-mail: journal@paton.kiev.ua
http://www.nas.gov.ua/pwj

State Registration Certificate
KV 4790 of 09.01.2001

Subscriptions:

\$324, 12 issues per year,
postage and packaging included.
Back issues available.

All rights reserved.

This publication and each of the articles
contained herein are protected by copyright.
Permission to reproduce material contained in
this journal must be obtained in writing from
the Publisher.
Copies of individual articles may be obtained
from the Publisher.

CONTENTS

SCIENTIFIC AND TECHNICAL

<i>Kharlamov M.Yu., Krivtsun I.V., Korzhik V.N. and Petrov S.V.</i> Heating and melting of anode wire in plasma arc spraying	2
<i>Kuzmenko V.G.</i> On the subject of electric submerged-arc welding	8
<i>Labur T.M.</i> Strength and features of fracture of welded joints on high-strength aluminium alloys at low temperature	13
<i>Knysh V.V., Solovej S.A. and Bogajchuk I.L.</i> Optimisation of the process of strengthening of welded joints of 09G2S steel by high-frequency mechanical peening	20
<i>Nazarenko O.K., Matvejchuk V.A. and Galushka V.V.</i> Simulation of the effect of high-voltage cables on current ripple in welding guns with automatic bias	24
<i>Kuchuk-Yatsenko V.S.</i> Peculiarities of resistance welding of copper with aluminium alloys using nanostructured foil of Al-Cu system	28
<i>Lyushinsky A.V.</i> Application of nanopowders of metals in diffusion welding of dissimilar materials	31

INDUSTRIAL

<i>Engindeniz E., Kaplan E., Ganioglu E., Yuksel F., Bayezid N. and Rosert R.</i> Manufacture of outstanding thick-walled constructions	35
<i>Razmyshlyayev A.D., Mironova M.V., Kuzmenko K.G. and Vydmysh P.A.</i> Efficiency of melting of electrode wire in submerged-arc surfacing with influence of transverse magnetic field	39
<i>Bartenev I.A.</i> Technological peculiarities of cladding of high alloys	43
<i>Shlensky P.S., Dobrushin L.D., Fadeenko Yu.I. and Ventsev S.D.</i> Chambers for explosion welding of metals (Review)	47
To 130th anniversary of the first method of arc electric welding	51

BRIEF INFORMATION

International Scientific-Practical Seminar in Kiev	53
New Book	55



wire through the anode spot being uniformly distributed over its section $z = L_w$. In addition, the entire wire is heated by arc current I flowing through it. It is assumed that the wire is in transverse position relative to the plasma flow around it at distance Z_w from the exit section of the plasma torch nozzle, and that the exit section of the wire feeder nozzle is at distance L_p from the plasma torch axis. Also, it is assumed that the wire melting rate is equal to the wire feed speed, and that the molten metal crossing section $z = L_w$ is detached and carried away by the plasma flow.

The thermal state of the anode wire under the plasma arc spraying conditions is determined by a set of the following physical processes: convective-conductive heat exchange of the plasma flow and surrounding gas with the side surface of the wire, thermal radiation energy exchange between the plasma and wire surface, effect of the electric arc introducing heat through the anode spot, volumetric Joule heating of the wire by the electric current flow, losses of heat with the molten metal carried away by the plasma flow, and cooling of the wire surface due to entrainment of the energy of evaporation of its material atoms by the vapour flow.

Assuming that the temperature field in the wire is characterised by the axial symmetry, the problem of finding it is reduced to solving the quasi-stationary thermal conductivity equation written down in the cylindrical coordinate system:

$$\begin{aligned} \gamma_w C_w v_w \frac{\partial T_w}{\partial z} = \frac{1}{r} \frac{\partial}{\partial r} \left(\chi_w r \frac{\partial T_w}{\partial r} \right) + \\ + \frac{\partial}{\partial z} \left(\chi_w \frac{\partial T_w}{\partial z} \right) + j^2 \rho_w, \end{aligned} \quad (1)$$

where $T_w(r, z)$ is the spatial distribution of temperature in the wire; $\gamma_w(T)$, $C_w(T)$, $\chi_w(T)$ and $\rho_w(T)$ are the density, effective specific heat, thermal conductivity coefficient and specific electrical resistance of the wire material, respectively; and j is the density of the electric current.

Consider the statement of boundary conditions for equation (1). Allowing for the above heat exchange mechanisms, the boundary condition on the wire surface (at $r = R_w$) can be expressed as follows:

$$\left(-\chi_w \frac{\partial T_w}{\partial r} \right) \Big|_{r=R_w} = Q_c + Q_r - Q_v, \quad (2)$$

where Q_c is the flow density of the energy due to convective-conductive heat exchange of the wire with the plasma and ambient gas; Q_r is the flow density of the energy of thermal radiation of the plasma absorbed by the wire surface; and Q_v is the flow density of the evaporation energy carried away from the wire surface.

The following symmetry conditions were specified for the wire axis:

$$\frac{\partial T_w}{\partial r} = 0. \quad (3)$$

Assuming that the wire goes out from the nozzle with temperature T_0 , the boundary condition at $z = 0$ will be written down as follows:

$$T_w(r, 0) = T_0. \quad (4)$$

To determine the boundary condition at the molten tip of the wire, it is necessary to allow for the heat released in a region of the anode fixation of the arc, as well as for the heat losses related to evaporation of the wire material and detachment of the melt by the plasma jet. As a result, the boundary condition at $z = L_w$ will be defined as

$$\left(-\chi_w \frac{\partial T_w}{\partial z} \right) \Big|_{z=L_w} = Q_a - Q_v - Q_t, \quad (5)$$

where Q_a is the specific heat flow from the arc to the anode, and Q_t are the heat losses related to detachment and carrying away of the molten material of the wire.

Consider the above components of heat exchange in more detail. The calculation region of the wire is located both in a zone affected by the high-temperature core of the plasma flow heating the wire and in a relatively cold peripheral regions of the flow through which the heat is removed from the wire. Assuming that the spatial distributions of temperature $T_p = T_p(z)$ and velocity $u_p = u_p(z)$ of the plasma along the wire length are known (e.g. calculated on the basis of model [6]), the convective-conductive heat flow under the given conditions can be determined according to the Newton model of heat exchange [7]:

$$Q_c = \alpha(T_p - T_{ws}), \quad (6)$$

where α is the heat transfer coefficient, and $T_{ws}(z) = T_w(R_w, z)$ is the temperature of the wire surface.

Heat transfer coefficient α is related to Nusselt number Nu that characterises the convective heat exchange as follows:

$$\alpha = Nu \chi_p / (2R_w), \quad (7)$$

where $\chi_p(T)$ is the coefficient of thermal conductivity of the plasma.

The Nusselt number in the transverse flow of the argon plasma around a cylinder is determined by the following expression, according to [8]:

$$\begin{aligned} Nu = 0.5 Re^{0.5} Pr^{0.4} (\gamma_p \eta_p / \gamma_{pw} \eta_{pw})^{0.2}, \\ Re = \frac{2R_w \gamma_p u_p}{\eta_p}, \quad Pr = \frac{C_p \eta_p}{\chi_p}, \end{aligned} \quad (8)$$

where Re and Pr are the Reynolds and Prandtl numbers, respectively; $\gamma_p(T)$, $\eta_p(T)$ and $C_p(T)$ are the density, dynamic viscosity and specific heat of the plasma at a constant pressure calculated at a temperature of the undisturbed flow; and $\gamma_{pw} = \gamma_p(T_{ws})$ and



$\eta_{pw} = \eta_p(T_{ws})$ are the density and viscosity of the plasma at a temperature of the wire surface.

The density of the heat flow due to radiation heat exchange can be calculated by using the known relationship [7]:

$$Q_r = \beta \sigma_0 (T_p^4 - T_{ws}^4), \tag{9}$$

where β is the emissivity factor of the wire material, and σ_0 is the Stefan–Boltzmann constant.

The heat flow due to evaporation of the material from the wire surface can be calculated from the following expression:

$$Q_v = \varepsilon nu, \tag{10}$$

where ε is the latent evaporation heat per atom, and n and u are the concentration and velocity of atoms of the metal vapour near the evaporation surface calculated by the procedure from study [9].

Specific heat flow to the anode, Q_a , is determined by a number of technological parameters, such as the arc current, composition of the electrode wire, kind of the plasma gas etc., and is of an order of $(0.8–1.5) \cdot 10^9 \text{ W/m}^2$ under the conditions considered [10].

Heat losses Q_t can be determined proceeding from an assumption that the velocity of the melting front and, hence, detachment of the molten material of the wire is equal to wire material feed speed v_w . Then

$$Q_t = C_w \gamma_w v_w T_w(r, L). \tag{11}$$

As a result, the spatial distribution of temperature in the consumable anode wire during plasma arc spraying can be determined by solving equation (1) with boundary conditions (2)–(5) and closing relationships (6)–(11).

Mathematical formulation of the stated problem can also be presented in a simpler form. For example, although the temperature in a cross section of the wire is distributed non-uniformly, this difference is insignificant. This is related to high thermal conductivity of the material of the spraying wire, as well as to its rather small diameter (about 1–2 mm). Then, integrating equation (1) with respect to radius yields the following unidimensional thermal conductivity equation:

$$\gamma_w C_w v_w \frac{\partial \bar{T}_w}{\partial z} = \frac{\partial}{\partial z} \left(\chi_w \frac{\partial \bar{T}_w}{\partial z} \right) + W, \tag{12}$$

where $\bar{T}_w(z)$ is the wire temperature averaged across the section, and W is the power of the heat sources.

The left and right boundary conditions for equation (12) will preserve the form of (4) and (5), the difference being that temperature $\bar{T}_w(z)$ averaged across the wire section appears in the said relationships instead of wire temperature $T_w(r, z)$. The heat flows through the side surface of the wire that appear in condition (2) transform to the volume heat sources

after integration of equation (1). The power of these sources can be determined from the following formula:

$$W = [I^2 \rho_w / (\pi R_w^2) + 2\pi R_w (Q_c + Q_r - Q_v)] / \pi R_w^2. \tag{13}$$

At this point we can consider description of the model of heating and melting of the wire in plasma arc wire spraying to be completed.

Now consider the procedure for solving the stated problem. Because the coefficients of equation (12), boundary condition (5) and closing relationships (6)–(11) are non-linear, it is very difficult to obtain an analytical solution of this equation. Therefore, the problem considered was solved numerically by the finite difference method [11, 12]. Equation (12) was approximated by the three-point scheme. Non-symmetrical differences against the wire speed were used for approximation of the convective term. The under-relaxation method was employed to improve convergence of the solution [12]. No explicit separation of interface between the phases in the wire was used in the calculations. Instead, the use was made of the shock-capturing method [11]. In this connection, effective heat capacity $\bar{C}_w(T)$ allowing for the latent melting heat was used instead of specific heat $C_w(T)$ of the wire material:

$$\bar{C}_w(T) = C_w(T) + W_w^m \delta(T - T_w^m), \tag{14}$$

where T_w^m is the melting temperature; W_w^m is the latent melting heat of the wire material, and $\delta(x)$ is the delta function.

To evaluate the thermal state of the wire in spraying it is necessary to know distributions of thermal and gas-dynamic characteristics of the flow of the arc plasma in a wire location region. These characteristics were calculated by using the earlier developed software [6] intended for quantitative evaluation of parameters of the turbulent flow of the arc plasma under the plasma arc spraying conditions. It was assumed for the calculations that the anode wire is located at distance $Z_w = 6.3 \text{ mm}$ from the exit section of the plasma torch nozzle. Distributions of the thermal and gas-dynamic characteristics of the plasma in this section under different operating conditions of the plasma torch are shown in Figure 2.

Numerical investigations were carried out for a steel wire, the thermal-physical characteristics of which were taken from study [4]. Wire parameters and spraying conditions were varied within the following ranges: wire diameter 1.4–1.6 mm, wire feed speed 6–15 m/min, arc current 160–240 A, and plasma gas (argon) flow rate 1.0–1.5 m³/h. Distance from the wire tip to the plasma jet axis was varied from 0 to 1 mm, and extension (distance from the feeder nozzle to the wire molten tip) was assumed to be equal to 12 mm.

Consider the modelling results. A very important aspect in analysis of the thermal state of the wire

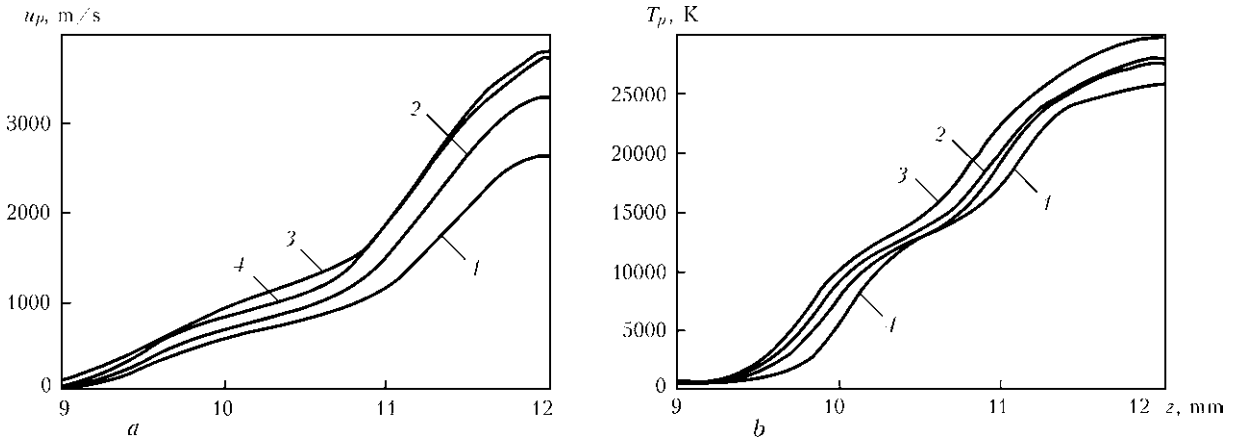


Figure 2. Distribution of velocity (a) and temperature (b) of plasma along the spraying anode wire (molten tip of the wire is located on the plasma jet axis): 1 – $I = 160$; 2, 4 – 200; 3 – 240 A, argon flow rate of $1 \text{ m}^3/\text{h}$; 4 – argon flow rate of $1.5 \text{ m}^3/\text{h}$

during spraying is evaluation of different components of its heat exchange with the arc plasma. Within the problem under consideration, interaction of the wire with external heat sources takes place through its side surface and through the melt on its tip.

Heating of the side surface of the wire is provided by two components – convective and radiation heat exchange with the plasma jet flowing around the wire (Figure 3). Contribution of these components to the energy balance of the spraying wire surface is approximately identical, near the molten tip of the wire the intensity of the said heat sources substantially growing, which is related to high values of temperature (up to 30,000 K) and velocity (up to 3800 m/s) of the plasma in the near-axis zone of the jet. As a result, the temperature of the wire in the $11 < z < 11.9 \text{ mm}$ region may exceed the boiling temperature of its material (3133 K). In this case the wire material intensively evaporates, and the wire cools down (see Figure 3, curve 4). In turn, this leads to a drop of the total heat flow through the side surface of the wire (Figure 3, curve 1). A reversed situation takes place in the wire regions located at a distance from the jet axis, i.e. the wire temperature becomes insignificant, as the wire is cooled by a cold gas flowing around it.

The heat balance of the wire surface region near section $z = L_w$ (see Figure 3) and directly in this section (Figure 4) should be considered separately. It can be seen from Figure 3 that in this region ($11.7 < z < 12 \text{ mm}$) the role of evaporation cooling substantially decreases and, hence, the resultant flow to the wire grows. Because of the direct dependence of values of the heat losses related to evaporation of the wire material on the temperature, this situation is caused by a dramatic decrease in temperature of the wire surface in the given region (Figures 5–8), this being associated with intensive removal of heat through section $z = L_w$. Moreover, the heat losses increase here with increase in temperature (see Figure 4). At low values of the temperature in the given section the heat losses are caused mainly by detachment of the molten material of the wire by the transverse plasma flow. At higher temperatures the key role in the heat balance of the section considered is played by evaporation cooling.

The effect of another heat source, i.e. the energy released due to the electric current flowing through the wire, is of low significance. In particular, contribution of the Joule heating near the molten tip of the wire is less than 1 % of the total action of all the sources (13) heating the wire. Therefore, heating and melting of the wire in plasma arc spraying are provided

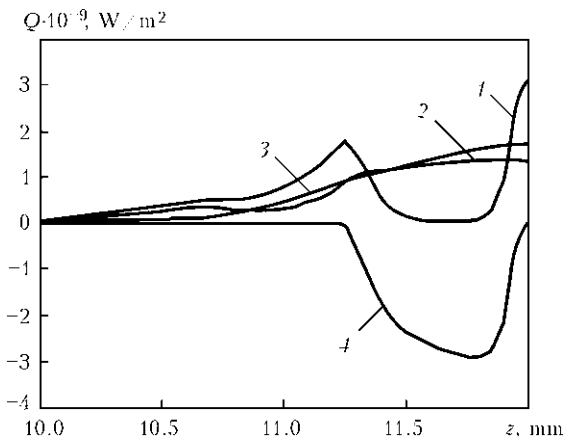


Figure 3. Distribution of components of heat flow along the length of the wire towards its surface ($I = 200 \text{ A}$; argon flow rate of $1 \text{ m}^3/\text{h}$; $2R_w = 1.4 \text{ mm}$; $v_w = 9 \text{ m/s}$, molten tip of the wire is located on the plasma jet axis): 1 – total heat flow; 2 – Q_c ; 3 – Q_r ; 4 – Q_e .

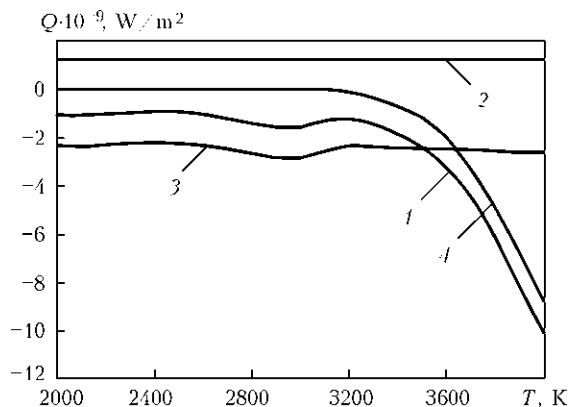


Figure 4. Total heat flow (1) introduced through section $z = L_w$ and its components (2 – Q_a ; 3 – Q_i ; 4 – Q_e) depending on the melt temperature in the given section

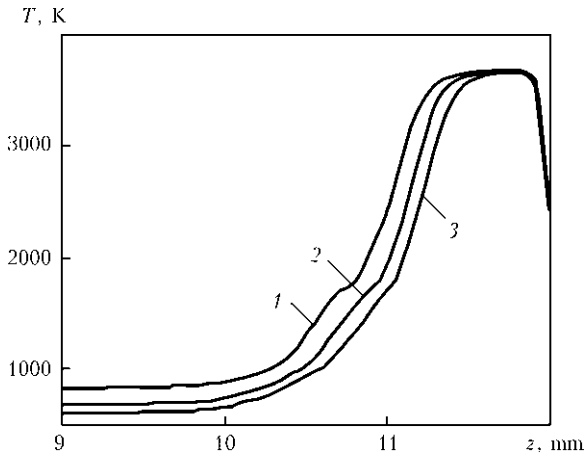


Figure 5. Distribution of temperature along the length of the wire depending on its diameter: 1 – 1.2; 2 – 1.4; 3 – 1.6 mm

primarily by the effect of the high-temperature high-velocity plasma jet.

Figures 5–8 show temperature fields in the wire resulting from variations of technological parameters of the spraying process. The effect of the wire diameter on the limiting-state temperature field is shown in Figure 5. As follows from the calculated data shown in this Figure, in case of heating of the large-diameter wire the length of the region heated above a specified temperature decreases. The same situation takes place also with increase in the wire feed speed. Decrease in the length of the high-temperature region near the molten tip of the wire (Figure 6) in this case results from the fact that the speed of the wire fed to the arc is in excess of the rate of distribution of heat in the wire due to the heat conduction mechanism. In addition, the heat losses due to the molten metal drops grow with increase of the wire feed speed. As a result, at a wire feed speed of 15 m/min the size of the molten region is 0.8 mm, and at a wire feed speed of 5 m/min it amounts to 1.35 mm.

The above results were obtained at an assumption that the molten tip of the wire is located on the plasma jet axis ($L_w = L_p$). Consider now how displacement of the wire tip with respect to the plasma jet axis affects the thermal state of the wire. As follows from

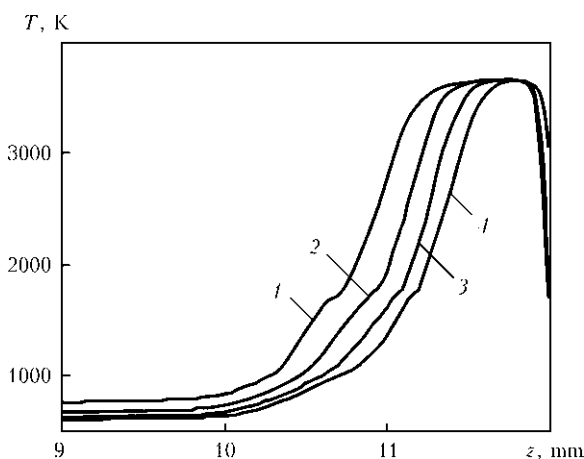


Figure 6. Distribution of temperature in the wire at different wire feed speeds: 1 – 5; 2 – 9; 3 – 12; 4 – 15 m/min

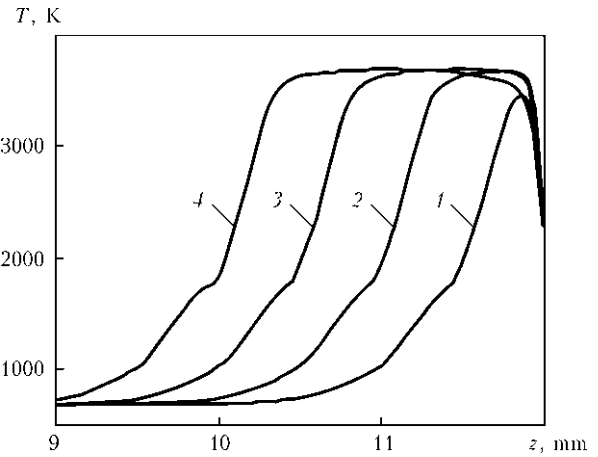


Figure 7. Distribution of temperature along the length of the wire depending on displacement of its molten tip relative to the plasma jet axis: 1 – $L_w - L_p = -0.5$; 2 – 0; 3 – 0.5; 4 – 1 mm

Figure 7, position of the molten tip of the wire has a considerable effect on the size of the heating and melting regions. For instance, if the wire is fed ahead of the plasma jet axis, the area of the side surface affected by the jet core grows. Given that heating of the wire is provided primarily due to the effect of the convective-conductive and radiation heat exchanges, the amount of heat accumulated in the wire increases. As a result, e.g. at $L_w - L_p = 0.5$ mm (see Figure 7, curve 3), the length of the molten region is 1.55 mm. In a case where the molten tip of the wire does not reach the jet axis, thus being on the periphery of the plasma flow, the share of the convective-conductive and radiation heating of the wire substantially decreases. E.g. at $L_w - L_p = -0.5$ mm the length of the molten region is 0.55 mm (Figure 7, curve 1). The results obtained are indicative of the fact that the plasma arc spraying process considered is characterised by the self-regulating possibilities. That is, the certain position of the molten tip of the wire relative to the plasma torch axis and length of the melt held on its tip set in with the spraying process parameters maintained at a steady-state level. Probable fluctuations of the process parameters during spraying lead to a

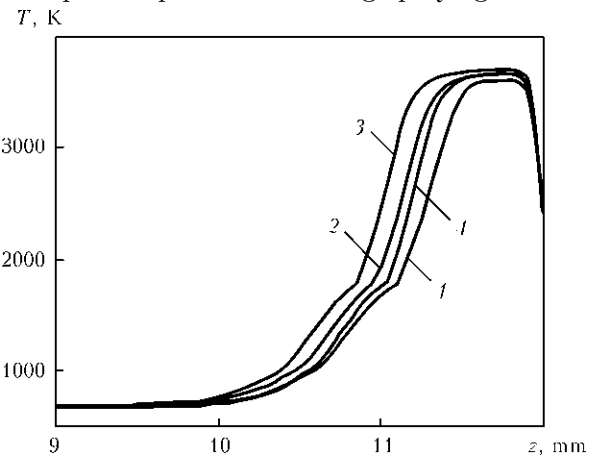


Figure 8. Distribution of temperature along the length of the wire at different operating parameters of the plasma torch: 1 – $I = 160$; 2, 4 – 200; 3 – 240 A, argon flow rate of 1 m³/h; 4 – argon flow rate of 1.5 m³/h



corresponding change in the above characteristics. However, in this case the amount of the heat input will be either insufficient for heating and melting of the wire and, as a result, it will come to its optimal position, or, if the wire goes ahead of the jet axis, the intensity of heating will be substantially increased and size of the molten metal region will grow as long as it can stay on the wire tip. Detachment of the melt by the plasma jet decreases the length of the wire. As a result, its tip will also come to the optimal position with respect to the jet axis.

Finally, Figure 8 shows the effect of operating parameters of the plasma torch on heating and melting of the spraying wire. At high values of the arc current the plasma velocity and temperature are higher. Hence, the role of the convective-conductive and radiation heat exchanges in the energy balance of the wire and length of its molten tip grow. Increase of the gas flow rate leads, first of all, to increase in the plasma velocity. In this case, the length of the molten region decreases to some extent.

CONCLUSIONS

1. The developed mathematical model can be applied to predict the temperature field and volume of molten metal of the live wire in plasma arc spraying.

2. As established by mathematical modelling, heating and melting of the anode wire in plasma arc spraying are caused primarily by the effect of the high-temperature plasma flow around the wire.

3. The model suggested allowed deriving dependencies of spatial distribution of temperature and volume of molten metal of the wire on such spraying

process parameters as the arc current, plasma gas flow rate and wire feed speed.

4. To construct the complete self-consistent model of the plasma arc spraying process it is necessary to develop a model of flow of the melt at the wire tip and formation of drops of the electrode metal, which, together with the plasma flow and wire heating models, would allow predicting the size, initial temperature and speed of introduction of fine particles formed as a result of melting of the wire to the plasma jet.

1. Kudinov, V.V., Bobrov, G.V. (1992) *Spraying deposition of coatings. Theory, technology and equipment*. Moscow: Metallurgiya.
2. Rykalin, N.N. (1951) *Calculations of thermal processes in welding*. Moscow: Mashgiz.
3. Sanyal, S., Chandra, S., Kumar, S. et al. (2004) An improved model of cored wire injection in steel melts. *ISIJ Int.*, **44**(7), 1157–1166.
4. Hu, J., Tsai, H.L. (2007) Heat and mass transfer in gas metal arc welding. Pt 1: The arc. *Int. J. Heat and Mass Transfer*, **50**, 833–846.
5. Hu, J., Tsai, H.L. (2007) Heat and mass transfer in gas metal arc welding. Pt 2: The metal. *Ibid.*, **50**, 808–820.
6. Kharlamov, M.Yu., Krivtsun, I.V., Korzhik, V.N. et al. (2007) Mathematical model of arc plasma generated by plasmatron with anode wire. *The Paton Welding J.*, **12**, 9–14.
7. Yudaev, B.N. (1988) *Technical thermodynamics. Heat transfer: Manual for non-energy production higher techn. institutions*. Moscow: Vysshaya Shkola.
8. Dresvin, S.V., Donskoj, A.V., Goldfarb, V.M. et al. (1972) *Physics and engineering of low-temperature plasma*. Ed. by S.V. Dresvin. Moscow: Atomizdat.
9. Knight, Ch.J. (1979) Theoretical modeling of rapid surface vaporization with back pressure. *AIAA J.*, **17**(5), 519–523.
10. Nemchinsky, V.A. (1994) Plasma parameters near a small anode in a high-pressure arc (gas metal arc welding). *J. Phys. D: Appl. Phys.*, **27**, 2515–2521.
11. Samarsky, A.A., Vabishchevich, P.N. (2003) *Computational heat transfer*. Moscow: Editorial URSS.
12. Anderson, D., Tannehill, J., Pletcher, P. (1990) *Computational hydromechanics and heat exchange*. Vol. 1. Moscow: Mir.

TO THE ATTENTION OF THE READERS!

The next regular information-statistical book SVESTA-2010: Welding. Robots. Steel (Economic-Statistical Data on Welding Production) is placed on the site of the E.O. Paton Electric Welding Institute of the NAS of Ukraine – www.paton.kiev.ua.

The authors-compilers of the book: [V.N. Bernadsky], O.K. Makovetskaya. Ed. by Prof. K.A. Yushchenko, Prof. L.M. Lobanov. – English language; 119 p.; 94 tables; 90 figures.

Book SVESTA-2010 was prepared and published by the E.O. Paton Electric Welding Institute (PWI) of the National Academy of Sciences of Ukraine with the assistance rendered by the International Institute of Welding (IIW) and European Welding Federation (EWF).

The book contains systematised economic-statistical information on state-of-the-arc and trends in development, consumption and market of welding engineering, as well as on world and national markets of technological welding robots and steel, which was the key structural material in 2006–2009.

The book includes statistical information on the world as a whole and on separate countries – members of IIW of the European, American and Asian regions, such as Bulgaria, Germany, Italy, Poland, Rumania, Great Britain, Russia, Ukraine, Brazil, USA, China, India, Japan, and South Korea. All the information is presented in the form of tables and diagrams, the sources of receiving this information being indicated.





ON THE SUBJECT OF ELECTRIC SUBMERGED-ARC WELDING

V.G. KUZMENKO

E.O. Paton Electric Welding Institute, NASU, Kiev, Ukraine

Results of investigation of the nature of flux melting in electric submerged-arc welding with slag bubble formation are described. It is established that the flux melts without formation of a slag bubble by the gas-plasma flows of the arc in the convective heat exchange mode. These conclusions are confirmed by visual observations of electric arc running under flux, using a procedure specially developed for this purpose. Moreover, an extended plume of liquid slag forms in the post-arc zone, which is separated from the weld metal by a wedge-like layer of solid slag. The process of slag crust formation is also due to high heat-insulating properties of welding fluxes.

Keywords: *electric submerged-arc welding, slag bubble, thermophysics, flux heat conductivity, hydrodynamics, visual observation of arcing, process diagram*

Some postulates of this work are given in papers, published in the way of discussion in «Automaticheskaya Svarka» [1, 2] and «Svarochnoe Proizvodstvo» [3, 4] journals.

The concept of electric arc welding (Figure 1) was formed in the middle of the XX century [5, 6], proceeding from the data of arcing zone examination by X-rays, based on which the authors came to the conclusion that the arc functions in the atmosphere of a slag bubble, forming from the melting flux.

Several remarks can be made on the investigation procedure: absence of preliminary identification of the differences between liquid slag and solid flux in the pre-arc zone, fragmentary nature of the filmed material, because of the short time of filming exposure (0.02 s), complexity of identifying the thin slag shell against the background of flux grains, and other factors, casting doubt on the obviousness of the above conclusions.

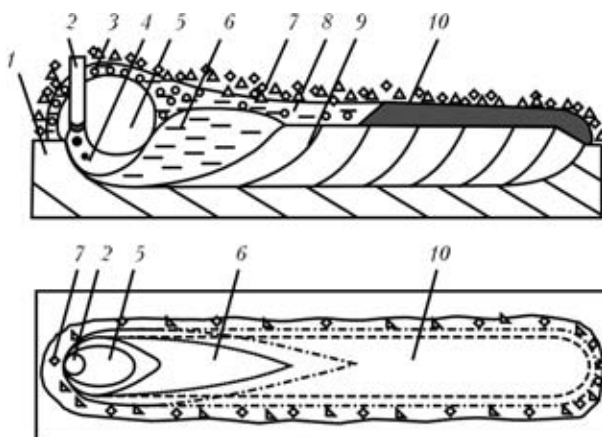


Figure 1. Schematic of the process of electric submerged-arc welding according to the current concepts: 1 – base metal; 2 – electrode wire; 3 – slag bubble; 4 – arcing zone; 5 – crater; 6 – weld pool; 7 – flux; 8 – liquid slag; 9 – weld; 10 – slag crust

© V.G. KUZMENKO, 2011

A feature of the electric arc column is its ability to push out of its space the solid and liquid components that is accompanied by formation of a cavity in the flux grain bulk. It was this cavity, possibly, that was recorded on the obtained rentgenograms. The question is, whether there is enough time for the liquid slag interlayer creating a closed shell around the arc, to form during welding in the flux volume ahead of the arc? This question is essential for assessment of the mechanism of weld pool metal protection from the influence of the components of the ambient air atmosphere.

Similar research was performed also by other authors [7–9]. So in [7] the X-ray image was sent to electron-optical tube, thus allowing the arcing process to be observed in its dynamics and electrode metal transfer to be studied both in manual electrode and flux-cored wire, and in submerged-arc welding. Nonetheless, based on the results of the performed research it is impossible to unambiguously determine the presence of slag shell in submerged-arc welding, particularly in the pre-arc zone. In order to determine the actual situation, we have conducted studies, including both theoretical calculations and special experiments.

The slag bubble in the case of its actual existence can be regarded as some dynamically stable formation, insulating the arcing zone from ambient air, and also having the function of liquid slag supplier, which is consumed for weld pool shielding. Slag bubble should be able to restore itself, and during welding should provide transfer of sufficient quantity of heat from the arc to solid flux beyond the slag shell. Using the known expression [10, 11], the time for heat transfer through the front wall of slag shell was determined, which was required to bring a certain amount of solid flux to melting temperature:

$$\tau = \frac{Q\delta}{\lambda(t_{st2} - t_{st1})F},$$

where Q is the heat that should be consumed for heating a certain amount of flux up to melting temperature; δ is the thickness of slag bubble shell; λ is the coef-



ficient of slag heat conductivity; $t_{st1} - t_{st2}$ is the temperature difference on the surfaces inside and outside the shell, respectively; F is the area of shell surface.

Such thermophysical properties of slags as specific heat capacity, density and heat conductivity, assumed by us for calculations, were taken from published sources [12–24]. Values of the thickness of slag bubble wall and temperature on its inner surface were assigned, and the temperature on the bubble outer surface was taken equal to flux melting temperature (1200 °C). For slag bubble wall inner surface the temperature was taken to be approximately equal to slag boiling temperature (3000 °C).

As shown by calculations, values of the speed of slag bubble shell restoration ahead of the moving arc (speed of shifting of flux melting isotherm) (Figure 2) are 3–4 times lower than the actual welding speed that calls in question the probability of formation of a liquid slag wall ahead of the arc in the respective welding process.

Existence of a slag bubble in submerged-arc welding is possible only in the presence of a sufficiently fine equilibrium between gas pressure in its volume, on the one hand, and interphase (surface) slag tension and flux mass, on the other, as well as at the absence of strong disturbance factors in the zone of slag bubble formation. Let us consider this in the real welding process as far as possible.

In welding the arc applies strong pressure to the edge of melting plate and weld pool liquid metal that is caused by its strong gas-plasma flows, the velocity of which, by various data, is equal from 75 to 2200 m/s [25–34]. As a result of reflection from the melting edge of metal being welded, these flows change their direction to the side opposite to arc motion. Here, a considerable portion of weld pool liquid metal is pressed out and a crater forms. Gas-plasma flows drive away liquid slag even more intensively, as its density is much lower than that of metal. This is confirmed by the data earlier obtained by us by indication method [1, 3] on the nature of metal and slag displacement after welding. Metal and slag acquire the maximum speed exactly at the first moment of contact with the arc. Presence of strong disturbance of metal and slag resulting from the arc impact prevents formation of the slag bubble in the considered welding process in connection with shifting of its supporting zone at a high speed that is confirmed by the data of investigations of liquid slag distribution along the weld pool obtained by ejection of its contents into a special collector with uniformly located sections [1, 3]. Figure 3 shows slag distribution along the weld pool at application of three standard fluxes of AN-60, AN-26S and AN-15M grades obtained by the above procedure. As follows from experimental results, welding slag is nonuniformly distributed along the welding zone. A considerable part of it is driven by the arc into the weld pool tail zone, and a marked

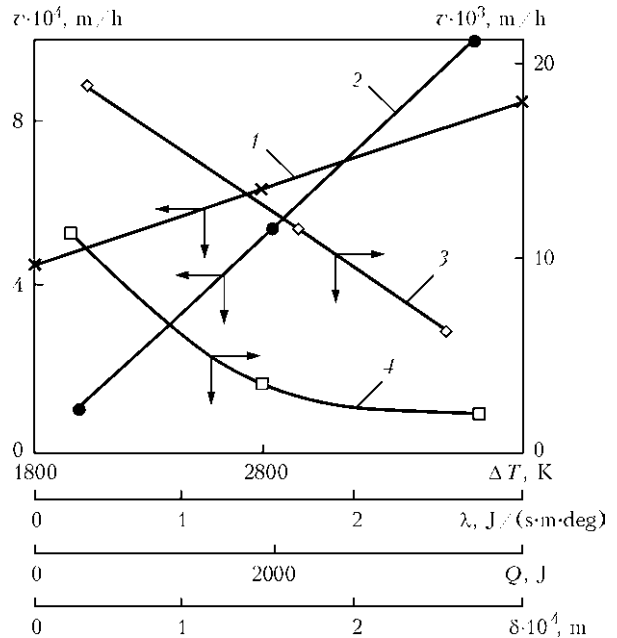


Figure 2. Change of the speed of restoration of slag bubble shell v in the pre-arc zone in electric submerged-arc welding depending on thermophysical characteristics: 1 – temperature gradient $\Delta T(t_{st2} - t_{st1})$ (shell thickness $\delta = 2$ mm; heat capacity of slag of $1 \times 1 \times 2$ mm volume $Q = 1177$ J; $\lambda = 1.5$ J/(s·m·deg)); 2 – coefficient of slag heat conductivity λ ($\delta = 2$ mm; $Q = 1177$ J of slag of indicated volume; $\Delta T = 2300$ K); 3 – heat capacity Q of slag of indicated volume ($\delta = 2$ mm; $\lambda = 2$ J/(s·m·deg); $\Delta T = 2300$ K); 4 – thickness of slag bubble shell δ ($Q = 1177$ J of slag of indicated volume; $\Delta T = 2300$ K; $\lambda = 1.5$ J/(s·m·deg))

tendency to lowering of liquid slag mass towards the melting metal edge is found in its head part. To obtain a clearer picture, similar experiments were conducted to monitor the presence of liquid slag on weld pool front edge, using lower arc voltage (21 V) that allowed limiting the volume of melting flux, which was masking the experimental results. In Figure 4 it is

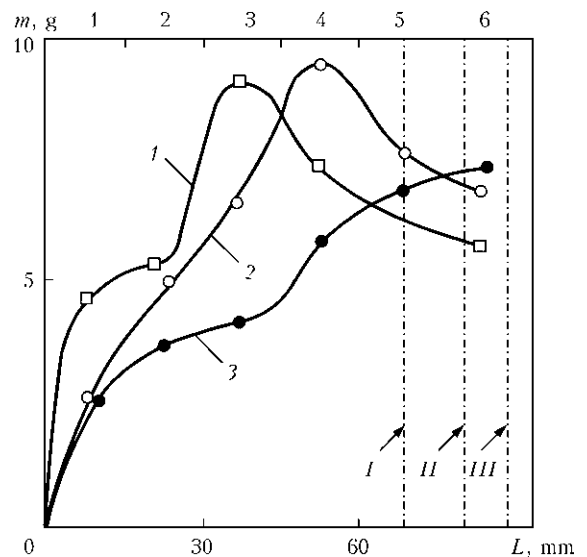


Figure 3. Distribution of mass m of slag along length L of weld pool in electric submerged-arc arc welding with fluxes of AN-60 (1), AN-26S (2) and AN-15M (3) grades established by turning over its contents into a collector with pockets 1–6, uniformly placed along the weld pool, and subsequent weighing of slag (arrows are weld pool boundaries at application of the above flux grades in the sequence corresponding to designated row I–III)

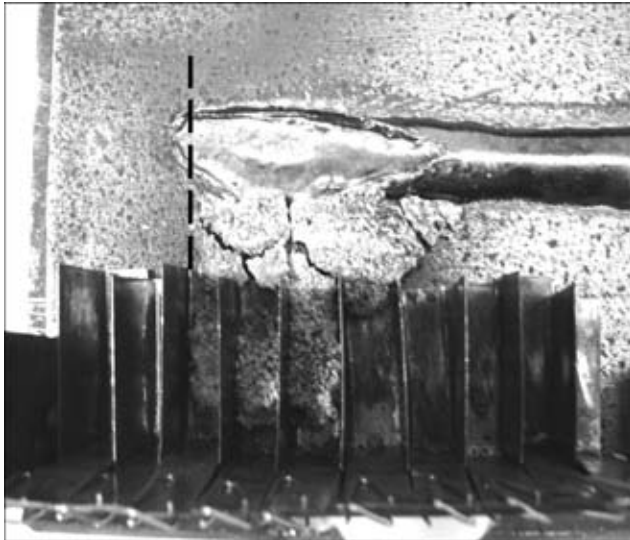


Figure 4. Distribution of molten slag along the weld pool in electric arc welding after removal of unmolten flux and slag crust (experimental phase)

clearly seen that liquid slag is absent on the edge in front of weld pool melting metal (marked by a dashed line), and it is not found also on a certain portion of weld pool head part, where the arc runs. This is confirmed by curves plotted by the data of weighing the contents of each of the collector pockets (Figure 5, *a*). Thus, investigations of slag distribution along the weld pool did not demonstrate its presence on the weld pool front edge that, essentially, eliminates the possibility of slag bubble existence in electric submerged-arc welding.

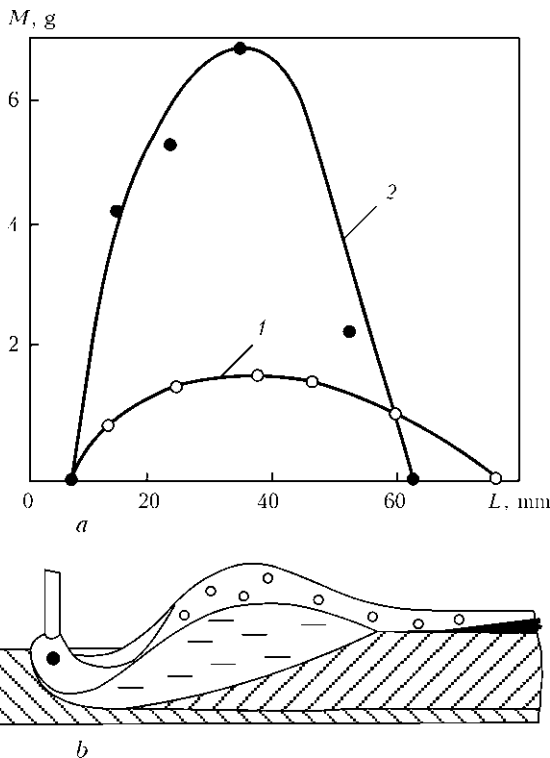


Figure 5. Curves of distribution of mass *M* of liquid slag (1) and metal (2) along the weld pool in electric submerged-arc welding obtained by application of an improved procedure of weld pool turning over and control of object mass (*a*), and schematic of the above-mentioned process (*b*)

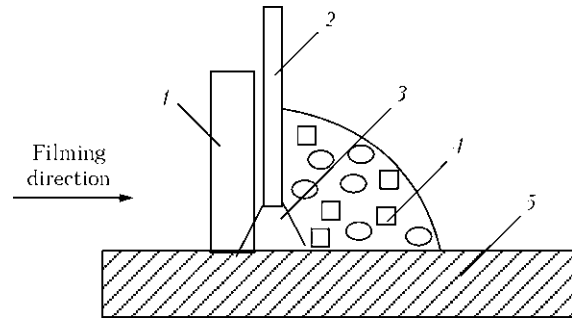


Figure 6. Schematic of an experiment on visual observation of the arcing process in electric submerged-arc welding: 1 – window glass; 2 – electrode; 3 – electric arc; 4 – flux; 5 – steel plate

In order to reveal the presence of slag bubble in electric submerged-arc welding, we conducted one more experiment. For this purpose individual beads were deposited on plates, in which a gradual starting from 25 mm (complete shielding of the arc), and then millimetre by millimetre lowering of flux pouring level was performed. All the experiment stages were recorded by a video camera. It was supposed that at a certain level of flux pouring it will be possible to see the pulsing cupola of the slag bubble. However, despite the monotonic lowering of the flux layer thickness, it was not possible to capture this moment in the filmed video material. Just baring of the arc without slag bubble formation and, vice versa, sagging of flux portion in the arcing zone were observed. The flux sagging was caused by formation of a crater in the metal, reduction of flux volume in melting and slag ejection by the arc towards weld pool tail part.

To provide a more convincing confirmation of slag bubble absence, we developed a procedure that enables visual observation of the arcing zone directly during electric submerged-arc welding (Figure 6). Here, window glass was used as a transparent screen and slag-forming material at the same time. The procedure was developed, taking into account the main postulates of our earlier thermophysical and hydrodynamic investigations. Here two alternative points of view were assessed. According to the first one, if formation of the gas bubble occurs during welding, then glass melting, formation of a shell around the arc from the glass melt and its shielding, respectively, take place. In the opposite case, glass melts in the post-arc space, no arc shielding occurs, and the arc can be observed directly. Results of experiments in the form of arcing phases successive in time in electric submerged-arc welding, are given in Figure 7. Studying the filmed material led to the conclusion that no arc shielding occurs during welding, the arc is clearly visible during the entire welding process, and no slag bubble forms around it. Liquid slag does not rise above the running arc level, but is concentrated on weld pool surface. This is readily visible in Figure 7 by the bright strip (tail) of hot slag in the post-crater zone of weld pool. This confirms the absence of slag shielding of weld pool crater zone and the essential role of gas shielding. At the same

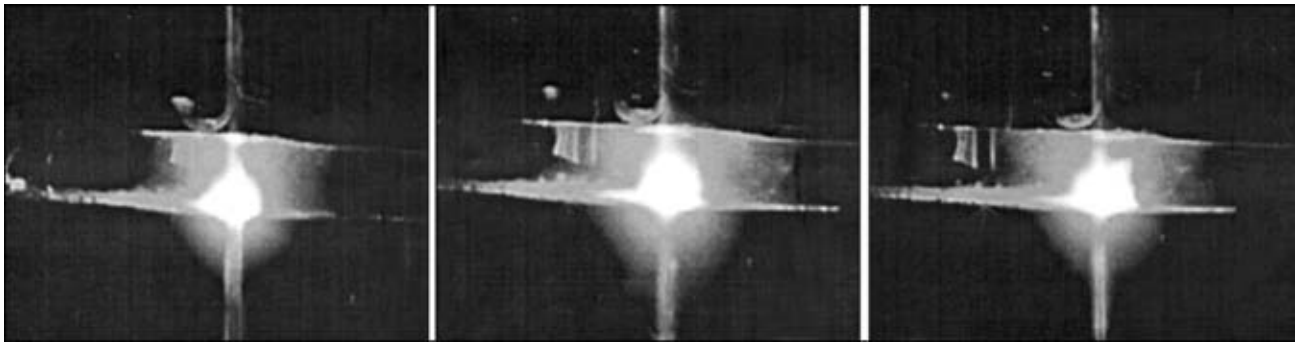


Figure 7. Three successive fragments of arcing phases in electric submerged-arc welding obtained in an experiment (see Figure 6) when welding process runs from left to right

time, the above circumstance became the subject of discussion [35–37] and were the basis for development by us of a new class of surface-fluorinated welding fluxes with 0.5–3.0 wt.% fluorine content in the surface layer of their grains. Such fluxes, even porous and of basic type, have a low susceptibility to hydration, high resistance to weld metal porosity because of rust and improved sanitary-hygienic characteristics in welding [38–40].

To obtain a complete picture of the process of electric submerged-arc welding, we studied the features of cooling and solidification of welding slag in the post-arc zone [3]. Unlike the generally accepted schematic of the welding process (see Figure 1), availability of an extended region of liquid condition of slag is established, which goes far beyond the weld pool limits. These data were obtained as a result of application of the traditional procedure of weld pool turnover [3]. High heat-insulating properties of slag have a great influence on the cooling rate and configuration of the zones of solidified and liquid slag. In this case, mostly heat removal into the metal takes place that is related to a change of the temperature field due to displacement of the electric arc along the weld axis. Here the slag solidifies, first of all in those points on weld metal surface, where its temperature decreases to slag melting temperature. In the direction away from the arc, further gradual lowering of temperature and monotonic increase of thickness of solidifying slag take place with separation and thermal insulation of the tail located above the liquid slag volume. A new schematic of the process of electric submerged-arc welding, taking into account the features of slag cooling down in the post-arc zone given in Figure 8, provides an explanation for the earlier unconsidered mechanism of flux solidification in electric arc welding. A considerable mass of overheated slowly cooling slag above the weld pool acts as its thermal extension that increases the length of time of weld metal staying in the liquid state and promotes its degassing. A large volume of liquid slag above the solidifying and solidified metal is a cavity that absorbs the gases evolving from the weld metal. Owing to presence of an elastic wedge-like film of slag on the surface of solidifying weld metal, it is possible to apply in electric submerged-arc welding fluxes with a higher melting temperature than that of the metal being welded. This also accounts sometimes for porosity formation in the lower part of the slag crust at intensive gas evolution

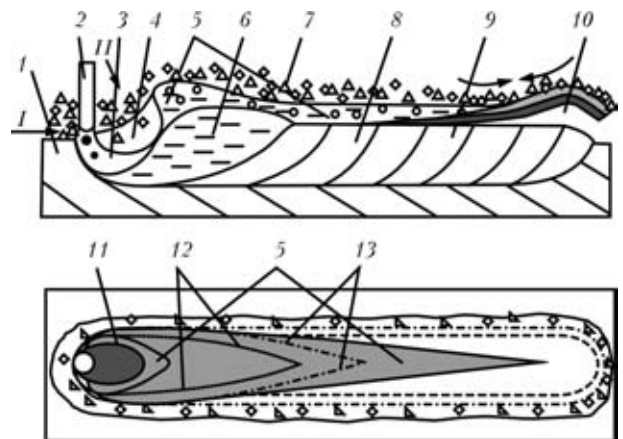


Figure 8. Precised schematic of the process of electric submerged-arc welding: 1 – base metal; 2 – electrode metal; 3 – arc plume; 4 – crater; 5 – liquid slag and its extended tail; 6 – weld pool; 7 – flux; 8 – weld; 9 – glass-like, wedge-like solidifying slag layer; 10 – crystalline layer of solidifying slag; 11 – crater zone not covered by liquid slag; 12, 13 – line of melting isotherm of flux and slag, respectively; I, II – ways of flux penetration into the arc

from the metal that does not come to its surface. Differences in the rates of cooling of slag layer adjacent to the weld and above-lying layer lead to essential differences in their structure. Slag layer contacting the weld surface cools down faster and forms a glass-like structure, whereas the above-lying slag layer is completely or partially solidified, owing to its thermal insulation. It has a much greater coefficient of thermal compression than that of glass-like slag layer, leading to bending of this two-layer structure, and is spontaneous separation from the cooling weld (see Figure 8). Such a mechanism of slag crust separability is particularly effective, when high-silicon welding fluxes are used.

CONCLUSIONS

1. Procedure of X-ray examination of the arcing zone in electric submerged-arc welding used in works [5, 6], does not give sufficient grounds to confirm the fact of existence of a slag shell around the arc, particularly in the pre-arc zone.

2. Use of general equation of heat conductivity and Fourier law as applied to unidimensional problem in calculations of the rate of heat transfer from the arc through the shell to pre-arc zone flux, depending



on slag thermophysical characteristics, temperature gradient and thickness of slag bubble shell showed that the speed of shell restoration (speed of shifting of flux melting isotherm) is by 3–4 orders of magnitude lower than the real welding speed.

3. As a result of an extremely low speed of restoration of the shell pre-arc component, no flux melting through formation of a slag bubble occurs in electric arc welding. Under the real welding conditions, the arc rolls over the flux, entraps it and melts it under the impact of its own gas-plasma flows in the convective mode more effective in terms of energy.

4. Configuration of the zones of solidified and liquid slag in the post-arc zone and their temperature in electric submerged-arc welding are determined by heat removal into the metal, and owing to high thermally insulating properties of the flux, they are accompanied by formation of an extended liquid slag tail, separated from the weld metal by a wedge-like layer of solidifying slag crust.

5. Change of slag cooling rate leads to formation of a two-layer structure of the slag crust (glass-like – near the weld, and crystalline – higher up). At its further cooling the differences in the values of the coefficient of thermal compression lead to bending of the slag crust that promotes its separability from the weld metal.

1. Kuzmenko, V.G. (1998) About continuity of slag shell in submerged-arc welding. *Avtomatich. Svarka*, **3**, 14–19.
2. Kuzmenko, V.G. (2000) On the features of flux melting in electric arc welding. *The Paton Welding J.*, **11**, 57–58.
3. Kuzmenko, V.G. (1999) Features of melting and solidification of flux in electric arc welding. *Svaroch. Proizvodstvo*, **10**, 16–22.
4. Badianov, B.N. (1999) New scheme of submerged-arc welding process. *Ibid.*, **6**, 18–29.
5. Ostapenko, N.G., Medovar, B.I. (1947) X-ray analysis of submerged arc zone. *Avtogemoe Delo*, **11**, 16–20.
6. Grebelnik, P.G. (1950) X-ray analysis of automatic submerged-arc welding process. *Avtomatich. Svarka*, **6**, 18–29.
7. Pokhodnya, I.K. (1964) Method of analysis of electrode melting and transport process in welding. *Ibid.*, **2**, 1–10.
8. Gobarev, L.A., Mazel, A.G., Shmeleva, I.A. et al. (1973) Analysis of submerged arc in welding using pulse X-ray apparatus. *Ibid.*, **2**, 69–70.
9. Eichhorn, F., Dilthey, U. (1971) High-speed X-ray photography for submerged arc welding. *Metal Construction and British Welding J.*, **3**(12), 453–456.
10. Kasatkin, A.G. (1973) *Processes and apparatuses of chemical technology*. Moscow: Khimiya.
11. Kuehling, H. (1982) *Reference book on physics*. Moscow: Mir.
12. Rykalin, N.N. (1951) *Calculations of thermal processes in welding*. Moscow: Mashgiz.
13. Litovsky, E.Ya., Puchkelevich, N.A. (1982) *Thermophysical properties of refractory materials*. Moscow: Metallurgiya.
14. Krzhizhanovsky, R.E., Shtern, Z.Yu. (1973) *Thermophysical properties of inorganic materials*. Leningrad: Energiya.
15. Misnar, A. (1968) *Heat conductivity of solids, liquids, gases and their compositions*. Moscow: Mir.
16. Chekhovskiy, V.Ya., Ulashchik, A.N. (1987) Heat conductivity of slags in solid and molten states. *Teplofizika Vys. Temperatur*, **5**(5), 924–928.
17. Yavojskiy, Ya.I. (1967) *Theory of steelmaking processes*. Moscow: Metallurgiya.
18. (1964) *Steelmaking*. Vol. 1. Moscow: Metallurgiya.
19. Sakura, T., Emi, T., Ohata, H. et al. (1982) Determination of heat conductivity of slag melts by modified method of laser beam. *Nihon Kinzoku Gakkaisha*, **46**(12), 1131–1138.
20. Egorov, V.N., Kondratenkov, V.I., Killeso, V.S. (1972) Thermophysical properties of some glasses and pyroceramics. *Teplofizika Vys. Temperatur*, **5**, 95–99.
21. Serebrennikov, N.I., Geld, P.V. (1968) Enthalpy and temperature of slag melting in aluminothermic fabrication of some ferroalloys. *Izvestiya Vuzov. Series Tsvet. Metallurgiya*, **4**, 39–44.
22. Maurakh, M.A., Mitin, B.S. (1979) *Liquid refractory oxides*. Moscow: Metallurgiya.
23. Vajsburd, S.E., Zedina, I.N. (1970) Thermal properties of some silicates in liquid state. In: *Physical chemistry of molten slags*. Kiev: Naukova Dumka.
24. Bobylev, I.B., Anfilogov, V.N. (1983) Method of calculation of molten slag density. *Metally*, **4**, 37–44.
25. Erokhin, A.A. (1979) Force effect of arc on molten metal. *Avtomatich. Svarka*, **7**, 21–26.
26. Chigarev, V.V., Shchetinin, S.V. (2001) Distribution of welding arc pressure. *The Paton Welding J.*, **9**, 8–11.
27. Suzdalev, I.V., Yavno, E.I. (1981) Device for analysis of nature of distribution of welding arc force effect. *Svaroch. Proizvodstvo*, **3**, 37–38.
28. Kovalev, I.M., Krichevskiy, E.M., Lvov, V.N. (1974) Effect of metal motion in welding pool on arc stability and weld formation. *Ibid.*, **11**, 5–7.
29. Mechev, V.S. (1983) Welding arc pressure on molten metal. *Ibid.*, **9**, 8–10.
30. Potekhin, V.P. (1986) Role of welding arc pressure in formation of undercuts. *Ibid.*, **8**, 38–39.
31. Wieneke, R. (1957) Ueber physikalische Vorgänge in Lichtbogen. *Schweissen und Schneiden*, **9**(9), 428–434.
32. Petrunichev, V.A. (1958) Pressure of high power arc on welding pool. *Ibid.*, **7**, 14–17.
33. Leskov, G.I. (1970) *Electric welding arc*. Moscow: Mashinostroenie.
34. Nebylitsyn, L.E., Lenivkin, V.A., Dyurgerov, N.G. (1976) Determination of parameters of plasma jet in consumable electrode welding. *Avtomatich. Svarka*, **2**, 8–10.
35. Lyubavskiy, K.V., Timofeev, M.M. (1951) Influence of variation of high-manganese flux composition on its properties. *Avtogemoe Delo*, **6**, 5–9.
36. Kirdo, I.V., Podgaetskiy, V.V. (1949) On effect of fluxes on porosity of automatic weld caused by rust. *Trudy po Avtomatich. Svarke pod Flyusom*, **6**, 36–62.
37. Podgaetskiy, V.V., Novikova, T.P. (1960) On emission of silicon fluoride in heating of flux during welding and drying. *Avtomatich. Svarka*, **6**, 19–22.
38. Kuzmenko, V.G., Guzej, V.I. (2004) Hydration of fluxes with a locally-changed chemical composition of grains. *The Paton Welding J.*, **6**, 41–43.
39. Kuzmenko, V.G., Guzej, V.I. (2005) Pore formation in weld metal in submerged arc welding with surface saturation of grains with fluorine. *Ibid.*, **2**, 14–17.
40. Kuzmenko, V.G., Guzej, V.I. (2006) Sanitarian-hygienic characteristics of welding fluxes with locally-changed chemical composition of grains. *Ibid.*, **2**, 37–39.



STRENGTH AND FEATURES OF FRACTURE OF WELDED JOINTS ON HIGH-STRENGTH ALUMINIUM ALLOYS AT LOW TEMPERATURE

T.M. LABUR

E.O. Paton Electric Welding Institute, NASU, Kiev, Ukraine

The regularities of variation in strength values of nonconsumable electrode welded joints on aluminium alloys of different alloying systems at low temperature (down to 20 K) were analyzed. Peculiarities of their fracture in different heat-affected zones are noted.

Keywords: aluminium alloys, nonconsumable electrode argon-arc welding, welded joints, strength, failure, low testing temperature, fractures

Owing to their structural capabilities and mechanical properties, aluminium alloys are an attractive material for low-temperature operation. They have high specific strength and are not prone to brittle fracture [1–3]. High-strength alloys of three alloying systems – Al–Mg–Mn (AMg6N), Al–Cu–Mn (1201) and Al–Cu–Li (1460) – became the most widely accepted by designers and technologists for fabrication of welded products for cryogenic engineering (Table). At application of permanent joints of components and structures from such alloys, it is necessary to determine their strength level and establish their fracture features at low temperature. This will allow determination of optimum temperature intervals of operation of aluminium alloy welded structures that is important, as a certain chemical and structural heterogeneity develops in the weld metal and HAZ during welding that determines fracture characteristics.

The subject of this work is establishing the regularities of the change of physico-mechanical properties and features of fracture of welded joints on high-strength aluminium alloys AMg6N, 1201 and 1460 in a broad temperature range (300–20 K). Sheets of the above alloys 4 mm thick were butt welded by mechanized nonconsumable electrode argon-arc welding that is the most widely accepted method of manufacturing

products for cryogenic applications. Welding was performed by a pulsed-arc of asymmetrical square-wave current of different polarity [4]. To prevent formation of defects in welded joints the welded edges were scraped to the depth of not less than 0.1 mm. Welding of AMg6N alloy was performed with welding wire of SvAMg63 grade, for 1201 alloy Sv1201 wire was used, and for 1460 – alloy test wire of Al–Cu system (see the Table). Wire diameter was 2 mm in all the cases. Proceeding from the results of X-ray inspection, the quality of the studied welds was recognized to be satisfactory.

Assessment of physico-mechanical properties was performed under the conditions of uniaxial and off-center tension at the rate of $3.3 \cdot 10^{-5}$ m/s at the temperature of 300, 200, 77 and 20 K. Samples were cooled using dry ice (at 200 K), liquid nitrogen (at 77 K) and hydrogen (at 20 K). At uniaxial tension flat smooth samples with notch radius of 0.25 mm along the weld axis were tested (GOST 227–77). At off-center tension, when tension and bending are applied simultaneously, flat samples of $57 \times 36 \times 4$ mm size with notch of 11 mm depth and 0.1 mm radius at the tip were used [5]. Theoretical coefficient of stress concentration was equal to 10. Notch tips in welded joint samples were located strictly along weld axis, in the fusion zone and HAZ zone located at 5 mm distance from the fusion line, as dissolution of alloying elements occurs at welding heating, and solid solution

Composition (wt.%) of commercial high-strength aluminium alloys and filler wires used in welding

Systems	Alloy and wire grades	Cu	Mg	Mn	Ti	Zr	Fe	Si	Other elements
Al–Mg–Mn	AMg6N	0.1	5.8–6.8	0.5–0.8	0.02–0.10	–	0.40	0.40	–
	SvAMg63	0.1	5.6–6.8	0.5–0.8	0.10	0.15–0.35	0.05	0.05	–
Al–Cu–Mn	1201	5.8–6.8	0.02	0.2–0.4	0.02–0.10	0.10–0.25	0.30	0.20	0.05–0.15 V
	Sv1201	6.0–6.8	0.02	0.2–0.6	0.02–0.10	0.10–0.25	0.15	0.08	0.05–0.15 V
Al–Cu–Li	1460	3.1–3.5	–	–	0.10–0.20	0.08–0.09	0.30	0.20	2.00–2.20 Li
	Test Al–Cu		–	–	–	–	–	–	0.07–0.08 Sc

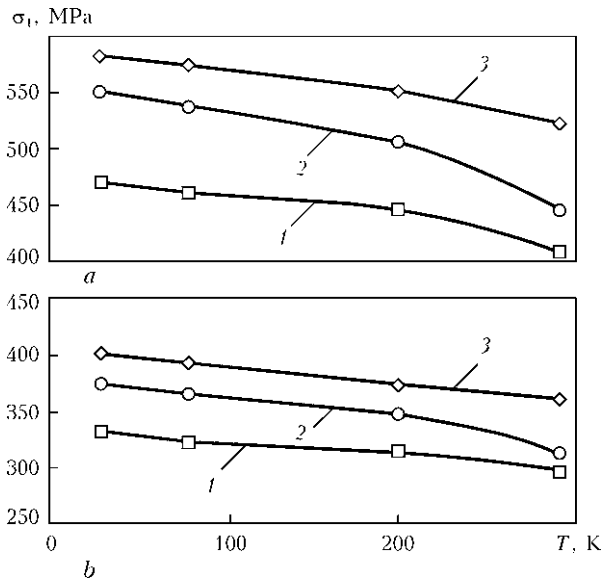


Figure 1. Influence of low-temperatures on ultimate tensile strength σ_t of notched samples of aluminium alloys AMg6N (1), 1201 (2) and 1460 (3) (a) and their welded joints (b)

decomposition and phase formation depend on heating source and temperature-time parameters of welding [4]. Tested for comparison were similar base metal samples of all the studied aluminium alloys, cut out in the direction transverse relative to rolling direction, the most unfavourable for rolled sheets.

Fracture mode of base metal and welded joints of the above alloys at different temperatures was studied in scanning electron microscope (SEM) JSM-840 with Link-860/500 microanalyzer system at accelerating voltage of 15, 20 and 30 kW. This instrument allows diagnosing the macro- and microstructure of welded joint fractures to study the kinetics and mechanism of crack propagation, as well as revealing the causes for the impact of various factors, in particular, change of their structure in welding, loading conditions and temperature [6–8].

As a result of experimental study, it was established that the values of ultimate tensile strength σ_t of samples of welded joints of AMg6N, 1201 and 1460 alloys at room temperature uniaxial tension were equal to 330, 350 and 400 MPa, respectively. Base metal strength here was by 20–25 % higher than that of welded joints (Figure 1). Lowering of testing temperature to 77 K increases by 10–20 % σ_t values for base metal (of AMg6N, 1201 and 1460 aluminium alloys).

Ultimate tensile strength values of welded joints compared to room temperature increase by only 5–10 %, remaining lower than those of base metal. Of the studied alloys, AMg6N alloy and its welded joints have a lower susceptibility to low-temperature strengthening. A similar dependence of σ_t is found at transition from 77 to 20 K temperature. Ultimate tensile strength of weld metal of 1201 and 1460 alloys here rises by more than 70 and 100 MPa, respectively.

Comparison of strength values of samples of base metal and welded joints shows that they differ from each other in the entire studied temperature range (from 20 up to 300 K), despite an increase of ultimate tensile strength (Figure 1). With lowering of testing temperature the rate of strength increase is 1.5–1.8 times higher for base metal than for welded joints. Among the studied alloys AMg6N alloy has a lower susceptibility (by 10–15 %) to low-temperature strengthening.

A similar tendency of strength variation is noted also under the conditions of off-center tension (Figure 2). At testing temperature of 300–77 K nominal breaking stress σ_{br} of AMg6N alloy rises only slightly (by 3–5 %), and in liquid hydrogen medium at 20 K temperature it decreases to room temperature level. In 1201 and 1460 alloys this strength characteristic rises monotonically in all the studied temperature range reaching $\sigma_{br} = 510$ and 630 MPa at 20 K. The physics of this phenomenon is related to the value of atom diameter (0.3120 nm) of magnesium as the main alloying element of AMg6N alloy. Lower value of atom diameter (0.256 nm) of copper contained in 1201 and 1460 alloys, compared to magnesium, promotes a more active movement of dislocations, with achievement of a uniform stress field distribution at lowering of ambient temperature [4, 5].

Welded joints of the studied alloys have lower values (by 100–200 MPa) of breaking stress at all values of testing temperature (Figure 2, a, d). Level of σ_{br} lowering is determined by alloying system of the alloy, as well as by the degree of inhomogeneity by alloying element and impurity content as a result of their segregation along the grain boundaries and formation of zones with a coarse structure under the impact of welding heating. Minimum level of σ_{br} values is noted in welded joints of AMg6N alloy. Temperature of testing welded joint samples has differing influence on the rate of stress increase in the weld and HAZ metal.

Marked differences between the studied aluminium alloys are found at determination of specific work of crack propagation (SWCP). All the alloys demonstrate a general regularity of lowering of SWCP at the change of testing temperature (Figure 2, b, e). This is related to the fact that at testing temperature below 77 K strong energy barriers are created in the path of dislocation motion [9–11] that reduce the probability of manifestation of thermal fluctuations required for dislocation mobility and, thus, limit plastic deformation, the degree of lowering of which is indicated by SWCP values. AMg6N alloy has a minimum level of fracture energy in the entire temperature range that is, possibly, due to insufficient purity of initial metal as to interstitial impurities or features of their crystalline, dislocation or electronic structure [2, 3].

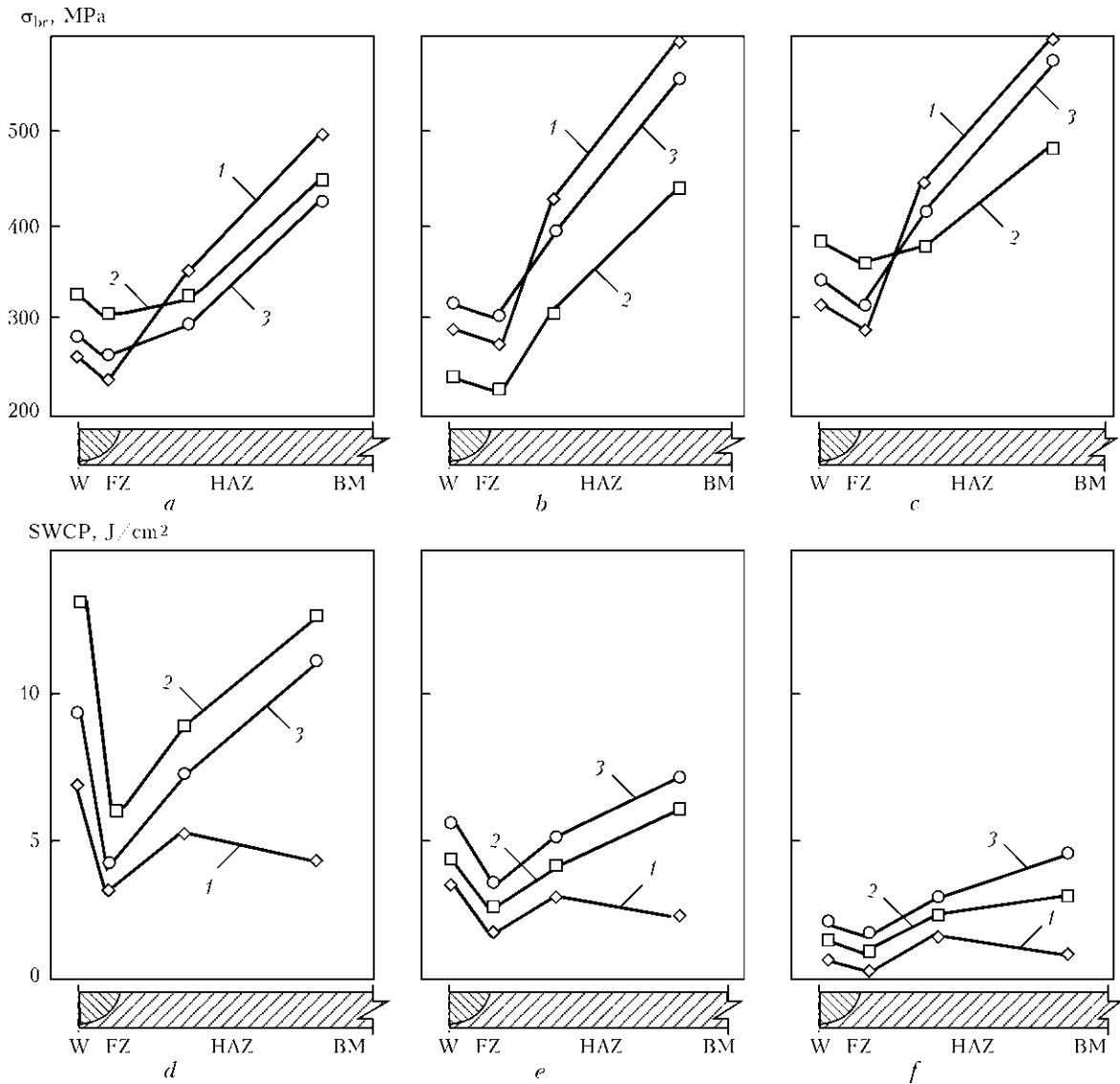


Figure 2. Dependence of nominal breaking stress σ_{br} (a-c) and SWCP (d-f) in different zones of welded joints of high-strength aluminium alloys 1460 (1), AMg6N (2) and 1201 (3) on testing temperature of 293 (a, d), 77 (b, e) and 20 (c, f) K: W – weld; FZ – fusion zone; BM – base metal

σ_{br} values in different zones of welded joints of AMg6N, 1201 and 1460 alloys decrease with lowering of testing temperature to 20 K, as a result of low-temperature strengthening characteristic for base metal (see Figure 2, a, d). However, σ_{br} values for different aluminium alloys differ from each other and from the base metal. In the latter case they are lower by 150–200 MPa that is close to the change of strength of welded joints at uniaxial tension. Rate of stress increase is determined by the alloy chemical composition and thermal impact of welding heating. Joints of 1201 and 1460 alloys were found to have a higher susceptibility to low-temperature strengthening than AMg6N alloy joints.

SWCP values of welded joints are more than 1.5 times higher compared to base metal in the entire studied temperature range (see Figure 2, b, e). Degree of SWCP lowering is also determined by alloy composition and depends on the change of structure in the joint zone under the impact of the welding cycle.

Joints of 1201 and 1460 alloys are characterized by higher values compared to AMg6N alloy that may be due to magnesium atom dimensions.

Fusion zone metal has minimum values of fracture resistance at all the values of testing temperatures. Their level depends on the composition of welded alloys (see Figure 2). For an alloy with magnesium, σ_{br} is equal to 310 MPa, SWCP is $6 J/cm^2$, and for an alloy with copper they are 260 MPa and $4 J/cm^2$, respectively. Lower σ_{br} values of fusion zone metal are indicative of the susceptibility to fast localisation of deformation, and, as a consequence, to low capability of uniform deformation under the conditions of off-center tension. At lowering of testing temperature σ_{br} values increase by 10 %, whereas SWCP values decrease by 30–40 %, that is related to formation of the least favourable metal structure in welding under the impact of welding heat [4]. The greatest lowering of values (by 180–220 MPa) is noted in joints of 1460 alloy containing lithium. Welded joints of 1201 alloy

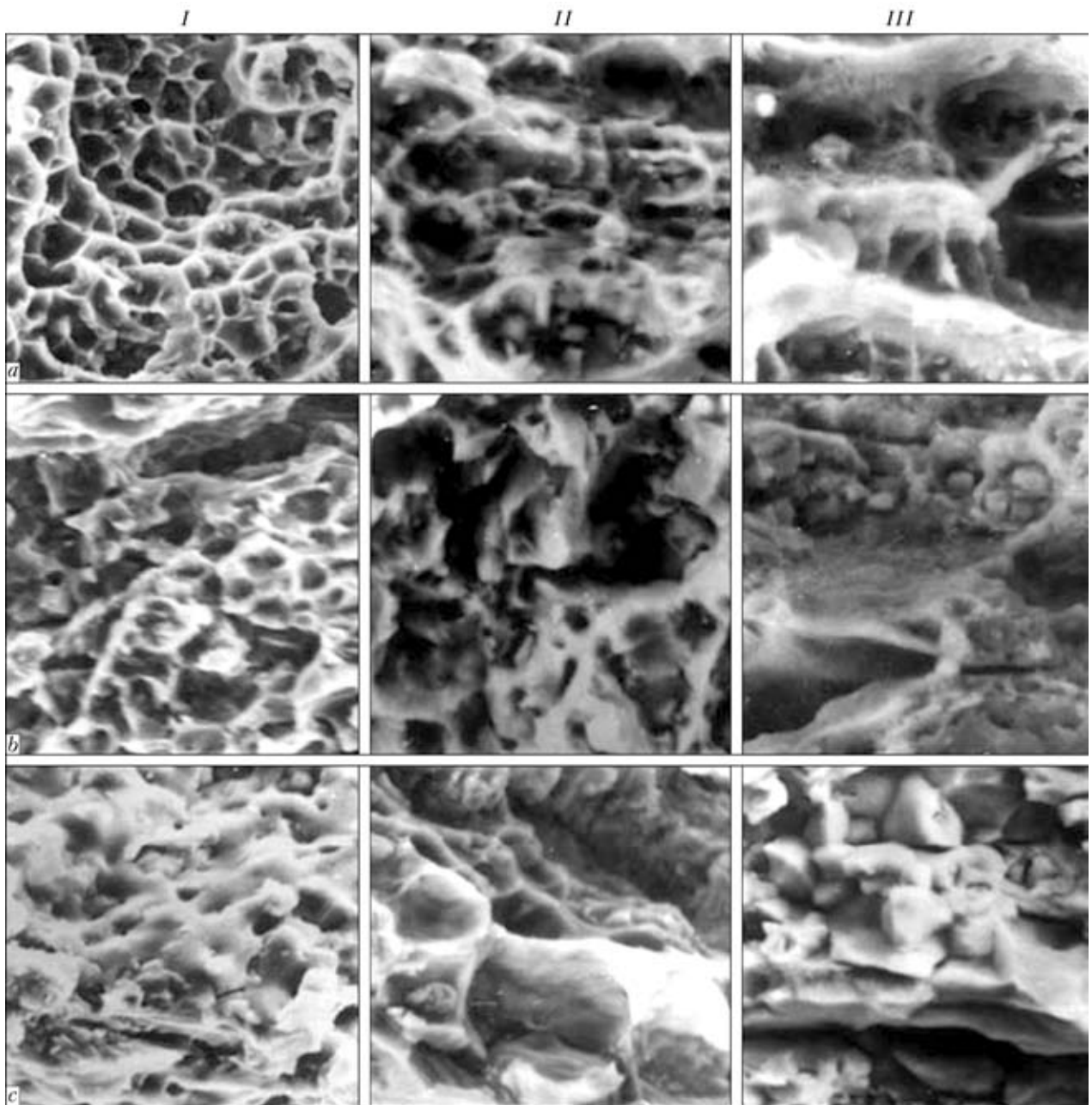


Figure 3. Fractograms of fracture surface of individual zones of welded joint of AMg6N alloy tested at the temperature of 293 (a), 77 (b) and 20 (c) K: I – W; II – FZ; III – HAZ

in the temperature range of 77–20 K have higher values of fracture resistance characteristics (σ_{br} and SWCP). Even in the dangerous fusion zone where a coarse structure forms, promoting the inevitable formation of technological defects, at testing temperatures of 20 K values of these properties are higher than for other studied alloys.

Fractographic studies of fracture surfaces of welded joints revealed that fractures of samples tested at room temperature have pit-like structure (Figures 3–5). Fracture surfaces were found to have micropores, presence of which is indicative of crack development by the mechanism of microvoid initiation, growth and coalescence, characteristic for aluminium alloys. Spherical shape of the pits, decorated by developed ridges along the edges, indicates the ability

of welded joint metal to deform intensively, resisting crack initiation under the impact of nominal tensile stresses. This is manifested particularly in AMg6N alloy, having the highest values of pit diameter and depth (Figure 3). Crack initiation sites are inclusions of intermetallics of 0.1–10.0 μm size, which form during alloy manufacture, as well as secondary phase particles of the type of dispersed particles of intermediate inclusions of 0.05–0.50 μm size and phase precipitates of 0.01–0.50 μm size. Pit formation, mode of fracture of brittle intermetallic particles or their delamination on the interface depend on the alloy composition, determining the properties of welded joints, pit shape, volume coefficient and state of structural component interface.

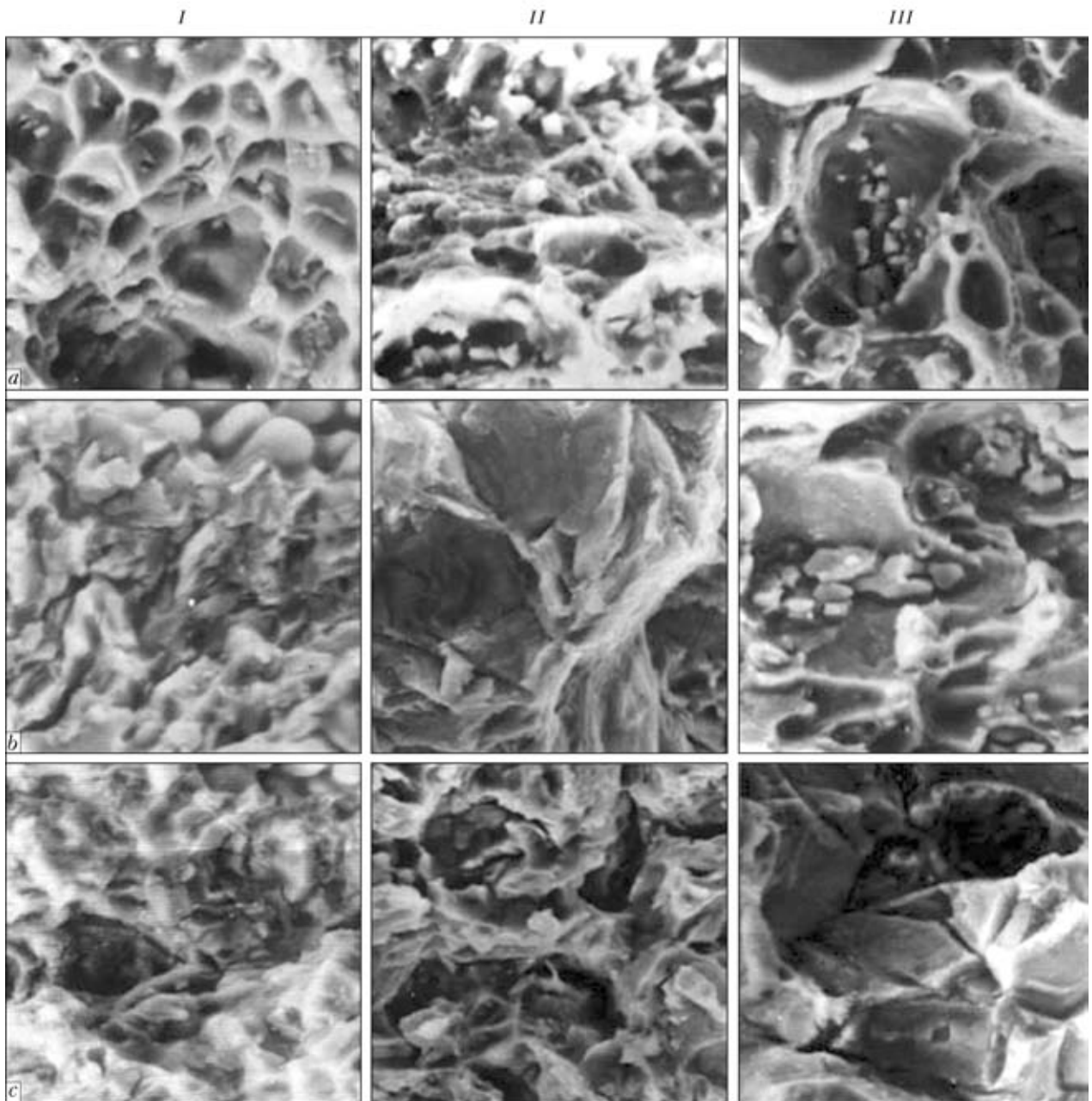


Figure 4. Fractograms of fracture surface of individual zones of 1201 alloy welded joint at low testing temperature (*a-c* and *I-III* – see Figure 3)

Relief topography of the weld and HAZ has certain differences. Weld metal is characterized by deep equiaxed pits with traces of particles initiating microcracks, observed on their bottom (see Figures 3–5). Such particles are coarse precipitates of excess phase formed under the conditions of welding cycle, as well as insoluble intermetallic inclusions. They are usually non-coherent to the matrix and lead to porosity on the interphases at plastic deformation of the metal [3]. Found features of the relief are indicative of the fact that the leading mechanism of microvoid formation in the structure of aluminium alloys and their welded joints is non-uniformity of plastic deformation and its localizing in the metal microvolume near the particles.

Structural inhomogeneity (difference in particle size and their spacing) in the fusion zone is reflected

in non-uniformity of pits on fracture surface. Regions are observed, where a multitude of finer pits are found on the large pit surface that is indicative of stage-by-stage nature of void formation and is the result of gradual fracture of finer inclusion particles. Individual microcracks are visible on grain boundaries. Their presence points to a high sensitivity of metal of this welded joint region to the impact of a complex stressed state at simultaneous tension and bending. HAZ metal relief preserves the orientation of pit sequences characteristic for wrought semi-finished products that was acquired during cold rolling. It is the most pronounced in AMg6N alloy with work hardening equal to approximately 20 %.

Lowering of testing temperature changes fracture topography (see Figures 3–5). Increase of the sections

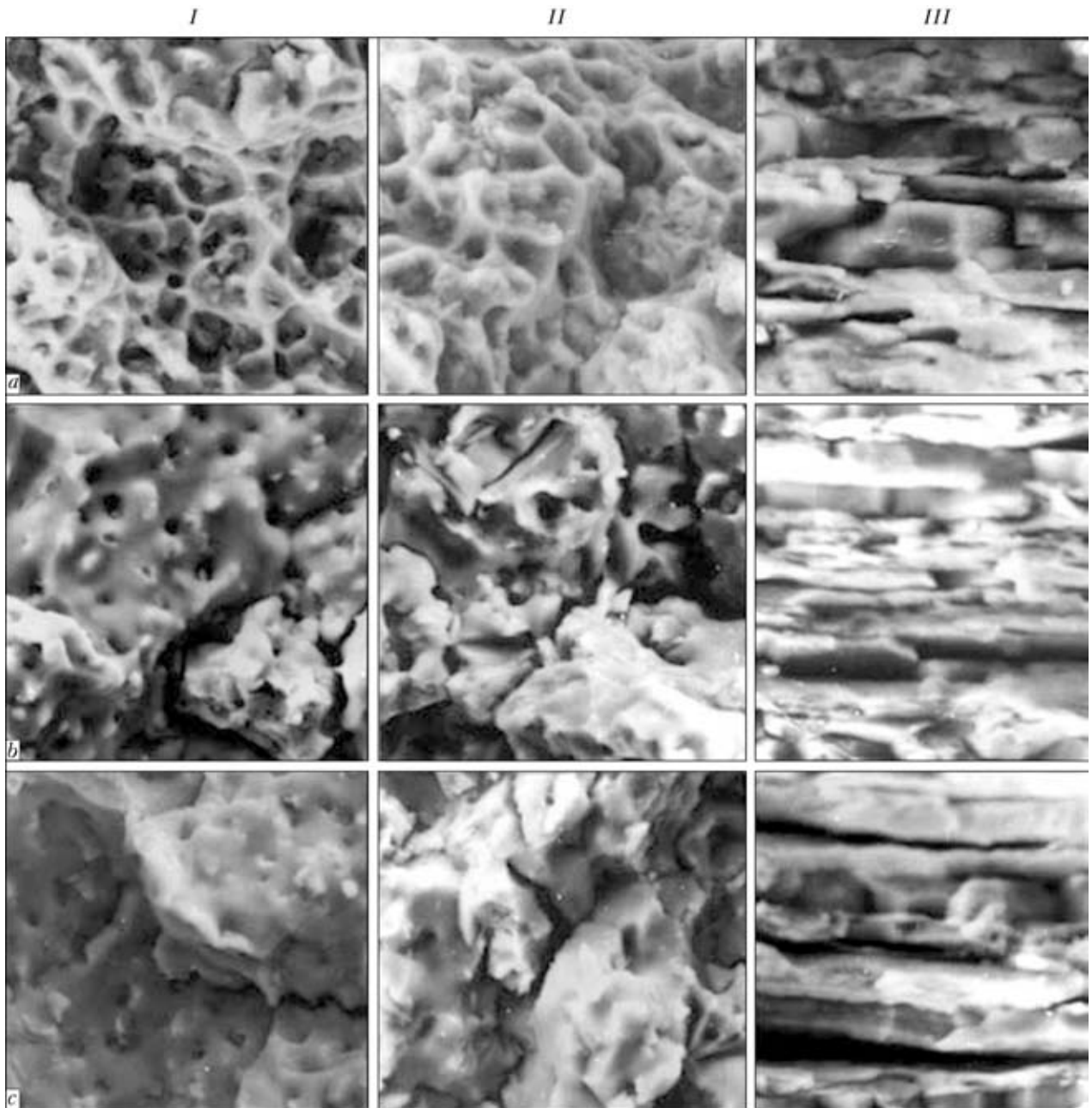


Figure 5. Fractography of fracture surface of individual zones of 1460 alloy welded joint at low testing temperature (*a-c* and *I-III* – see Figure 3)

of intergranular fracture by the tearing mechanism should be regarded as one of the main fractographic indications, even though individual fragments of tough relief are also observed, particularly in AMg6N and 1460 alloys. Further lowering of testing temperature to 20 K causes an increase of the number and extent of sections with microcracks located along grain boundaries, as well as area of fragments with metal delamination. This was less pronounced in fractures of weld metal, where a large number of tough ridges are located around the pits (see Figure 3). Increase of the fraction of intergranular and intercrystalline failures on fractures of welded joints of AMg6N alloy at lowering of testing temperature is accompanied by development of a net of fine and shallow pits that points to a lowering of its fracture resistance. Their

formation can be caused by lowering of cohesion forces of structural components and embrittlement of intermetallic phases [1].

A considerable number of tough fracture regions in fractures of 1201 alloy and its welded joints at all the testing temperatures compared to AMgN and 1460 alloys, determines on the whole its high performance under low temperature conditions (see Figure 4). Weld metal fracture remains tough in the entire temperature range. Fracture mode in HAZ zones is practically identical to that in the base metal. At lowering of testing temperature, however, the fusion zone preserves the tendency to formation of microcracks along the grain boundaries, that is related to the presence of a coarse structural heterogeneity which develops during welding. Non-uniform dimensions of micro-



voids, formed at cracking of coarse phase inclusions, are indicative of their stage-by-stage fracture during matrix deformation up to the moment, when the crack length has reached critical dimensions.

In welded joints of aluminium-lithium alloy 1460 susceptibility to intergranular fracture is manifested at temperatures of 77 and 20 K (see Figure 5). This is related not only to the presence of coarse intermetallic inclusions in the structure, but also to formation of zones free from precipitates on the boundary between solid solution grains, hindering development of plastic deformation of the metal [3]. Their formation is due to alloy composition and welding heating conditions, which promote intensive development of structural heterogeneity by alloying element and impurity content as a result of their segregation along grain boundaries. With increase of volume fraction of such zones in the welded joint structure an increase of stress concentration level is found that is indicated by formation of flat sections of the relief along the boundaries of crystallites and grains on broken sample fractures. On the other hand, no such significant lowering of fracture resistance characteristics values is found in welded joint samples at low temperatures, as is observed in the base metal (see Figure 2). Slant fracture of samples is indicative of shear fracture under the impact of tangential stresses with formation of a tough pit structure. Their small dimensions and presence of cleavage sections decorated by slip lines, point to a local nature of deformation that runs along the slip planes. Increased resistance of metal of 1460 alloy welded joints to crack propagation at low temperature is attributable to presence of copper in its composition, as well as dispersed precipitates of scandium phase, uniformly distributed across all the structural sections of welded joints [3]. Refinement of weld metal structure and absence of recrystallization in the HAZ in welding provide fracture resistance of welded joint metal, despite presence of intergranular fracture regions in the fusion zone (Figure 5). It should be noted that this fact is confirmed by industrial testing of aluminium-lithium alloys of 1460 type and their welded joints. Obtained results enabled application of these alloys in pilot production of welded structures for aerospace engineering [2].

Proceeding from the results of investigations of aluminium alloy welded joints at low temperature, it can be stated that the condition of grain boundaries in structural zones of welded joints on AMg6N, 1201 and 1460 aluminium alloys affects their strength level and fracture mode. Negative impact of welding heating is manifested only in the presence of extended sections with unfavourable structure in the base metal, which form in connection with excess content of alloying elements, impurities and phase clusters located along the rolling line. To prevent structural component embrittlement, it is necessary, using advanced technologies, to strictly specify the content of impurities and volume of welding heat input, when making joints of the above alloys.

CONCLUSIONS

1. Strength σ_t of welded joints of AMg6N, 1201 and 1460 aluminium alloys at uniaxial tension and nominal breaking stress σ_{br} at off-center tension increase by 10–20 % at lowering of testing temperature from 300 to 20 K. AMg6N alloy features a lower susceptibility to low-temperature strengthening. Here, SWCP of welded joints decreases, depending on alloy composition and testing temperature. Crack initiation sites are intermetallic inclusions, particles of secondary phases and phase precipitates, which become brittle at low temperature.

2. Minimum values of fracture resistance properties at all values of testing temperature are characteristic for the zone of weld fusion with base metal, which depends on welded alloy composition. This is due to inhomogeneity of structure, namely difference in particles dimensions and distance between them in this welded joint zone that is expressed in non-uniformity of the depth and dimensions of tough pits on fracture surface.

3. It is established that crack propagation in welded joints of aluminium alloys AMg6N, 1201 and 1460 at room temperature runs by the mechanism of initiation, growth and coalescence of microvoids, characteristic for ductile materials. Lowering of testing temperature to 20 K leads to a change of fracture mechanism from the tough to quasi-tough. Here, an increase of the number and extent of regions with microcracks and fragments of structure delamination along the grain boundaries formed by the tearing mechanism is found on the fracture surface. This was manifested to a smaller degree on weld metal fractures, where a considerable number of tough ridges are located around the pits.

4. It is rational to apply welded joints of AMg6N alloy containing magnesium in structures operating in the temperature range of 300–77 K. High strength and low susceptibility to brittle fracture in the fusion zone of welded joints of 1201 and 1460 alloys containing copper, allows these materials to be applied in cryogenic engineering structures.

- (1967) *Aluminium alloys at low temperatures*. Ed. by I.N. Fridlyander. Moscow: Metallurgiya.
- Ishchenko, A.Ya., Labur, T.M., Bernadsky, V.N. et al. (2006) *Aluminium and its alloys in current welded structures*. Kiev: Ekotekhnologiya.
- Krivov, G.A., Ryabov, V.R., Ishchenko, A.Ya. et al. (1998) *Welding in aircraft construction*. Ed. by B.E. Paton. Kiev: MIITsV.
- Labur, T.M., Ishchenko, A.Ya., Taranova, T.G. et al. (2005) Features of crack initiation and propagation under the conditions of off-center tension of Al–Li alloy 1441 welded joints. *The Paton Welding J.*, **11**, 6–10.
- Gordeeva, T.A., Zhegina, I.P. (1978) *Analysis of fractures in evaluation of material reliability*. Moscow: Mashinostroenie.
- Ivanova, V.S., Kudryashov, V.G., Shtovba, Yu.K. et al. (1974) Fractography and fracture toughness of aluminium and titanium alloys. *Tekhnologiya Lyog. Splavov*, **3**, 65–70.
- (1982) *Fractography and atlas of fractograms*: Refer. Book. Moscow: Metallurgiya.
- Rabkin, D.M., Lozovskaya, A.V., Sklabinskaya, I.E. (1992) *Metals science of welding of aluminium and its alloys*. Kiev: Naukova Dumka.
- Solntsev, Yu.P., Stepanov, G.A. (1985) *Structural steels and alloys for low temperatures*. Moscow: Metallurgiya.
- (1990) *Structural levels of plastic deformation and fracture*. Ed. by V.E. Panin. Novosibirsk: Nauka.
- Vladimirov, V.I. (1984) *Physical nature of metal fracture*. Moscow: Metallurgiya.



OPTIMISATION OF THE PROCESS OF STRENGTHENING OF WELDED JOINTS OF 09G2S STEEL BY HIGH-FREQUENCY MECHANICAL PEENING

V.V. KNYSH, S.A. SOLOVEJ and I.L. BOGAJCHUK
E.O. Paton Electric Welding Institute, NASU, Kiev, Ukraine

Based on investigation of the depth of plastically deformed metal layer after application of high-frequency mechanical peening, optimum parameters for strengthening low-alloyed steels were established, which enable plastic deformation of metal to the depth of down to 1 mm.

Keywords: *strengthening of welded joints, high-frequency mechanical peening, plastically deformed metal layer, micro-hardness, optimization*

Owing to its advantages, high-frequency mechanical peening (HFMP) or ultrasonic impact treatment is an advanced method of surface plastic deformation of metal that is finding ever wider application to increase fracture resistance of welded joints [1–9]. Starting from 1959, when the energy of ultrasonic oscillations was used for the first time for redistribution of residual stresses in welded joints [10], strengthening treatments with application of ultrasonic energy became successfully applied in improvement of service properties of welded joints in various metal structures. In a considerable part of publications special attention was given to effectiveness of HFMP technology application for improvement of cyclic fatigue life of welded joints, but, as a rule, without consideration of the issues of establishment of optimum strengthening parameters [11]. The main controllable technological parameters at strengthening by HFMP technology include oscillation amplitude of end face of waveguide of manual impact tool, ultrasonic generator frequency, diameter of strikers of replaceable working heads, linear speed of HFMP performance and force of impact tool pressing down. It should be noted that HFMP equipment was continuously improved, developing from stationary equipment with consumed power of 13 kW into compact and mobile one with consumed power of 300–500 W. In this connection, the issue of determination of optimum strengthening parameters should be solved, depending on applied equipment, pursued goals and solved tasks.

In order to improve fatigue resistance of welded joints, HFMP technology is used to treat a narrow zone of transition of weld to base metal that results in formation of a characteristic groove, under which a work-hardened (plastically deformed) metal layer is located. Achievement of maximum depth of plastically deformed metal layer under the groove bottom

as a result of HFMP can be the main criterion of establishment of optimum strengthening parameters.

The purpose of this work was establishing the optimum parameters of strengthening of welded joints on 09G2S steel in order to improve their fatigue resistance. Here ultrasonic equipment with piezoelectric transducer USP-300 of 300 W power batch-produced by «Ultramet» Company (Ukraine) was used. Experimental studies of the depth of plastically deformed metal layer were conducted on samples from low-alloyed steel 09G2S widely applied in welded metal structures.

Starting from 1970s, practically all HFMP equipment (including USP) has been made with an intermediate impact element. Therefore, as shown in works [12, 13], with such a schematic of HFMP realization the force of impact tool pressing down to the surface being treated should be equal to about 50 N. Here, the change of pressing-down force from 30–80 N does not affect treatment efficiency, i.e. we will consider this technological parameter established.

Oscillation amplitude of the end face of manual impact tool waveguide and ultrasonic generator frequency in USP-300 equipment have constant values and are equal to 30 μm and 22 kHz, respectively. Thus, the main technological parameters that may be varied in this equipment, are diameter of strikers of replaceable working heads and linear speed of HFMP performance. Therefore, in this work the influence of these parameters on the depth of plastically deformed metal layer under the groove bottom was studied, which was determined by microhardness measurements. This is the simplest and most widely applied method to assess the depth of work-hardened metal layer [13, 14].

Depth of plastically deformed metal layer and characteristic groove after HFMP were determined by the following procedure. Three blanks of 110 \times 80 mm size were cut out of the rolled sheet 30 mm thick. Finishing was performed around the blank contour with subsequent grinding of the blank working surface from two sides and annealing. HFMP of the working surface of made samples of 100 \times 70 mm size



was conducted along three lines with 25 mm spacing (Figure 1). The first sample was strengthened using a replaceable single-row four-striker head with 2 mm diameter of cylindrical strikers, the second sample was strengthened with a single-row four-striker head with 3 mm cylindrical strikers, and the third sample was strengthened with a single-row three-striker head with 4 mm cylindrical strikers. HFMP treatment of each sample was performed in four passes by reciprocal motions of manual impact tool, but at three different peening speeds (1, 5 and 10 mm/s). At determination of peening speed, peening time was selected equal to the total treatment time of sample surface along a 100 mm line in four passes of the work tool of 100, 20 and 10 s, respectively. As a result, three grooves formed on the sample surface, corresponding to the preset constant speeds of tool displacement. A clock-type indicator was used to measure the groove depth, depending on striker diameter and linear speed of HFMP performance. From Table 1, presenting measurement results, one can see that the depth of characteristic groove after peening essentially depends on the speed of HFMP performance. Maximum groove depth (0.14 mm) is achieved at surface treatment with single-row four-striker head with 3 mm cylindrical strikers and 1 mm/s speed of HFMP performance. In [15] it is shown that there exists a satisfactory correlation between the groove depth and fatigue life of welded joints, while provision of the required groove depth can be the criterion of treatment quality.

In order to study the depth of plastically deformed layer by microhardness measurement method transverse sections were prepared by cutting samples into 12 parts by the schematic given in Figure 1. To eliminate the influence of edge effects one-sided transverse microsections were prepared from the six extreme parts (see Figure 1, 1–3, 10–12), and two-sided microsections — from the remaining six parts (see Figure 1, 4–9). Thus, there were 6 points on 12 parts of the sample for measurement of microhardness characteristic for this striker diameter (2, 3 or 4 mm) at the set speed of HFMP performance (1, 5 or 10 mm/s). Microhardness on the surface of transverse sections was measured normal to peening direction in-depth of base metal, starting from the surface layer of groove bottom and up to stabilization of microhardness characteristic. LECO M-400 was used as measuring instrument, the principle of operation of which

Table 1. Groove depth (mm) depending on striker diameter and HFMP linear speed

Striker diameter, mm	Linear speed of HFMP, mm/s		
	1	5	10
2	0.11	0.07	0.05
3	0.14	0.11	0.04
4	0.09	0.07	0.05

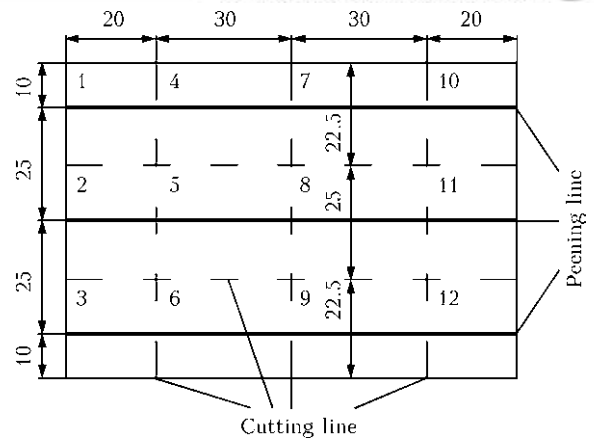


Figure 1. Schematic of sample cutting up after HFMP

is based on pressing in a diamond indenter with 0.1 N force. Measurement step here was 50 μm near the surface and 100 μm farther from it. Obtained results were averaged by six measurement values (see Figure 2). Note that at such a small force on the indenter the applied method becomes sensitive not only to metal strengthening due to the usually observed at HFMP increase of dislocation density and their redistribution

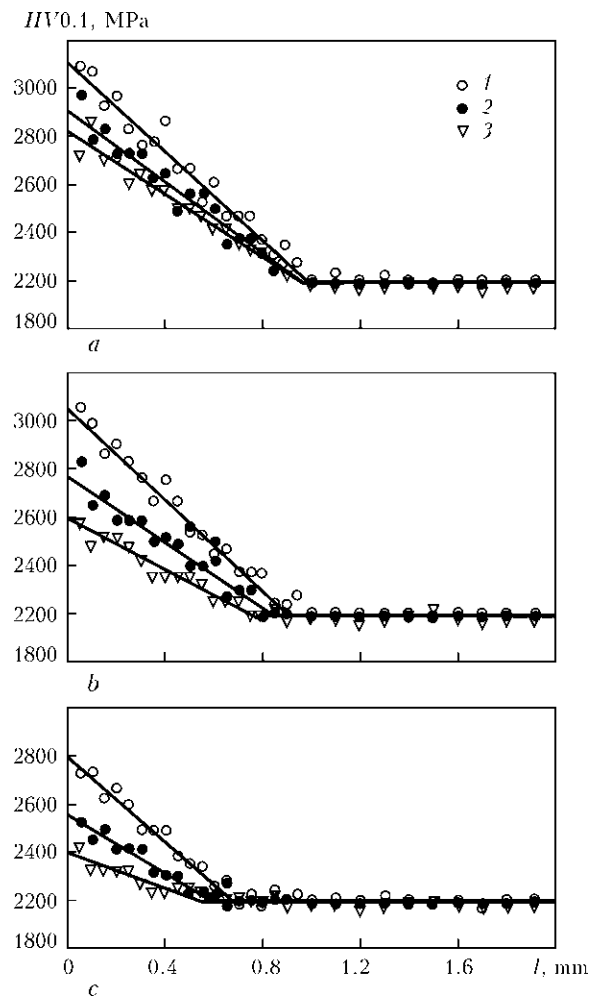


Figure 2. Dependence of hardness of subsurface metal layer strengthened by HFMP using single-row head with diameter of cylindrical strikers of 2 (a), 3 (b) and 4 (c) mm on distance from groove bottom *l* in-depth of the metal at speed of HFMP performance of 1 (1), 5 (2) and 10/s (3) mm



inside the grains (formation of subgrain boundaries and cell boundaries) [16, 17], but also to an increase of the level of residual compressive macrostresses [16, 18].

As is seen from Figure 2, at strengthening of samples of 09G2S steel by HFMP technology the maximum depth of plastically deformed layer (approximately 1 mm) is achieved when using single-row four-striker head with 2 mm diameter of cylindrical strikers. At strengthening by HFMP technology, using single-row four-striker head with 3 mm cylindrical strikers, maximum depth of plastically deformed layer decreases to about 0.8 mm, and when single-row three-striker head with 4 mm cylindrical strikers is used, it is about 0.6 mm. For the considered range of speeds of HFMP performance, the depth of plastically deformed layer is determined, mainly, by diameter of striker pins (by impact force in the contact zone), as well as tool displacement speed, as change of work-hardened layer depth for one striker diameter, depending on tool displacement speed, does not exceed 0.1 mm. Hardness of plastically deformed layer of metal depends both on striker diameter, and on peening speed. At treatment at the considered speeds by 2 mm strikers the hardness of surface-deformed layer of metal directly under the groove is 1.3–1.4 times higher than base metal hardness, for 3 mm strikers it is 1.2–1.35 times, and for 4 mm strikers is 1.1–1.25 times. For all the samples a lowering of hardness is observed when moving away from the surface into the metal depth. Here, hardness decreases with increase

of the speed of HFMP performance. As the depth of plastically deformed metal layers (1.0 and 0.9 mm) and their maximum hardness values ($HV0.1-3100$ and $HV0.1-3050$ MPa) practically do not differ, when using replaceable single-row four-striker heads with 2 and 3 mm striker diameter at low peening speeds (1 mm/s), cylindrical strikers of 3 mm diameter are the most advantageous in terms of technology from the view point of lowering of stress concentration factor, and provide the greatest groove depth (0.14 mm). Therefore, the optimum parameters at treatment of 09G2S steel welded joints by HFMP technology are 3 mm diameter of strikers of replaceable working heads and linear speed of HFMP performance of about 60 mm/min. Despite the fact that technological parameters of strengthening by high-frequency peening are established for low-alloyed steel 09G2S, they can be taken as the optimum ones for most of the low-alloyed steels, as the latter have close mechanical properties.

Metallographic investigations of metal grain structure in the peening zone were also conducted to establish the nature of grain transformation as a result of strengthening by HFMP technology on transverse microsections of samples from 09G2S base metal, earlier used to determine the depth of plastically deformed metal layer by microhardness method after strengthening by HFMP technology at the speed of 1, 5 or 10 mm/s, using single-row four-striker heads with 3 mm strikers. «Neophot-32» microscope was

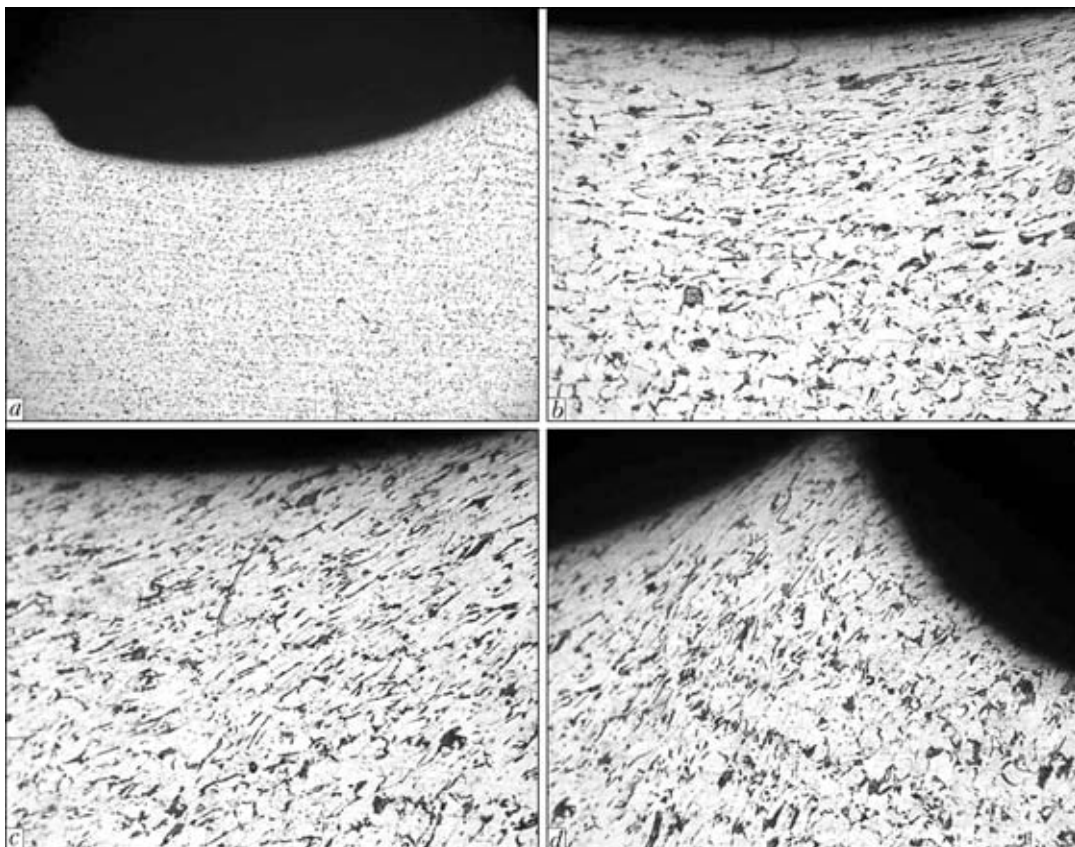


Figure 3. Microstructures of groove zones: a – $\times 50$; b–d – $\times 200$ (for descriptions see the text)



Table 2. Degree of grain deformation in subsurface metal layer strengthened by HFMP using a single-row head with 3 mm striker diameter

HFMP speed, mm/s	Studied region	$K_{f_{av}}$	δ , mm
1	1	11.80	200
	2	6.10	500
	3	3.61	600
5	1	8.50	125
	2	6.50	150
	3	2.94	245
10	1	No intensive deformation of grains was found	
	2		
	3		

used for analysis. Change of structure of low-alloyed 09G2S steel as a result of HFMP was studied at different magnifications (Figure 3).

General view of the groove zone is given in Figure 3, *a*. Subsurface zone with structural changes can be conditionally subdivided into three regions. In the first zone (Figure 3, *b*) deformed ferrite grains are located practically parallel to the tangent to groove bottom, and to sample surface, respectively. Pearlite component of the structure is also elongated. Moving away from the groove bottom to the edge, a certain change of grain shape and dimensions (second region) is found. In this region (Figure 3, *c*) grains are located at an angle to sample surface, but remain parallel to the tangent to groove surface. On the boundary with base metal not subjected to HFMP (third region), isolated deformed grains are observed, located practically normal to sample surface (Figure 3, *d*). Thus, intensive plastic deformation, leading to a change of grain shape, runs through grain elongation in the direction normal to the groove, which is formed by the surface of a sphere of cylindrical striker end face. Such grain behaviour in the surface layers of Armco-iron was reported by the authors of [19], where at compression in the ultrasonic field an essential elongation of grains is observed in the direction parallel to the treated surface. Results of analysis of grain shape change at intensive deformation induced in the subsurface layer by HFMP technology are presented in Table 2. Obtained data show that grain form factor $K_{f_{av}}$ (characterizing the degree of ferrite grain deformation) and depth of propagation of grains, which have changed their shape δ , depend on the speed of HFMP performance. At low peening speeds $K_{f_{av}}$ and δ values are maximum. In [20] parameter γ is used to determine the actual deformation of surface layer e at attrition, which is similar to grain form factor $K_{f_{av}} \cdot \sqrt{3}e = \gamma = a/b$, where a , b are the elongated grain length and width, respectively. It is shown that grain shape change is caused by intensive deformations of

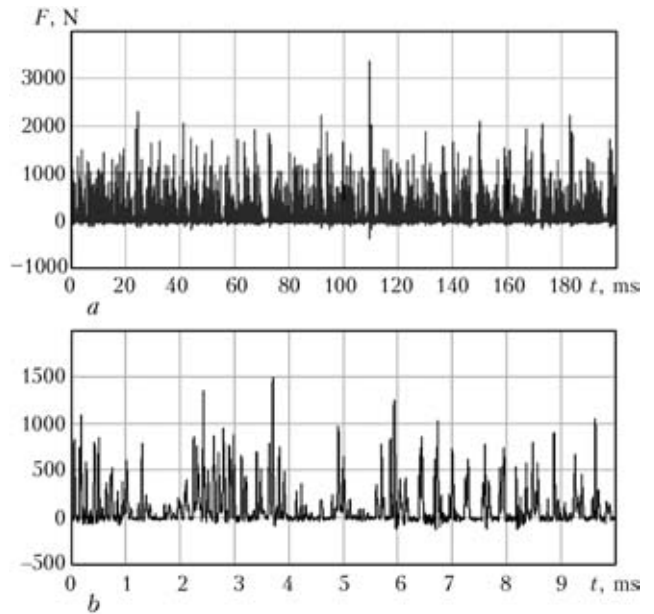


Figure 4. Oscillograms of impact force of 3 mm striker, when using USP-300 equipment, recorded in 200 ms (*a*) and with a scan of first 10 ms (*b*)

the order of $e \geq 1$. Lower degrees of deformation do not lead to grain shape change, but cause accumulation and redistribution of dislocations inside grains.

In our case, the size of the zone with significant changes of grain shape under the groove (zone with a high degree of deformation $e > 1$) is limited by 200 μm , whereas the zone of plastically deformed metal layer, according to microhardness measurements, is equal to 1 mm. The high level of residual compressive stresses forming during deformation at HFMP [16, 18, 21], which have some influence on microhardness value, should be also taken into account.

A piezoceramic transducer and high-resolution oscillograph were used to record also the oscillogram of the force of impact of 3 mm striker on the surface during HFMP performance (Figure 4). As is seen from Figure 4, *a*, application of the load during treatment is performed by blocks of pulses of different width with maximum values of impact force in the block, exceeding 1000 N. Here, duration of force impact pulses is not longer than 100 μs (Figure 4, *b*). Frequency of appearance of pulses above 1000 N is equal to approximately 1 kHz. In individual blocks the impact force is higher than 2000 N, whereas the maximum fixed value of impact force in 200 ms was equal to 3400 N.

CONCLUSIONS

1. Based on investigation of the depth of plastically deformed metal layer after application of HFMP by batch-produced equipment of 300 W power, the following optimum parameters for strengthening low-alloyed steels were established: 3 mm striker diameter and 1 mm/s linear speed of HFMP performance.

2. Performance of HFMP technology at the established optimum parameters allows plastic deformation



of metal to the depth of down to 1 mm with formation of a characteristic groove of down to 0.14 mm depth. The size of the zone under the groove with considerable changes of grain shape (grain form factor $K_{fv} = 11.8$) is equal to 200 μm .

3. At HFMP treatment of metal surface the load is applied by blocks of pulses of different width with maximum value of impact force in the block higher than 1000 N. Duration of such pulses of force impact does not exceed 100 μs , and frequency of their appearance is equal to approximately 1 kHz.

- Zhao, X., Wang, D., Huo, L. (2011) Analysis of the S-N curves of welded joints enhanced by ultrasonic peening treatment. *Materials & Design*, 32(1), 88–96.
- Abston, S. (2010) The technology and applications of ultrasonic impact technology. *Austral. Welding J.*, 55, 20–21.
- Yin, D., Wang, D., Jing, H. et al. (2010) The effects of ultrasonic peening treatment on the ultra-long life fatigue behavior of welded joints. *Materials & Design*, 31(7), 3299–3307.
- Marquis, G. (2010) Failure modes and fatigue strength of improved HSS welds. *Eng. Fract. Mech.*, 77, 2051–2062.
- Wang, T., Wang, D., Huo, L. et al. (2009) Discussion on fatigue design of welded joints enhanced by ultrasonic peening treatment (UPT). *Int. J. Fatigue*, 31(4), 644–650.
- Kudryavtsev, Y., Kleiman, J., Lugovskoy, A. et al. (2007) Rehabilitation and repair of welded elements and structures by ultrasonic peening. *Welding in the World*, 51(7/8), 47–53.
- Kuhlmann, U., Duerr, A., Guenther, P. et al. (2005) Verlängerung der Lebensdauer von Schweisskonstruktion aus hoherfesten Baustählen durch Anwendung der UIT-Technologie. *Schweißen und Schneiden*, 57(8), 384–391.
- Huo, L., Wang, D., Zhang, Y. (2005) Investigation of the fatigue behaviour of the welded joints treated by TIG dressing and ultrasonic peening under variable-amplitude load. *Int. J. Fatigue*, 27(1), 95–101.
- Statnikov, E.S., Muktepavel, V.O., Blomqvist, A. (2002) Comparison of ultrasonic impact treatment (UIT) and other fatigue life improvement methods. *Welding in the World*, 46(3/4), 20–32.
- Mordvintseva, A.V. (1959) Ultrasonic impact treatment of welded joints for removal of residual stresses. *Trudy MVTU im. N.E. Bauman*, Issue 45, 32–43.
- Lobanov, L.M., Kirian, V.I., Knys, V.V. (2006) Improvement of fatigue resistance of welded joints in metal structures by high-frequency mechanical peening (Review). *The Paton Welding J.*, 9, 2–8.
- Prokopenko, G.I., Nedoseka, A.Ya., Gruz, A.A. et al. (1995) Development and optimization of equipment and process of ultrasonic peening of welded joints for relaxation of residual stresses. *Tekhnich. Diagnostika i Nerazrush. Kontrol*, 3, 14–22.
- Kravtsov, T.G., Sevryukov, V.V. (2001) *Ultrasonic peening of ship parts and welded structures*. Nikolaev: UGMTU.
- Nekhoroshev, O.N., Pershin, V.P., Semukhin, B.S. (2006) Application of ultrasonic peening method on welded joints of structural steels. *Vestnik TGA-SU*, 2, 120–125.
- Degtyaryov, V.A., Shulginov, B.S., Knys, V.V. (2009) Deformation criterion of the efficiency of strengthening of welded joints by high-frequency mechanical peening. *The Paton Welding J.*, 10, 39–41.
- Mordyuk, B.N., Milman, Yu.V., Iefimov, M.O. et al. (2008) Characterization of ultrasonically peened and laser-shock peened surface layers of AISI-321 stainless steel. *Surface and Coating Technology*, 202, 4875–4883.
- Volosevich, P.Yu., Prokopenko, G.I., Knys, V.V. et al. (2008) Structural changes in weld zone of St3 steel in ultrasonic peening and their influence on improvement of fatigue resistance. *Metallofizika i Nov. Tekhnologii*, 30(10), 1429–1443.
- Mordyuk, B.N., Prokopenko, G.I. (2007) Ultrasonic impact peening for surface properties' management. *J. Sound and Vibrations*, 308(3/5), 855–866.
- Volosevich, P.Yu., Kozlov, A.V., Mordyuk, B.N. et al. (2003) Plastic deformation in ultrasonic field and its possibilities as applied to carbon saturation of surface layers of iron specimens. *Metallofizika i Nov. Tekhnologii*, 25(5), 679–692.
- Yurkova, A.I., Belotsky, A.V., Byakova, A.V. et al. (2007) Mechanism of iron dispersion in intensive plastic deformation by friction with simultaneous nitrogen diffusion. *Nanosistemy, Nanomaterialy, Nanotekhnologii*, 5(2), 565–588.
- Mordyuk, B.N., Prokopenko, G.I. (2006) Fatigue life improvement of α -titanium by novel ultrasonically assisted technique. *Materials Sci. and Eng.*, 437, 396–405.

SIMULATION OF THE EFFECT OF HIGH-VOLTAGE CABLES ON CURRENT RIPPLE IN WELDING GUNS WITH AUTOMATIC BIAS

O.K. NAZARENKO, V.A. MATVEJCHUK and V.V. GALUSHKA

E.O. Paton Electric Welding Institute, NASU, Kiev, Ukraine

The mechanism of formation of current ripple in welding electron guns with automatic bias caused by ripple of the cathode bombardment current is studied by using computer mathematical simulation. It is shown that when using the coaxial high-voltage cable the ripple of the cathode bombardment current does not affect the ripple of the beam current. In case of a multi-core cable or four separate single-core high-voltage cables the ripple of the cathode bombardment current causes the ripple of the beam current because of the parasitic capacitance currents flowing through the beam current control circuit. To decrease the beam current ripple factor to 0.05, the cathode bombardment current ripple factor at a frequency of 20 kHz should not exceed 0.05 either.

Keywords: electron beam welding, high-voltage cable, distributed capacitances, electron gun, triode emission system, automatic bias, cathode bombardment current ripple, beam current ripple

Despite the high-usage pulse modulation of the electron beam current with a depth of 100 %, it is impor-

tant that in the steady-state operation mode the peak-to-peak amplitude of the beam current ripple be no more than 5 % (ripple factor 0.05), which is specified by international standard EN ISO 14744-1 [1]. This requirement is caused, in particular, by the need to

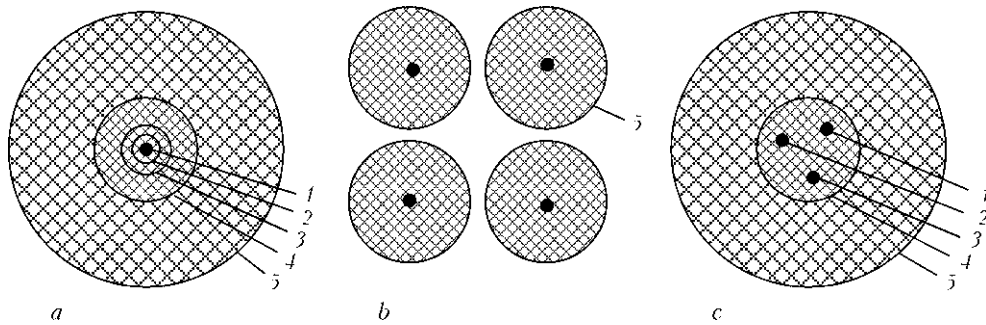


Figure 1. High-voltage cables used in welding guns with cathodes heated by electron bombardment and their parasitic capacitances C_p : *a* – coaxial cable, $C_{p(1-2)} = 300$, $C_{p(2-3)} = 400$, $C_{p(3-4)} = 500$, $C_{p(4-5)} = 100$ pF/m; *b* – four separate single-core cables, $C_p = 70$ pF/m; *c* – multi-core cable with conductors in current-conducting screen 4 used as a current conductor to the modulator, $C_{p(1-2)} = 150$, $C_{p(2-3)} = 70$, $C_{p(1, 2-4)} = 210$, $C_{p(3-4)} = 70$, $C_{p(4-5)} = 130$ pF/m; 1, 2 – current conductors to heater spiral; 3 – current conductor to cathode; 5 – external grounded screen

ensure a high consistency of the non-through penetration depth in heavy metal sections.

In the majority of cases the high-power (60–120 kW) welding electron guns use massive cathodes heated by electron bombardment, and the most efficient control of the beam current is provided by automatic bias [2], where an electronic valve with grid control is connected to the emission system cathode circuit [3]. In this case, minus of the accelerating voltage source is connected to the modulator (control electrode) of the emission system of the gun.

In the former USSR the guns of this type were equipped with coaxial high-voltage four-core cables of the 4KVEL-60 or 4KVEL-165 grades, and there were no problems with the welding current ripple. But now, because the coaxial cables with the required electric strength between the cores are no longer produced, the use is made of four separate cables (Techmeta, France) or multi-core cables (E.O. Paton Electric Welding Institute). With these cables it is necessary to thoroughly filter the cathode bombardment current to avoid ripple of the welding current, which involves some difficulties associated with placement and reliability of electronic elements at a high potential in oil bath. The bombardment current usually amounts to 100 mA at a voltage of 1.5–5.0 kV. When changing from mains power supply to a supply with a frequency of 20–50 kHz, the effect of ripple of the cathode bombardment current becomes much more pronounced. For example, other conditions being equal, the beam current ripple factor in case of using the bombardment current source with a ripple frequency of 100 Hz is approximately 30 times lower compared to the bombardment current source with a ripple frequency of 20 kHz. The final causes of ripple of the welding electron beam current in the guns considered may be ripples of the accelerating voltage and potential of the modulator (control electrode) of the emission system. As according to the requirements of international standard EN ISO 14744-1 the mean level of the accelerating voltage ripple should not exceed 2% (in practice it is lower by an order of magnitude), allowing for dependence $I_b \sim U_{acc}^{3/2}$ the value of the beam current ripple for the above reasons should be

not higher than 3%. Apparently, in case of a higher beam current ripple its cause should be looked for in the modulator potential ripple.

Previously, the issues of using different high-voltage cables and associated beam current ripples were not discussed in the technical literature. That gave rise to conducting investigations the results of which are considered below.

Investigation procedure and objects. The high-voltage cables under investigation are shown in Figure 1. When changing from the coaxial cable to other types, we noticed formation of the beam current ripple, which disappeared immediately after a sudden shutdown of the cathode bombardment current (Figure 2). As the cathode cooled down, the beam current gradually fell to zero without any ripple. This result explicitly confirms the fact that the beam current ripple is caused by the cathode bombardment current ripple, but it gives no understanding of the mechanism of this effect and does not allow it to be quantitatively estimated.

Therefore, we used computer mathematical simulation of the beam current control circuits with three types of the high-voltage cables, each 10 m long. Graphic windows of the computer mathematical simulator [4] are shown in Figure 3. They are made so that it is possible to reveal quantitative relationships and main ways of flowing of an alternating component of the cathode bombardment current through parasitic capacitances of a cable. The bombardment voltage source is shown here in the form of two series-connected sources: direct voltage source $V2 = 1500$ V and alternating voltage source $V3 = 1.5-150$ V with a frequency ranging from 50 Hz to 50 kHz, which is used to set the ripple factor within the range of interest, i.e. 0.005–0.1. The vacuum diode (heater cathode) is represented by resistor $R2 = 20$ kOhm = $U_{bomb}/I_{bomb} = 1500$ V/0.075 A, which is justified by constancy of the given load. Models of the welding gun and valve GMI-27 were made on the basis of study [5]. Model X5 of welding gun ELA-60-60 corresponds to its modulation characteristic (Figure 4, *a*), and valve model X6 – to the anode characteristic of electronic valve GMI-27 (Figure 4, *b*).

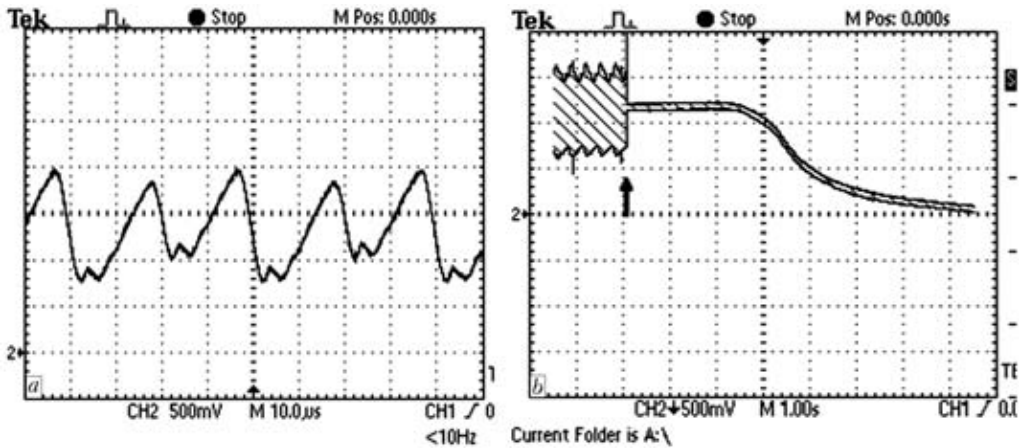


Figure 2. Oscilloscope of the beam current ripple (a) (time axis scale — one cell = 10 μs) and its termination (b) (one cell = 1 s) from the time point of shutoff of the bombardment current when using the multi-core cable. Frequency and ripple factor 50 kHz and 0.28, respectively; time point of shutoff of the bombardment current is marked by an arrow; beam current 12.5 mA; bombardment current 60 mA; bombardment voltage 1.5 kV; oscilloscope Tektronix TDS-2002

Results and discussions. In case of using the coaxial cable (see Figure 3, a) the alternating component of the bombardment current is closed by the filament-cathode circuit and parasitic capacitance C2, thus exerting no effect on the cathode-modulator potential difference and, hence, beam current ripple. Therefore, in this case there is no need to place the ripple filter at output of the cathode bombardment current source. It is enough just to rectify the bombardment current, as at a frequency of 20–50 kHz the losses in the cable are inadmissibly high. In case of four separate cables (see Figure 3, b) the alternating component of the cathode bombardment current is closed both by the filament-cathode circuit and by the accelerating voltage source-ground- parasitic capacitances C1 and C2

circuit shown by the dashed line, where the alternating voltage drop is formed at parallel-connected valve X6 and resistor R5. The latter causes the corresponding beam current ripple. When using the multi-core cable (see Figure 3, c), the alternating component of the cathode bombardment current also causes the alternating voltage drop at parallel-connected electronic valve X6 and resistor R5, as there is the circuit of closing of the alternating component of the cathode bombardment current through parasitic capacitances C2–C4.

Figure 5, a, b shows results of computer simulation of the effect of the beam current on the amplitude of the control voltage and beam current ripples for the same cables at three different bombardment current

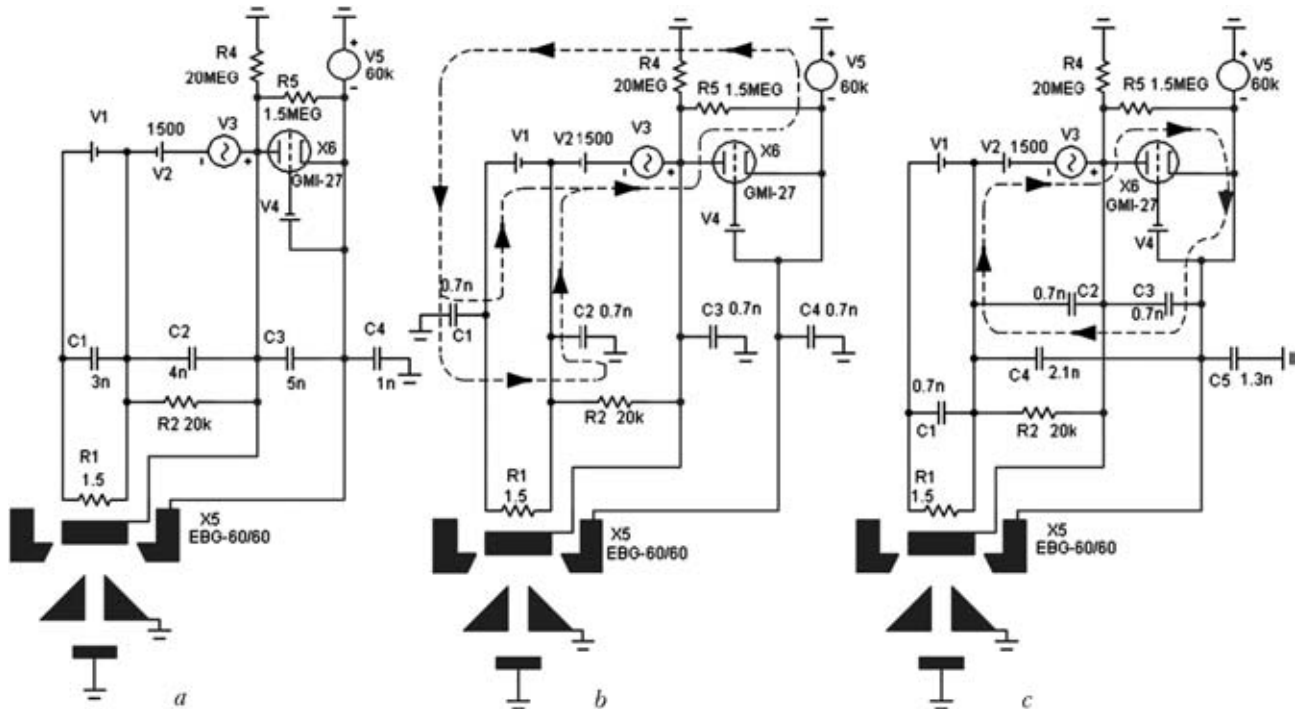


Figure 3. Graphic windows of the computer mathematical simulator of beam current control circuits for coaxial cable (a), four separate cables (b) and multi-core cable (c): V1 — heat source for spiral; V2 — source of direct bombardment voltage; V3 — source of alternating voltage; V4 — source of bias voltage; V5 — stabilised source of accelerating voltage; X5 — model of 60 kV and 60 kW welding gun; X6 — simplified model of tetrode GMI-27

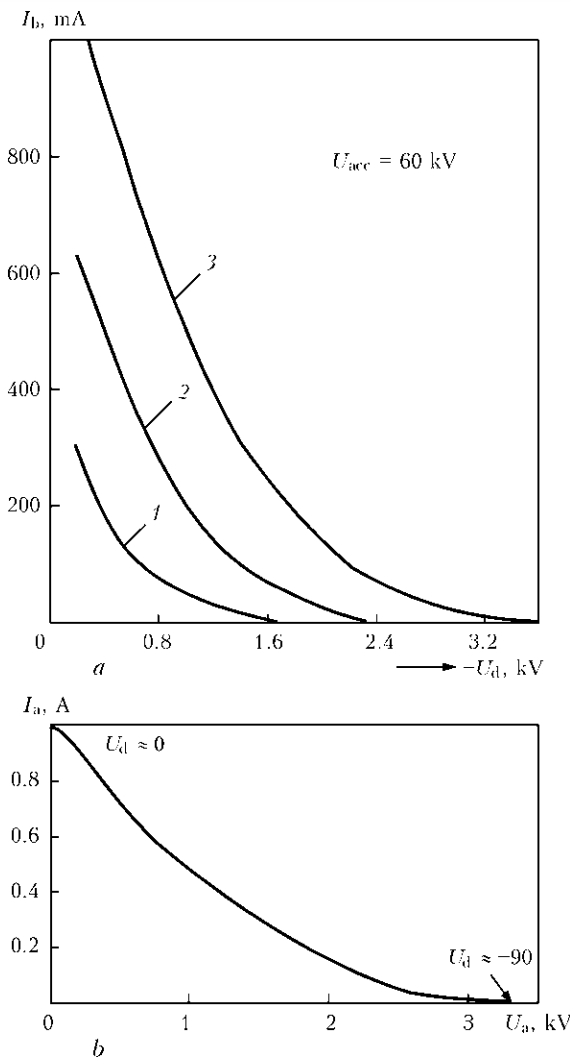


Figure 4. Modulation characteristics of the emission systems forming the beams with currents of 250 (1), 500 (2) and 1000 (3) mA (a), and certificate anode characteristic of valve GMI-27 (b)

ripple factors. The character of dependencies and, hence, the mechanism of formation of the beam current ripple are identical for both types of the cables, although when using four separate cables the ripple is a bit lower.

As follows from the simulation results, the effect of the bombardment current ripple increases with decrease of the beam current, and at a beam current of 1 mA and cathode bombardment current ripple of 10 % the amplitude of the beam current ripple with a frequency of 20 kHz becomes close to 100 %, which makes functioning of the secondary-electron observation and seam tracking systems impossible. Also, as shown by the above results, to decrease the beam current ripple factor to 0.05 (the maximum permissible value specified by international standard EN ISO 14744-1) it is necessary to limit the cathode bombardment ripple factor formed by the power source at a frequency of 20 kHz to the same value. Connecting an extra capacitance to the circuit between the cathode and modu-

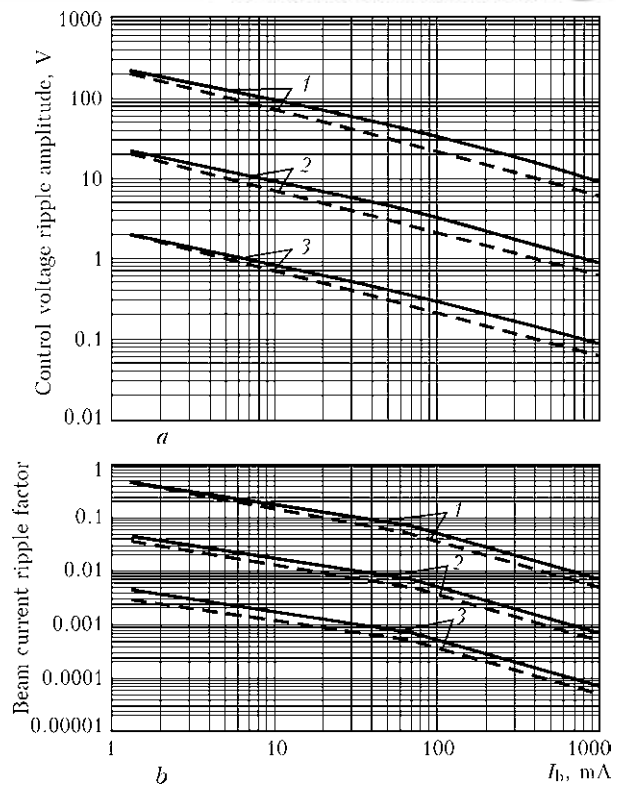


Figure 5. Dependence of the control voltage ripple amplitude (a) and beam current ripple factor (b) on the beam current when using four separate cables (dashed lines) and multi-core cable (solid lines); bombardment current ripple factor 0.1 (1), 0.05 (2) and 0.005 (3); cathode bombardment current ripple frequency 20 kHz

lator provides an efficient decrease of the beam current ripple amplitude, although it deteriorates, accordingly, the dynamic characteristics of the beam current control system.

CONCLUSIONS

1. The cathode bombardment current ripple exerts a substantial effect on the beam current ripple in case of using the multi-core cable or four separate cables, which is caused by parasitic capacitance currents flowing through the beam current control circuit.

2. When using these cables, to decrease the beam current ripple factor to 0.05, which is the maximum permissible value specified by international standard EN ISO 14744-1, it is necessary to limit the cathode bombardment ripple factor at a frequency of 20 kHz to the 0.05 value.

1. ISO 14744-1: Welding — acceptance inspection of electron beam welding machines. Pt 1: Principles and acceptance conditions.
2. Rolf, M. *Strahlstromsteuerung fuer eine Elektronenstrahlschweissmaschine*. Pat. 24 60 424 Deutsche. Int. Cl. H 01 J 37/24. Publ. March 17, 1977.
3. Nazarenko, O.K., Lanbin, V.S. (2007) Investigation of high-voltage control circuits of welding electron beam current. *The Paton Welding J.*, **5**, 17–20.
4. Amelina, M.A., Amelin, S.A. (2007) *Circuit simulation software Micro-Cap 8*. Moscow: Gor. Liniya Telekom.
5. Koren, N. (1996) Improved vacuum-tube models for SPICE simulation. *Glass Audio*, **8**(5).



PECULIARITIES OF RESISTANCE WELDING OF COPPER WITH ALUMINIUM ALLOYS USING NANOSTRUCTURED FOIL OF Al-Cu SYSTEM

V.S. KUCHUK-YATSENKO

E.O. Paton Electric Welding Institute, NASU, Kiev, Ukraine

Peculiarities of formation of welded joints of AD1 aluminium alloy with M1 copper using nanostructured foil of Al-Cu system as an insert are considered. Microstructure and chemical heterogeneity of welded joint metal were studied and mechanical rupture testing of welded joints was performed.

Keywords: resistance butt welding, nanostructured foil, eutectics, microstructure, intermetallics

Welding of aluminium with copper is applied in industry for manufacture of current conducting elements and units of electric machines, transformers, current conductors, busbars, power-consuming machines, chemical vessels and other products. The main problem in producing welded joints is formation of intermetallics of Al-Cu system in a weld which have con-high hardness and brittleness, thus significantly deteriorating mechanical and electric characteristics of the products. The negative influence of intermetallics is especially noticeable if thickness of their layer is more than 7–8 μm [1]. To decrease the thickness of layer of intermetallics one should minimize the time-temperature parameters of welding process and provide more concentrated heating.

In the present work the process of resistance welding of aluminium with copper was studied using nanostructured foil of Al-Cu system as embedded elements, which is featured by the formation of melt of eutectic composition in the joint zone at minimal heat input. Besides it was established in the works [2, 3] that application of such foils provides highly-concentrated uniform heating of parts being joined.

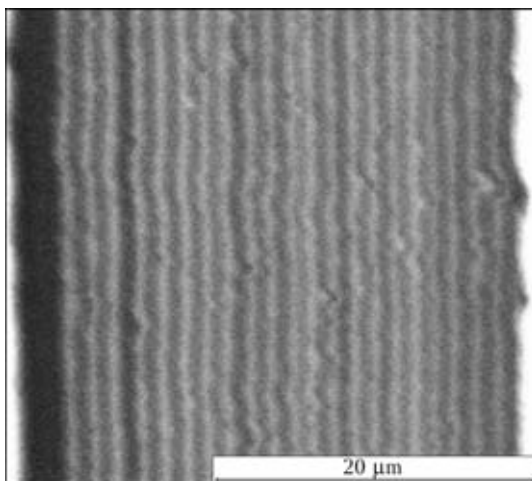


Figure 1. Microstructure of nanolayer foil of Al-Cu system

© V.S. KUCHUK-YATSENKO, 2011

The welding of specimens of 5 × 14 × 140 mm was performed using updated butt welding machine of the K766 type. The pressure during heating was 3–4 MPa, during upsetting it was 7.5–8.0 MPa, time of welding – 1.5–2.0 s.

The manufacture of nanostructured foils using method of electron beam evaporation with subsequent condensation of components was mastered at the E.O. Paton Electric Welding Institute [4]. The microstructure of a nanolayer foil of Al-Cu system (78 wt.% Al and 22 wt.% Cu) produced using micro X-ray spectral analysis is presented in Figure 1.

The analysis of microstructure and determination of chemical heterogeneity of the joints was performed using optical microscope «Neophot-32» and scanning electron microscope JSM-840 (Japan) with microanalyzer «Link-systems». The evaluation of strength properties of the joints was performed by investigation of microhardness using the LECO microhardness meter and performing mechanical rupture tests.

The experiments on resistance welding of aluminium alloy of the grade AD1 with copper M1 and comparative metallographic investigations were performed using foil of Al-Cu system and without it. In microstructure of transition zone of a joint produced without using foil, the width of a weld is not uniform (varied in the range of 1–10 μm). At 1–2 μm width of transition zone the structure of weld metal is homogeneous, the boundary with aluminium is wave-shaped (Figure 2, a, b). There is a shelf on the curves of distribution of copper and aluminium in the area located near the boundary with aluminium; a curve of distribution of copper grows gradually while that of aluminium is falling.

It is known that copper is not dissolved in aluminium at a room temperature and solubility of aluminium in copper reaches 7.6 wt.%. Al-Cu system is characterized by the presence of some intermetallic compounds, among which CuAl_2 is the nearest to aluminium.

Based on the diagram of state (see Figure 3) [5] it can be assumed that transition zone is composed of

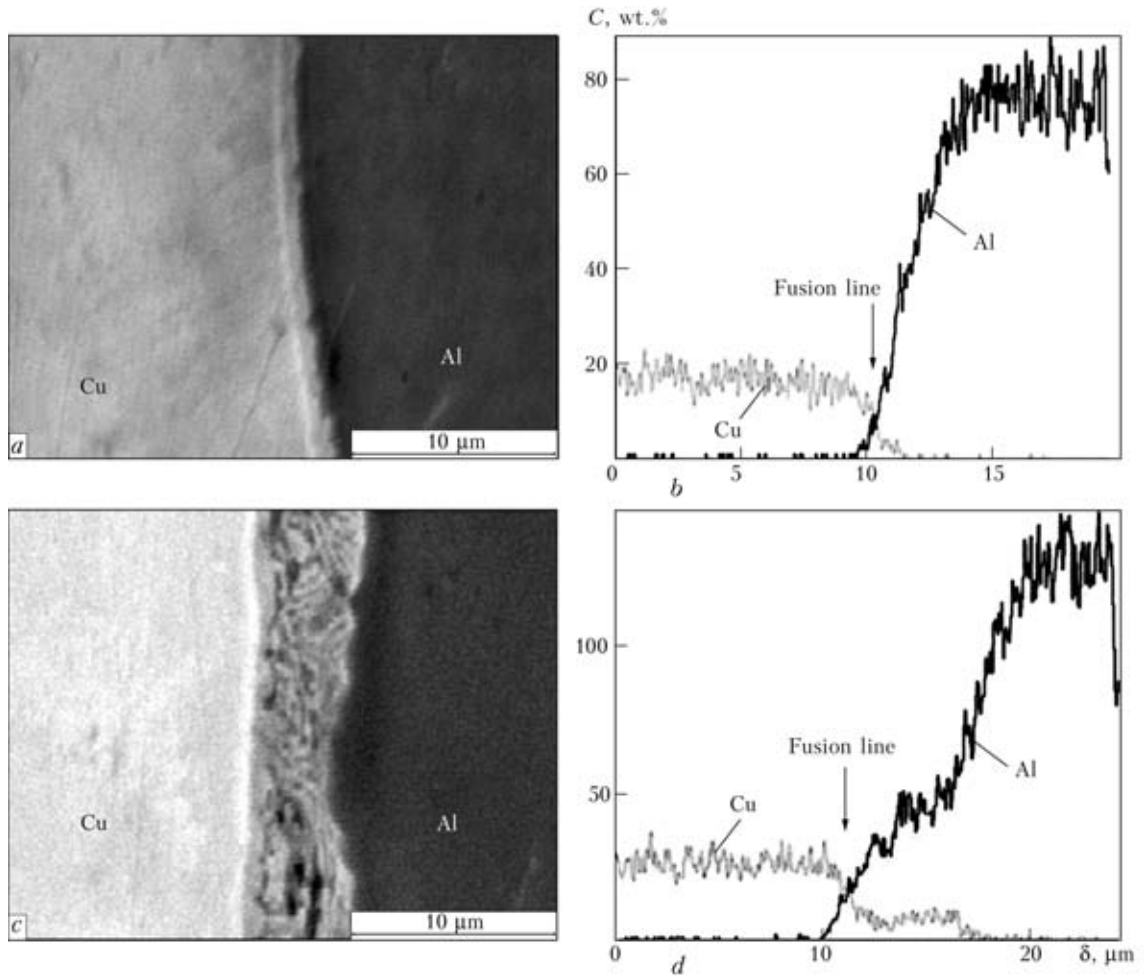


Figure 2. Microstructures (a, c) and curves of distribution of copper and aluminium content C (b, d) in transition zone of the joint, produced using resistance butt welding without using foil, on the zones of the width $\delta = 1-2$ (a, b) and 10 (c, d) μm

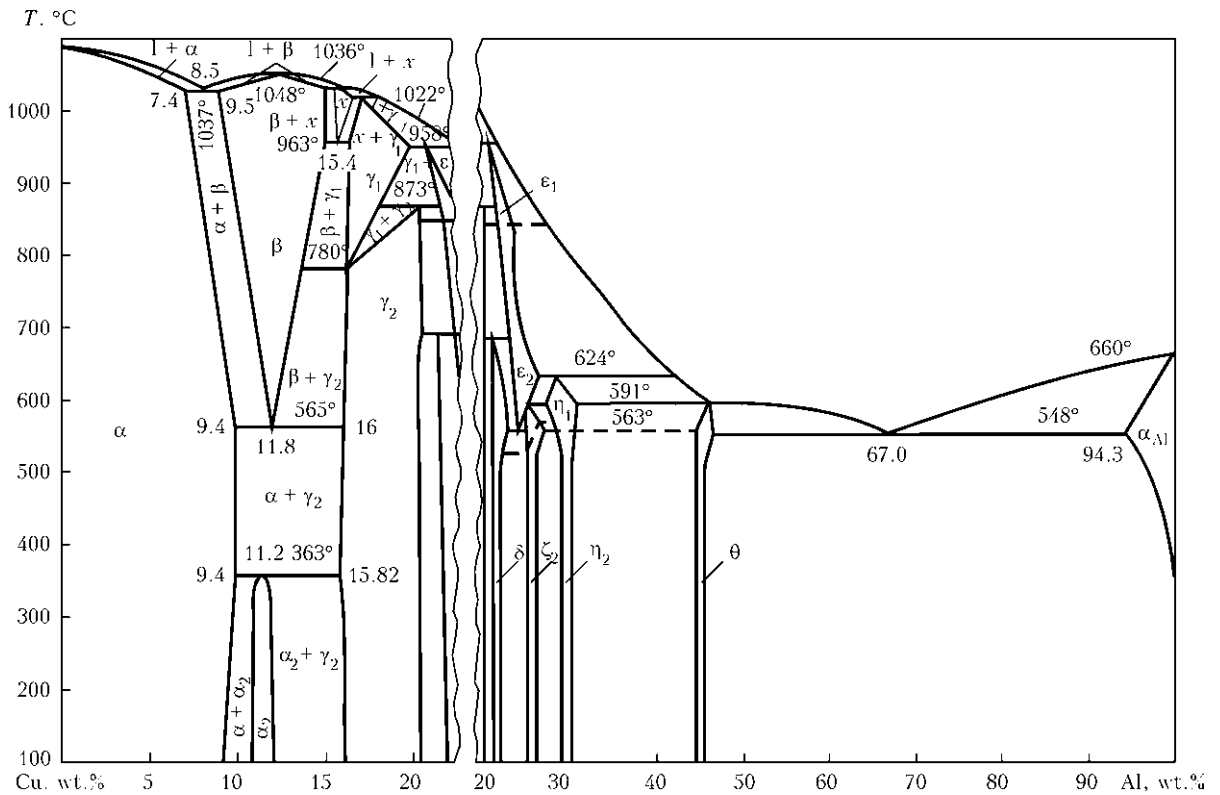


Figure 3. Temperature diagram of state of Al-Cu system

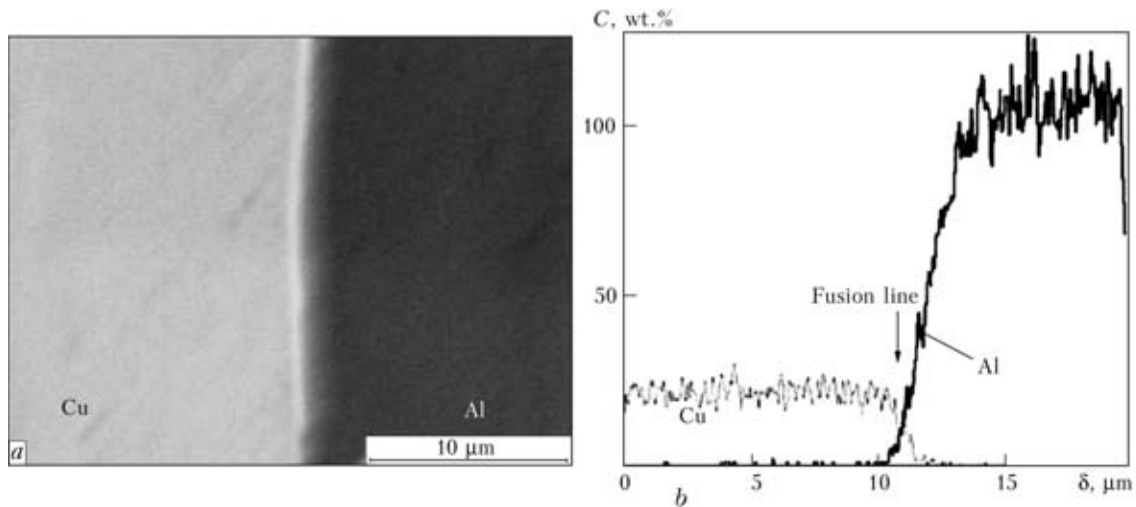


Figure 4. Microstructure (a) and curves of distribution of content of copper and aluminium (b) in transition zone of the joint produced by resistance welding using nanostructured foil of Al–Cu system

diffusion zone of copper and a layer of θ -phase (solid solution based on CuAl_2).

With increase in width of a weld to 10 μm the dendrites, growing from the boundary with copper, and eutectic colonies are formed in its metal (see Figure 2, c, d). The shelf corresponds to the eutectic colonies on the curves of distribution of aluminium and copper, in the area of dendrites a curve of distribution of copper is gradually falling and a curve of distribution of aluminium grows. In this case the transition zone is composed of eutectics $\text{Al} + \theta\text{-(CuAl}_2\text{)}$ and dendrites of α -phase (solid solution of aluminium in copper).

A weld produced using resistance butt welding using foil of Al–Cu system (Figure 4) has a width of 2–3 μm . The shape of the curves of distribution of aluminium and copper in the transition zone of width of above 1.5 μm evidences the gradual change of content of these elements. If intermetallic compounds are not detected, the eutectics is absent.

Mechanical rupture tests showed that maximal strength of specimens of welded joints produced using resistance butt welding with nanostructured foil was

75 MPa (the average value was 65–70 MPa). The fracture of specimens occurred along the near-weld zone on the side of aluminium. The maximal strength of welded joints produced without using foil was 50 MPa. During the tests the specimens were fractured along the weld.

Thus, the use of aluminium with copper in resistance butt welding and nanostructured foil of Al–Cu system as an embedded element prevents the formation of brittle intermetallic phases in weld metal and allows producing welded joints of equal strength.

1. Ryabov, V.R. (1983) *Welding of aluminium and its alloys with other metals*. Kiev: Naukova Dumka.
2. Kuchuk-Yatsenko, V.S., Shvets, V.I., Sakhatsky, A.G. et al. (2007) Features of resistance welding of aluminium alloys using nanolayered Al–Ni and Al–Cu foils. *Svarochn. Proizvodstvo*, **9**, 12–14.
3. Kuchuk-Yatsenko, V.S., Shvets, V.I., Sakhatsky, A.G. et al. (2009) Peculiarities of resistance welding of titanium aluminides using nanolayered aluminium-titanium foils. *The Paton Welding J.*, **3**, 11–14.
4. Movchan, B.A. (1998) Inorganic materials deposited from the vapor phase in vacuum. In: *Current materials science of 21st century*. Kiev: Naukova Dumka.
5. Mondolfo, L.F. (1979) *Structure and properties of aluminium alloys*. Moscow: Metallurgiya.



APPLICATION OF NANOPOWDERS OF METALS IN DIFFUSION WELDING OF DISSIMILAR MATERIALS

A.V. LYUSHINSKY

OJSC «Ramenskoe Instrument Engineering Design Bureau», Ramenskoe, Russia

Comparative analysis of compact materials, deposited and galvanic layers, and powders with different particle size used as such layers is presented. The processes of sintering of nanopowders and their adhesion through sintering to the surfaces of parts welded are studied. It is shown that the use of double mixtures of nanopowders allows intensifying the process of diffusion formation of the welded joint and provides the welds with preset mechanical and physical properties.

Keywords: *diffusion welding, powder intermediate layer, nanopowders of metals, intensification of process of joining, welding temperature, time of welding, pressure, structure of metal in zone of joining*

Technology of diffusion welding along with obvious advantages over the other methods of welding has one significant disadvantage, i.e. low efficiency of the process, which restrains its wide application in industry. In this connection there is a task for the specialists in area of welding to find a method for intensification of process of obtaining of solid state permanent joint.

In diffusion welding the cyclic changes of its main parameters — temperature T and pressure P [1, 2] — is the most simple method for intensification of this process. There are other methods, but they require a development of special technologies, creation of high-frequency and specialized equipment and precision fixture that means significant financial expenses.

Solution can be found due to existence of one more method for the intensification of process of diffusion welding. It provides solution of a complex of tasks and being based on application of the intermediate layers functioning during welding in various ways: reduction of chemical inhomogeneity in joining zone; relieve of the residual stresses and elimination of influence of a difference in values of coefficients of linear thermal expansion of materials being welded; prevention of their plastic deformation; significant reduction of the main parameters of diffusion welding with simultaneous assurance of high strength of joints.

Plastic metals (gold, silver, nickel, copper, aluminum, ect.) are applied, as a rule, for the intermediate layers in a form of foils, wires, powders and films which are deposited on the surfaces to be joined by galvanic method or vacuum deposition [3].

Activity of the surface of the foil, obtained by rolling of molten metal, is almost similar to compact welding materials. It is used as an intermediate layer mainly for preventing formation of intermetallics in the joining zone. Thickness of intermediate layers makes 0.05–1 mm. Their preparation for welding is similar to the preparation of surfaces of the parts to be joined.

Quality of the joints obtained through galvanic or deposited coatings mainly depends on their adhesion to the base metal. In turn the level of adhesion is determined by quality of surface preparation of the parts to be coated. Similarity of the structures of the base and deposited metals is an important factor for providing necessary adhesion. Moreover, mutual diffusion of the base and coating metals promotes their reliable adhesion during coating as well as in the process of diffusion welding, if the diffusion is accompanied by formation of solid solution.

Thin galvanic or deposited films are characterized by high values of surface area to volume ratio, different level of structure ordering, small mass as well as imperfect crystal lattice. This results in development of new effects and evident deviation from the effects taking place in the massive samples. Conditions of thermodynamic equilibrium in the thin films significantly differ from conditions in volume. The film is formed from many discrete nuclei at their strong off-orientation and displacement relatively to each other, that result in formation of the dislocations and network of vacancies over the interfaces of coalescing nuclei and development of elastic stresses in the film.

A powder body is unstable due to excess of free energy. This is first of all related with the presence of highly developed internal interfacial interface of the solid body with the pores [4].

Rising of particle size of metal powders increases their volume shrinkage during pressure sintering process, reduces temperature of beginning of evident shrinkage (Figure 1) and improves strength. The powders which at other things being equal (temperature, compression force, etc.) compacting with higher speed are considered to be more active. The higher powder particle size, the bigger its specific area and the greater system deviation from thermodynamic equilibrium.

Investigations of welded samples from nickel NP-2, made by diffusion welding at temperature $T_w = 550$ °C, pressure $P = 20$ MPa and time of welding $t_w = 30$ min using intermediate layers from nickel electrolytic powders PNE-1, carbonyl PNKOT-1 and nanopowders (NP), obtained as a result of thermal decomposition of $\text{Ni}(\text{COOH})_2 \cdot 2\text{H}_2\text{O}$ nickel formate with particle size

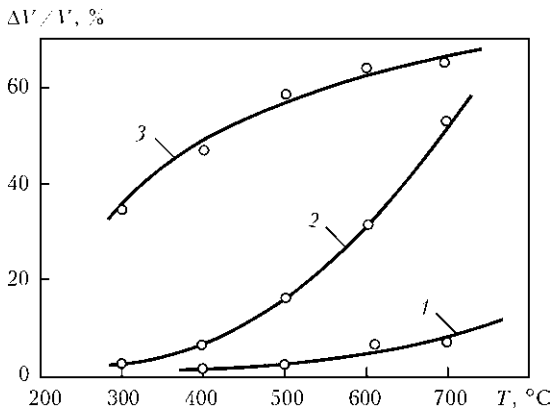


Figure 1. Dependence of volume shrinkage $\Delta V/V$ of electrolytic powder NPE-1 (1), carbonyl PNKTO-1 (2) and NP (3) on sintering temperature at $t = \text{const}$

$d = 39.75, 7.63$ and less than $0.10 \mu\text{m}$ and area of specific surface $S_s = 0.12, 0.48$ and $17.32 \text{ m}^2/\text{g}$, respectively, showed that maximum value of tensile strength $\sigma_t \geq 200 \text{ PMA}$ is achieved in welding through NP.

Compacting of the intermediate powder layer is a process of directed transfer of material mass. Diffusion of lattice vacancies over the layer surface takes place thorough their sinks representing itself interparticle boundaries. Amount of such sinks and, respectively, distance between them depends on particle size. Reducing the latter the amount of vacancy sinks increases that activate shrinkage process.

Speed of the processes of mutual sintering of the particles and their adhesion to the flat surface are increased reducing linear dimensions of the particles and are described by ratio [4]

$$X/R = R^{-3/5} f(t, T),$$

where X is the minimum radius of contact neck; R is the radius of particles; t is the time of sintering.

Defectiveness of the crystalline structure is increased together with rising of particle size and specific area of the powder for activation of process of diffusion welding using the powder layer at which two processes, i.e. sintering of powder particles between each other and their adhesion to the flat compact surface, take place simultaneously. For this metal powder are manufactured under non-equilibrium conditions at

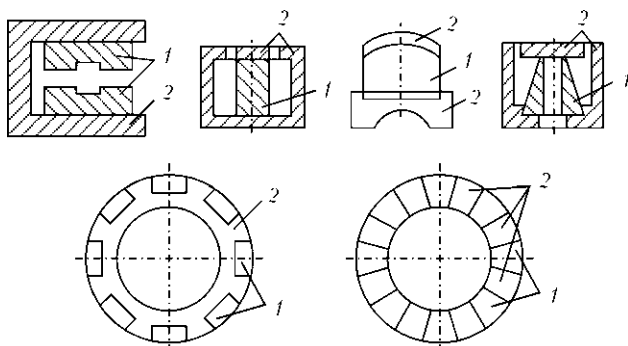


Figure 2. Schemes of the main variants of magnetic materials joining: 1 – constant magnets; 2 – magnetic circuit

lower temperature and high speed of heating and cooling when speed of cooling is higher than that of heating. Specifically, this is a scheme of obtaining of NP by thermal decomposition of formates and metal oxalates.

Thus, reduction of free energy, connected with the free surface of porous body and defects of its crystalline structure, is the main driving force of sintering process of powder intermediate layer and its adhesion to the base metal. Besides, increase of concentration of dislocations, along which high diffusion mobility of the atoms takes place, can be the reason of rise of powder activity in diffusion welding.

Technology of diffusion welding using powder intermediate layers is applied, for example, in aircraft instrument-making for manufacture of magnetic systems, in particular, for joining constant magnets of YuNDK type with 27KKh alloy, 10880 steel, permalloys and other materials (Figure 2). Diffusion welding was carried out under following conditions: $T_w = 550\text{--}600 \text{ }^\circ\text{C}$, $P = 20 \text{ MPa}$, $t_w = 30 \text{ min}$. Strength of weld metal made more than 200 MPa (fracture took place along the constant magnet), plastic deformation of parts was absent, initial magnetic properties of the magnetic materials were preserved, further heat and mechanical treatment were not necessary and welded assemblies were ready to further erection. If a comparison with technology of welding without activating layers ($T_w \geq 870 \text{ }^\circ\text{C}$, $P = 30 \text{ MPa}$, $t_w = 30 \text{ min}$) is made then in this case the strength of weld metal makes $5\text{--}7 \text{ MPa}$, plastic deformation is not less than 15% . Additional thermomagnetic treatment for renewal of the initial magnetic properties is required at that since process of welding is performed at temperature above Curie point. Besides, technological cycle for manufacture of one part was reduced by 30% using the powder intermediate layer.

Failure of quality welded joints occurs on the intermediate layer that indicates on complete processes of adhesion between the surfaces of sample and powder and full enough chemical interaction, the evidence of which is a fractogram of fractured surface of welded joint, obtained at $T_w = 600 \text{ }^\circ\text{C}$, $P = 5 \text{ MPa}$, $t_w = 30 \text{ min}$. It is reasonable to consider that the fractogram consists of three zones (Figure 3). It can be observed comparing zones 1 and 3 that the character of their surface (size and depth of pits) is similar and, zone 3, respectively, is a part of the powder intermediate layer along which the failure took place. It should be noted that failure of the specified sample occurred on two mechanisms: by means of coalescence of micropores (zones 1 and 3) and chip (zone 2). The failure, mainly, took place between the particles (intergranular character). This confirms the fact that process of sintering of powder rolling strip (intermediate layer) is carried out on a mechanism of grain-boundary slip of particles.

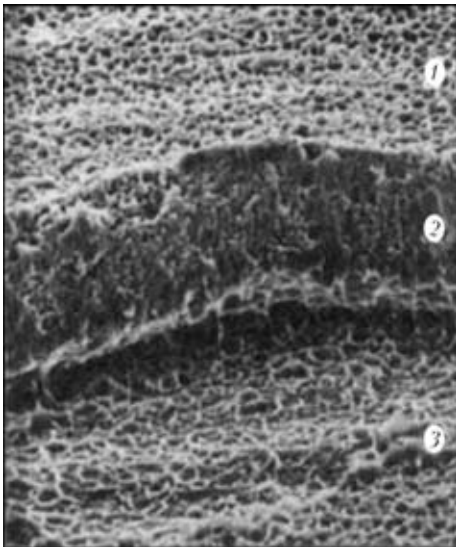


Figure 3. Fractogram ($\times 800$) of fracture surface of the welded joint sample: 1 – surface of sintered powder layer after fracture; 2 – section of intermediate sintered powder layer (thickness of layer after welding and fracture); 3 – places of pit

Thermo-activation analysis of process of welded joint formation and sintering of intermediate powder layer was carried out based of dependence of relative strength at fixed pressure of welding $P = 10$ MPa and relative strength $\bar{\sigma} = 0.8$. Their values correspond to value of activation energy of the process of welded joint formation, sintering of intermediate layer $E_a = 110$ kJ/mol and activation energy of the compact nickel. This allows making a conclusion that formation of welded joint through powder intermediate layer is controlled by process of its sintering, and the latter in turn – by grain-boundary self-diffusion.

Double component powder layers based on the most promising mixtures of NP nickel, copper and cobalt of different compositions were developed and investigated for increasing of mechanical properties of the joints and improvement of special properties of the magnetic systems as well as decreasing thermodeformation influence on welded parts and reduction of technological cycle of diffusion welding.

Kinetics of solid-phase sintering of double mixtures in contrast to single-component mixtures is complicated by the processes accompanying diffusion homogenizing. Excessive free energy of the powder mixture caused by presence of concentration gradient of the components can be very significant. This is energy-wise even when the system is not in equilibrium state according to any other parameter, for example, developed free surface, value of stresses in diffusion zone, etc. New compaction mechanism appears realizing which the movement of particles of different materials is related with their size, developed surface as well as with content of the components.

The intermediate layer, consisting of double component NP, was also applied for joining of hard alloys with steels in manufacture of special instruments.

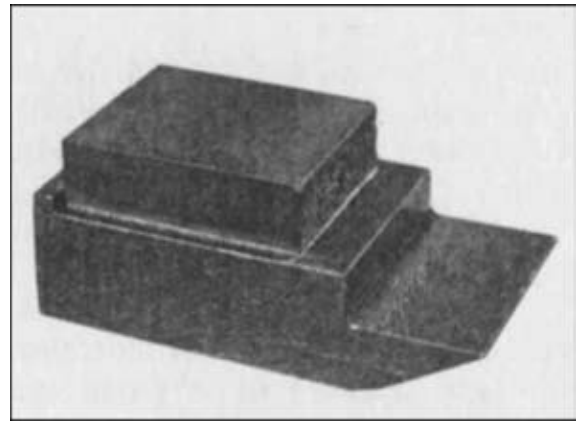


Figure 4. Appearance of the part from diffusion-welded hard alloy VK6 with steel U8

In many respects, strength of the welded joint of hard alloy with steels is determined by quality of preparation of surfaces to be joined, in particular, by roughness of higher than 1.25 and parallelism deviation of less than 0.02 mm. Therefore, their welding is carried out through porous shrinking intermediate layers leveling deviation of their sizes from required values. The intermediate powder layers based on Ni–Co, Ni–Cu, Cu–Co double mixtures with different content of components were investigated. The best result was obtained for intermediate layers from NP of Ni–Co system.

Diffusion welding of hard alloy VK6 (94 wt.% WC and 6 wt. % Co) with steels U8 (Figure 4) and 35 was carried out through spacer with 75 % Ni + 25 % Co. This composition, as showed our experiments, is optimum for specified pair of materials. The same spacer composition was used in welding of VK20 alloy (80 % WC and 20 % Co) under following conditions: $T_w = 850\text{--}900$ °C, $P = 10\text{--}15$ MPa, $t_w = 30$ min. Tensile strength made $\sigma_t = 600\text{--}900$ MPa, failure occurs along the hard alloy.

Mutual diffusion of elements being joined in welding of hard alloy with steels using the intermediate layers from mixtures of nickel and cobalt forms a

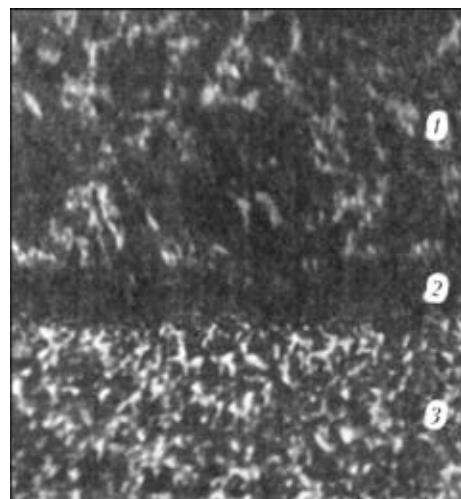


Figure 5. Microstructure ($\times 350$) of joining zone of hard alloy VK6 (1) with steel U8 (3) through powder intermediate layer (2)



transition zone. Virtually all elements of materials being joined take part in its formation. Nickel, which can diffuse in alloy to 25–30 μm depth along the grain boundaries, shows the highest activity in formation of the transition zone. As a result, on the one hand, cobalt is substituted to nickel in alloy (at that the grains of tungsten carbide partially dissolve in nickel forming nickel–cobalt solid solution) and, on the other hand, intensive development of the diffusion processes between cobalt in the alloy and cobalt in the spacer takes place.

Figure 5 shows a microstructure of joining zone of hard alloy VK6 with steel U8.

Application of the intermediate layers from NP mixtures in diffusion welding instead of brazing, for example, by copper or brass, for tool manufacturing allows saving up to 75 % of expensive and scarce alloy, increasing quality and reliability of hard alloy to steel

joint, rising service life of tool 1.4–1.5 times and reducing laboriousness for its manufacture. Unfortunately, specified technology has significant disadvantage, i.e. low efficiency in comparison with brazing but this is eliminated by high quality of the part. Application of multi-position fixture can increase efficiency of welding process.

Thus, process of diffusion welding can be intensified by means of application of highly active energy-rich intermediate layers based on NP. It is important that particles having maximum developed surface together with minimum size.

1. Kazakov, N.F. (1976) *Diffusion welding of materials*. Moscow: Mashinostroenie.
2. Karakozov, E.S. (1986) *Pressure welding of metals*. Moscow: Mashinostroenie.
3. Lyushinsky, A.V. (2006) *Diffusion welding of dissimilar materials*. Moscow: Akademiya.
4. Geguzin, Ya.E. (1967) *Physics of sintering*. Moscow: Nauka.



September 6–8, 2011
Mariupol

Organizers:

Ministry of Education and Sciences of Ukraine
Welding Society of Ukraine
Ukrainian Information Center «SCIENCE. TECHNIQUE. TECHNOLOGY»
Priazovsky State Technical University
Welding Department of the OJSC «Azovmash» Vocational School (Mariupol)

Program of the Conference

The Conference will consist from plenary and sectional sessions on the following subjects:

- improvement of quality and efficiency of processes of welding and related technologies
- issues of designing, manufacturing and operation of welded structures
- system for certification of products of welding engineering
- upgrading of staff training under conditions of multi-level system of high education.

Details by telephones:

(380629) 44 65 91, 44 65 79, 44 61 79, 44 64 13

INTERNATIONAL RESEARCH-AND-METHODICAL CONFERENCE ON CURRENT PROBLEMS OF WELDING AND RELATED TECHNOLOGIES, STUFF TRAINING

MANUFACTURE OF OUTSTANDING THICK-WALLED CONSTRUCTIONS

E. ENGINDENIZ¹, E. KAPLAN², E. GANIOGLU², F. YUKSEL², N. BAYEZID² and R. ROSERT¹

¹Altleiningen, Germany

²Istanbul, Gemlik, Turkey

Manufacture of specific elements up to a unit weight of 1000 t, used in current refinery projects, is presented. Constructions of the highest apartment and office tower in Moscow, Russia, as well as the football stadium «Shakhtar» in Donetsk, Ukraine, are described. In addition to the specific welding procedure variants, logistic issues during transport and assembly are discussed.

Keywords: arc welding, welded structures, thick-walled sheets, multi-pass welding, flux-cored wires, efficiency of welding process, unique constructions

CIMTAS was founded 37 years ago as subsidiary of the largest construction company ENKA in Turkey, and mainly produces pressure vessels, storage tanks, wind turbines and all kinds of steel constructions. While the Company headquarters are located in Istanbul on the European side of the Bosphorus, two production facilities are situated in Gemlik on the Asian side of Turkey. The town of Gemlik is located approximately 100 km south of Istanbul at the Sea of Marmara close to Bursa.

A total of 47,000 t of steel was processed in these facilities in the year 2007. Amongst others numerous pressure vessels were produced for the GASCO project in the United Arab Emirates and the LNG project in Angola. The construction of these petrochemical facilities is still on-going. In addition, the Company supplies a number of pressure vessels to the companies PETROFAC BG, Tunisia, and MAN. Six of these vessels had a unit weight of slightly more than 500 t. One vessel which is currently being manufactured will even reach a shipping weight of 1000 t.

In this paper we will describe the latest activities of the CIMTAS Corporation, which include the manufacture of extremely thick-walled pressure vessels, as well as building special steel and elevated steel constructions. Two of these buildings are the currently highest apartment and office building in Moscow, Russia, and the football stadium «Shakhtar» in Donetsk, Ukraine. These steel construction projects also require the use of thick-walled sheets currently exceeding a thickness of 200 mm.

High-rise building «Eurasia» in Moscow. Currently the highest building in Russia is being built in the city centre of Moscow. The two-tiered tower with 5 underground and 74 above ground floors is of 310 m high. The high-rise building houses office space, as well as apartments, shops, restaurants and a health club.

The multi-storey car park on the lower floors can accommodate up to 1000 vehicles. Figure 1 shows how the building is planned to look after its completion in May 2009.

The construction is made from steel and weights 27,000 t. The total net floor area of the building is 200,000 m². 24,000 components have been manufactured by welding, thereof 21,000 beams, 2300 box profiles as support columns and 700 braces. Steel grades S355 J2G3 and P 460 NL1 with a sheet thickness up to 404 mm were used for the base plates of the foundations and steels with sheet thicknesses up to 220 mm were used for the closed box profiles.

Football stadium «Shakhtar» in Donetsk. In June 2006 ENKA group was commissioned to build a 5 star stadium in line with UEFA and FIFA regulations in Donetsk.

In August of the same year the Company already started to excavate the foundations and will thus be able to finish this huge building in time in August 2008.

Figure 2 shows impressively the special form of the roof construction which weighs approximately



Figure 1. High-rise building «Eurasia» in Moscow

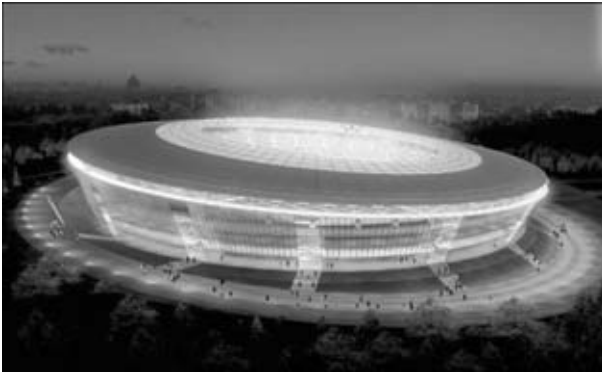


Figure 2. Football stadium «Shakhtar» in Donetsk

3800 t with the total steel weight of the construction amounting to 4300 t.

The architect had the idea to construct a harmonic roof without supports. This was realized by using space trusses spanning 60 m supported on space truss beams which protrude as far as the trusses. As shown in Figure 3, the space truss beams and the space truss are in one plane. The roof height is 54 m. Thanks to its roof which is dipping down to the south the stadium matches the contours of Leninsky park. This reduces the height of the roof by one third resulting in a significantly increased amount of sunlight shining on the lawn. However, in terms of structural design this means that all 12 truss beams have different dimensions. Therefore, the production of the elements and the subsequent assembly logistics were extremely time-consuming and expensive. The roof segments have been designed in such a way that they can compensate certain ground shifts caused by the coal mining activities which used to take place at this site. The

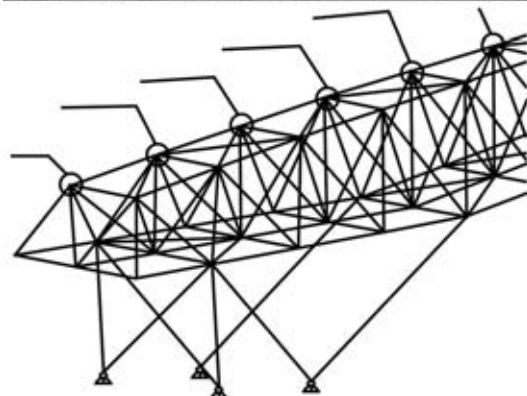
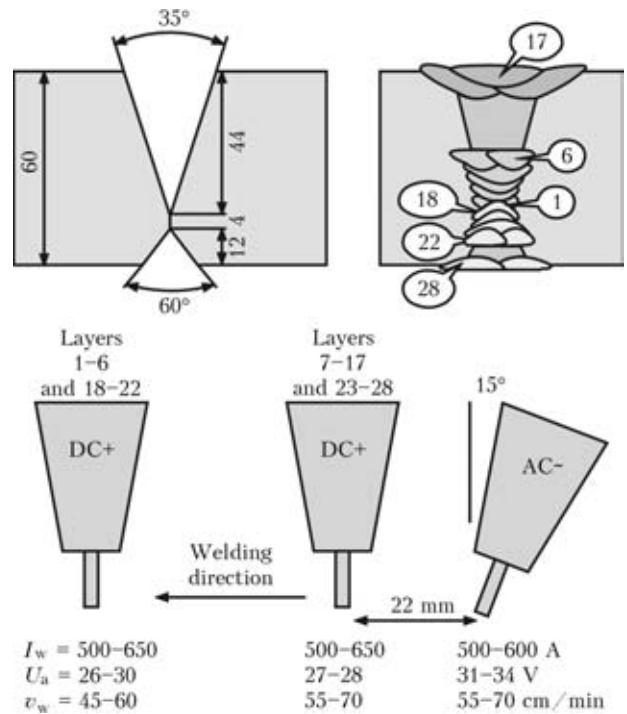


Figure 3. «Shakhtar» roof construction (May 2008)

stadium accommodates 50,000 football fans including 5000 VIP guests. The size of the construction site amounts to 255,000 m². The built-up area including the rising gradient is 46,780 m². The stadium cost approximately 180 mln Euros.

Another special feature of this stadium is the impressive lawn which has a size of 24,000 m². The glass facade which runs around the entire perimeter and includes some transparent roof constructions will make the stadium look like a jewel once the floodlights are turned on. It seems that the football club «Shakhtar» will be the owner of the most modern stadium in Eastern Europe for some time to come and the stadium is planned to be the venue of a semi-final game of the European Football Championship 2012.

Welding procedure variants. On account of the operating conditions and the practical experiences submerged-arc welding (SAW) was chosen as the main pre-production process, especially since the dimensions and geometries of the elements were predestined for this method. The use of flux-cored electrodes was considered for economic and qualitative reasons and qualified for wall thicknesses up to approximately 60 mm in twin-wire tandem variants. As can be seen



Impact work at -46 °C of welded bead with notch at the middle part, J/m ²	
Layers 1-17	Layers 18-28
224	134
180	202
190	164
Average 204.5	176.5

Figure 4. Scheme of SAW of steel SA 516 Cr 70 N (heat-treated at 630°C for 12 h) with flux-cored wire TC 731B 4.0 mm diameter and flux BF 10, and results of the procedure test

in Figure 4, 4.0 mm diameter basic flux-cored wires are used for this method with the first 5–6 beads at the root area on each side being welded using the single-wire technique.

Thanks to the cleaning effect of the basic slag formers contained in the welding flux the sealing run does not have to be ground or bored out. The wetting of the side walls is always error-free and the overlap is always guaranteed at the chosen process parameters and with a root face of 4 mm. This is the main reason for the superior cost effectiveness of this method compared to solid-wire welding. The repair quota is almost zero and the inconvenient non-productive times spent preparing the joints of the sealing run are no longer required. One of the reasons why the Company is extremely popular with customers and buyers is their brilliant impact toughness values which also contribute to its excellent reputation.

For the extreme wall thicknesses required in vessel production and for manufacturing the box profiles for the steel constructions mentioned above it was decided to use the twin-wire technology with two thick flux-cored wires 2.4 mm in diameter. After the pre-testing had been successfully completed this variant was approved in the scope of another procedure test and at the same time even upgraded to twin wire tandem. Figure 5 shows the documentation for a 197 mm thick

sheet SA 516 Gr 70 N. While commercial mobile welding tractors are available for twin-wire tandem applications, the twin-arc tandem machines had to be built in-house.

Figure 6 shows a mobile station with two automatic machines. Two welds are simultaneously welded onto the box girder to meet the manufacturing tolerances.

As can be seen, the commercial twin-wire tractor was coupled with a trailer bearing additional twin-wire reels. Thus the profile is welded using 8 reels simultaneously.

Figure 7 shows the welding time using the example of a 197 mm thick joint in comparison of all SAW procedure variants. This examination should be regarded as supplement to increase the cost effectiveness if flux-cored wire SAW is used. Although the reduction of the welding time achieved by using the flux-cored welding technology in comparison to the other procedure variants lies between 18.8 and 20.0 %, the Company reports cost savings in production of up to 30 % since, as already mentioned earlier, the down-times and repair times are minimized. Absolutely the same process parameters have been used for calculating the welding times represented in Figure 7.

These performance parameters are also used in production. The weld weight of the joint selected for this example was 76.6 kg/m. The weld reinforcement was

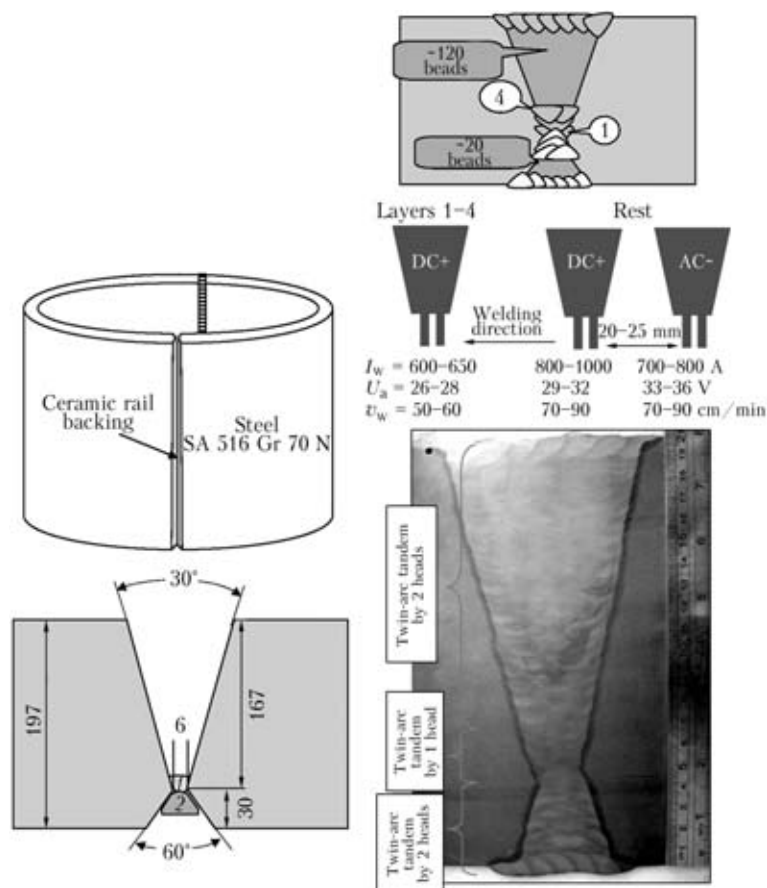


Figure 5. Scheme of twin-arc SAW and twin-arc tandem SAW of sheets 197 mm thick (heat-treated at 630 °C for 12 h) with two 2.4 mm flux-cored wires TC 731 B and flux BF 10, and test results: 1 – root made vertically rising using MF 713R and M21; 2 – formed ceramic rail backing

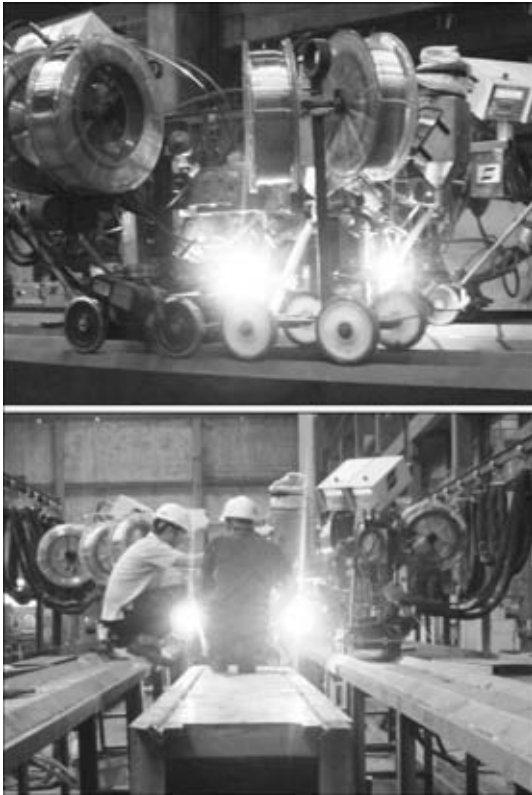


Figure 6. Mobile welding station with 2.4 mm flux-cored wires for twin-arc tandem SAW



Figure 8. Pre-production of the gusset plates for «Eurasia» (a) and «Shakhtar» (b) using flux-cored GMAW in Gemlik

taken into account with an average height of 2.5 mm. As expected, twin-arc tandem SAW using 4 flux-cored wires provides the best results.

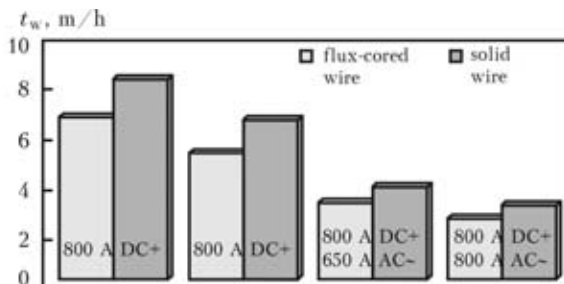
In addition to the SAW technology, GMA welding was used exclusively with flux-cored wires. In Figure 5 it can be seen that the welding of the root using a rutile flux-cored wire on ceramics is performed in a vertical position rising upwards. This bead is used primarily to fasten the vessel halves but later it also forms the backing for the subsequent SAW.

CIMTAS is the company with the longest experience in flux-cored wire welding in Turkey. Its employees have been welding using flux-cored wires and shielding gas for more than 25 years. When completing the building «Eurasia» and stadium «Shakhtar», for example, all fillet and butt welds for lower sheet thicknesses were performed using the GMAW procedure and seamless flux-cored wires. Two type wires containing rutile slag (E 71 T1 and E 81 T1-Ni1) and wire with metal powder filling (E 70 C-6 M9) were used.

Figure 8 shows how intensively the shielding gas flux-cored wire technique is used. It is even used during the assembly on the construction site. Other welding procedures, which were used for the manufacture of the elements shown above, include TIG, stud and laser welding, as well as electroslog strip cladding and firecracker welding using stick electrodes.

The latter is only used to a small extent and only on construction sites. The thin-walled tubes for the roof elements of the stadium «Shakhtar» were manufactured using laser welding.

Delivery of the elements. The continuously increasing weight of the units which had to be transported was a big challenge for the region at the Sea of Marmara. The capacity of the harbour facilities of the BORUSAN logistics company had to be gradually enlarged and qualified for the loading of the pressure vessels over the past 15 months. The distance on land which had to be covered between the production facility and the harbour is approximately 3 km. The



Parameter	One-arc welding with 4.0 mm wire	Twin-arc welding		
		2.4 mm two wires	4.0 mm two wires in tandem	2.4 mm four wires in twin-tandem
Flux-cored wire	6.54	5.10	3.10	2.43
Solid wire	8.06	6.38	3.73	3.0
Time saving, %	18.86	20.0	16.87	19.0

Figure 7. Comparison of the welding time for 197 mm thick joint (according to Figure 5)



Figure 9. Loading of a 500 t slug catcher surge vessel onto a freighter at Gemlik harbour

roads along this path also had to be stabilised and reinforced in a lot of places. Figure 9 shows the loading of surge vessel onto a freighter.

The heavy lorry has 31 axles. Currently all measures are taken to prepare the harbour for the transport of the 1000 t CO₂ absorber.

The maximum unit loads for «Eurasia» and «Shakhtar» amount to 70 t.

Therefore, they can be handled as is shown in Figure 10. The logistical problems mainly regard the timing. Due to the risk of freezing waters the elements can only be transported from April to October. To minimize storage costs procurement and production planning are precisely coordinated. Currently this causes relatively large problems since the worldwide steel market is suffering from shortages.

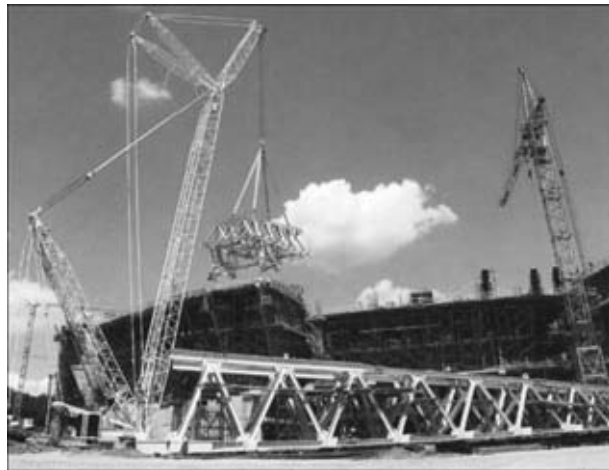


Figure 10. Handling of the roof girders in Donetsk

So, the concerned steel constructions are «Eurasia», the highest apartment and office building in Moscow, and the stadium «Shakhtar» in Donetsk. All projects include wall thicknesses of approximately 200 mm. The production facilities are located in Turkey. For the welding processes both the SAW and the GMAW procedures using flux-cored wires are applied. In addition to the qualitative advantages of the flux-cored wire technology, the economic aspect is also highlighted.

EFFICIENCY OF MELTING OF ELECTRODE WIRE IN SUBMERGED-ARC SURFACING WITH INFLUENCE OF TRANSVERSE MAGNETIC FIELD

A.D. RAZMYSHLYAEV, M.V. MIRONOVA, K.G. KUZMENKO and P.A. VYDMYSH
Priazovsky State Technical University, Mariupol, Ukraine

A device has been developed, which generates a transverse magnetic field (TMF), for the process of submerged-arc surfacing using wire. It is shown that in reverse polarity surfacing the impact of a constant and alternating TMF of 50 Hz frequency increases equally the coefficient of melting of electrode wire α_{melt} , both of ferromagnetic and nonmagnetic materials. Maximum increase of wire α_{melt} is 20–30 % at the magnitude of transverse component of TMF induction of 30–45 mT.

Keywords: submerged-arc surfacing, electrode wires, transverse magnetic field, induction, melting coefficient

Technological peculiarities of arc welding and surfacing process using transverse magnetic field (TMF) are considered in the works [1–8]. It is followed from them that in consumable electrode argon arc welding [2, 3] using electrode wire of 1–1.2 mm diameter and TMF influence, the decrease of penetration depth and increase of weld width are observed. During welding and surfacing using wire of 3 and 4 mm diameter under the flux AN-348A at the impact of TMF of 50 Hz frequency, the penetration depth decreased in 1.5 times and width of a weld (bead) negligibly increased

(efficiency of melting wires was not studied) [4]. For surfacing of beads using wire Sv-08GA of 2 mm diameter under the flux AN-348A, the change of frequency TMF in the limits of $f = 0–20$ Hz and induction of magnetic field $B_x = 0–0.015$ T (at reverse polarity) the data are given which are not quantitative but qualitative, i.e. only tendency of influence of frequency of induction of TMF on penetration depth of metal and width of a bead was established [5]. In the work [6] it was shown that in surfacing using wire Sv-08A of 4 and 5 mm diameter under the flux AN-348A on the plates of steel St3 under the impact of TMF of 50 Hz frequency, the depth of metal penetration decreased whereas width of a bead increased. It

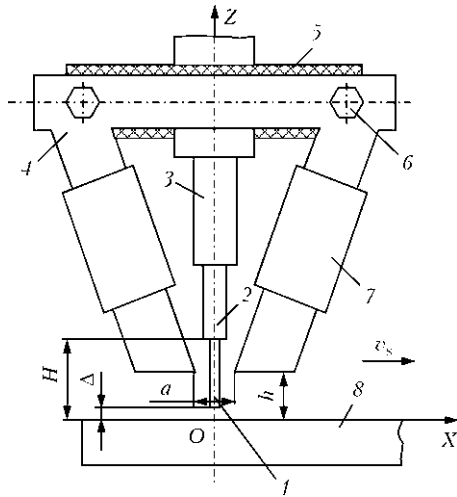


Figure 1. Scheme of the device for generating TMF (see designations in the text)

is also noted that during induction of TMF near the surface of a plate above 18–20 mT, the interruptions of an arc are observed, which did not allow applying higher values of induction. The impact of TMF on the coefficient of melting α_{melt} of 1.8–2 mm diameter wire in submerged-arc surfacing was studied only in the work [7]. It was established that influence of TMF results in negligible increase of α_{melt} , namely from 11.7 to 12.2 g/(A·h). In submerged-arc surfacing the electrode wires of 3–5 mm diameter are usually used, but there are no data about impact of TMF on α_{melt} of such electrodes. This problem required study because efficiency of the surfacing process is determined not only by the sizes of penetration zone of base metal, but also α_{melt} value of electrode.

The aim of this work was investigation of impact of TMF on the coefficient of melting α_{melt} of electrode wire of 3–5 mm diameter in submerged-arc surfacing.

To develop the controlling TMF, the device (Figure 1) was designed which represents a magnetic core 4 consisting of three sections: two inclined ones where coils 7 are located, and horizontal one connected with

inclined sections using bolted joints 6. The magnetic core is assembled of plates of electrotechnical steel of 0.5 mm thickness, the cross-section of an assembly is 30 × 20 mm. Two coils are manufactured of two-layer copper insulated wire of 2 mm diameter. The quantity of turns of one coil was 70. The device generating TMF was fixed to the welding machine ADS-1002 using yokes. The magnetic core 4 was isolated from the machine by the isolator 5. The automatic machine allowed varying the electrode stickout H , i.e. distance between current conducting jaws 2 and plate 8, and also distance h from the ends of magnetic core 4 to the surface of plate 8. The design of device allowed changing the distance between lower sections of magnetic core near the electrode edge (parameter a). The electrode wire 1 passed through nozzle 3. Figure 1 also uses the system of coordinates accepted for study of magnetic field (the beginning of coordinates was located at the surface of a plate under the axis of electrode).

In this work the constant or alternating TMF of 50 Hz working frequency was applied to control the electrode drops transfer, as far as such magnetic fields are the most simple to be realized in practice. To generate the mentioned magnetic fields in the coils of device the direct current from the welding rectifier VSZh-303 or alternate current from the welding transformer TM-402 was passed. In the zone of electrode drop and arc the measurements of induction components B_x and B_z were conducted using milliteslameter of the type EM-4305 with Hall sensor at measuring base 1 × 1 mm for the constant TMF and F-4356 type was used for alternating TMF. The measurements were carried out at $Z = 0, Y = 0$ in the points $X = 0, 5, 10$ and 20 mm. The distance from the edge of the electrode to the surface of the plate Δ were preserved constant ($\Delta = 5$ mm). The electrode stickout was $H = 25$ mm ($h = 25$ mm), and the distance between the lower ends of magnetic core along the horizontal was $a = 35$ mm. In the investigations of the induction of the magnetic field, the wires Sv-08GA and Sv-12Kh18N10T of 4 mm diameter were used and in capacity of base metal the plates of the steel 09G2S and 12Kh18N10T were used.

Figure 2 shows distribution of components of induction of B_x and B_z of constant and alternating TMF of 50 Hz frequency using welding wire Sv-08GA (ferromagnetic) of 4 mm diameter and base metal — the plate of steel 12Kh18N10T (non-magnetic material) at the current in coils $I_{\text{coil}} = 60$ A. The distribution of B_z induction of constant and alternating TMF of 50 Hz frequency bears incremental character depending on distance from the axis OZ to the poles of the device along the axis OX. In the zone under the end of electrode the component of induction B_z (Figure 2, curves 1, 3) is much smaller than B_x (Figure 2, curves 2, 4). It was also established that components of induction B_z and B_x practically increase in a linear way (in all points along the axis OX) at increase of direct

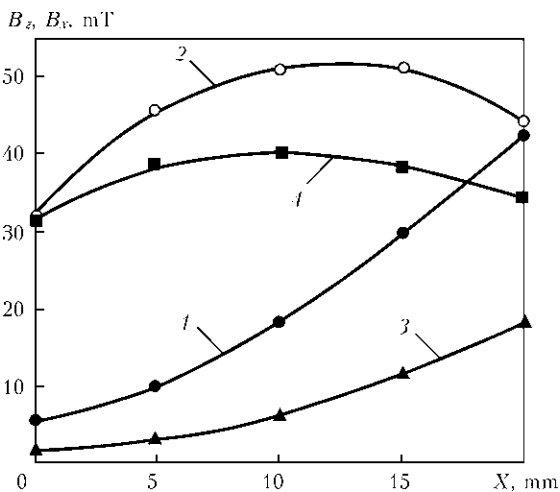


Figure 2. Distribution of components of induction B_z and B_x of TMF along the axis OX ($Z = 0, Y = 0, I_{\text{coil}} = 60$ A): 1, 3 — B_z ; 2, 4 — B_x ; 1, 2 — constant TMF; 3, 4 — alternating TMF of 50 Hz frequency

or alternate current of 50 Hz frequency in the coils of a device generating TMF.

The results of investigations about the influence of ferromagnetic properties of electrode wires and base metal on the components of induction B_x of constant and alternating TMF of 50 Hz frequency at the current in the coils $I_{\text{coil}} = 60$ A are presented in Figure 3. The obtained data show that using ferromagnetic wire and ferromagnetic plate of the component of the induction B_x in the zone under the end of the electrode is negligible, about 4 mT (Figure 3, *a*, curve 1). Using ferromagnetic wire Sv-08GA and plates of non-magnetic steel 12Kh18N10T, the component of induction B_x in the zone under the end of electrode has a value of an order 30–40 mT. Using electrode wire and base metal of non-magnetic materials the level of induction B_x of constant TMF (Figure 3, *a*, curve 3) is similar to the level, observed while using wire of ferromagnetic material Sv-08GA and base metal of non-magnetic steel 12Kh18N10T (Figure 3, *a*, curve 2). We supposed that level of induction $B_x \approx 30$ –40 mT in the zone under the end of electrode is sufficient for control of transfer of electrode metal drops.

The similar ferromagnetic properties of base and electrode materials influence the level of induction of alternating TMF of 50 Hz frequency. The component of induction B_x using electrode wire and base metal of non-magnetic materials practically coincides with the level obtained using ferromagnetic wire Sv-08GA and non-magnetic base metal of the steel 12Kh18N10T (Figure 3, *b*, curves 2, 3) and is considerably higher than that using ferromagnetic base metal and wire (Figure 3, *b*, curve 1), and this level of induction B_x (30–40 mT) is also sufficient to control the transfer of electrode drops in arc surfacing.

The influence of TMF on the coefficient of electrode metal melting α_{melt} in arc surfacing was defined according to the standard methods (by weighing method). The experimental surfacing procedures were performed using automatic machine ADS-1002 with the speed of electrode supply from the rectifier VDU-1202 independent of arc voltage (with falling external characteristics) at the reversed polarity on the plates of steel 12Kh18N10T. The wire Sv-08GA of 4 mm diameter and flux AN-348A, and flux AN-26P were used during surfacing using wire Sv-12Kh18N10T. The surfacing procedures were performed with and without impact of constant or alternating TMF of 50 Hz frequency. The recording parameters of surfacing mode (I_s , U_a) was performed using the devices of N390 type. In all experiments the parameters of the mode of surfacing without TMF were set preliminary according to the pointed indicators, and for $d_e = 4$ mm they were $I_s = 480$ –520 A, $U_a = 30$ –32 V, and $v_s = 27$ m/h. As far as during switching TMF the current of surfacing was decreased, the speed of electrode wire feed was increased to maintain arc voltage in the limits of $U_a =$

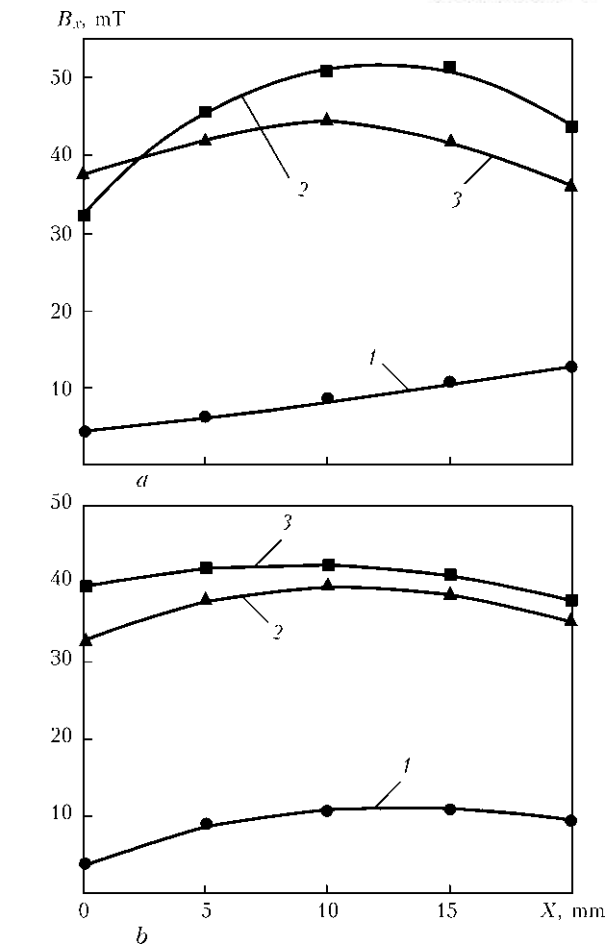


Figure 3. Distribution of induction B_x of constant (*a*) and alternating TMF of 50 Hz frequency (*b*) along the axis OX depending on ferromagnetic properties of welding wire of 4 mm diameter and base metal ($Z = 0$, $Y = 0$, $I_{\text{coil}} = 60$ A): 1, 2 – wire Sv-08GA; 3 – Sv-12Kh18N10T; 1 – plate 09G2S; 2, 3 – 12Kh18N10T

$= 30$ –32 V. The process of surfacing was not less than 30 s. Three surfacing operations were performed under each condition.

The data of investigations showed that during surfacing with the impact of both constant and alternating TMF of 50 Hz frequency and using ferromagnetic wire Sv-08GA at increase of induction B_x of TMF, the coefficient of its melting α_{melt} grows and at $B_x = 40$ –45 mT reaches maximal values (of about 17.5 g/(A·h)), while during surfacing without impact of TMF its values were 12.5–13.0 g/(A·h). Here α_{melt} of electrodes of ferromagnetic material (Sv-12Kh18N10T) grows at increase of induction of both constant and alternating TMF of 50 Hz frequency.

The increase of α_{melt} values of wires during surfacing with the impact of constant TMF is somewhat higher than during surfacing with the impact of alternating TMF of 50 Hz frequency (Figure 4, *a*). The maximal relative increase in α_{melt} ($\Delta\alpha_{\text{melt}}/\alpha_{\text{melt}}$) of wires of 4 and 5 mm diameters in surfacing with the impact of constant TMF is 27–30 % at the level of field induction $B_x = 40$ –45 mT, and for the wires of 3 mm diameter it is 23–25 % at the level of induction $B_x = 30$ –35 mT.

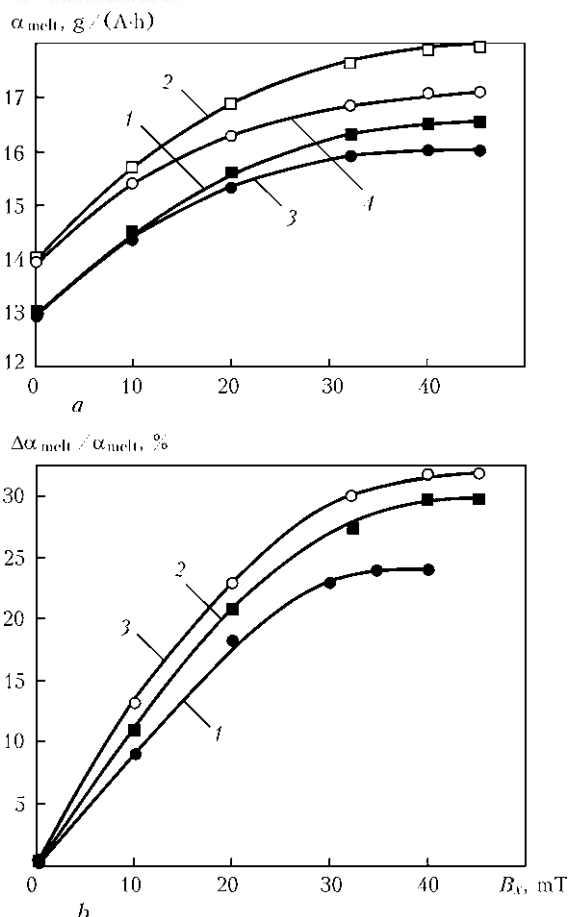


Figure 4. Influence of component of induction B_x of TMF on α_{melt} of electrode wires of 4 mm diameter (a) and increase in coefficient of melting of electrode wires $\Delta\alpha_{\text{melt}}/\alpha_{\text{melt}}$ (b): a: 1, 3 – Sv-08GA; 2, 4 – Sv-12Kh18N10T; 1, 2 – constant TMF; 3, 4 – alternating TMF of 50 Hz frequency; b: wire Sv-08GA, alternating TMF of 50 Hz frequency; 1 – $d_e = 3$ mm, $I_s = 340\text{--}350$ A; 2 – $d_e = 4$ mm, $I_s = 460\text{--}480$ A; 3 – $d_e = 5$ mm, $I_s = 700\text{--}720$ A

For the alternating TMF of 50 Hz frequency the relative increase in α_{melt} is accordingly 30, 25 and 20 % for the electrode diameters 5, 4 and 3 mm (Figure 4, b).

As is known [8, 9] the maximal increase in α_{melt} of a wire of 4 and 5 mm diameter in submerged-arc surfacing with the impact of longitudinal magnetic field (LMF) reaches 30 % (at reversed polarity of the process). Therefore, in submerged-arc surfacing at reversed polarity applying the impact of TMF the level of α_{melt} of wires grows practically to the same extent as in surfacing with the impact of LMF. It should be noted that during submerged-arc surfacing the impact of LMF does not increase the α_{melt} value of wires of non-magnetic materials [9], while the impact of TMF increases the α_{melt} value of wires both of ferromagnetic and non-magnetic materials.

The increase of α_{melt} of wires in surfacing in LMF occurs as a result of destroying (removal from the electrode end) of rotating drops [10]. At the impact of the constant TMF the drops are removed from the

electrode end (in a horizontal plane along the axis OY) under the action of electromagnetic force, formed by interaction of surfacing current (direction along the axis OZ) with the component of induction B_x of TMF directed along the axis OX . During surfacing at TMF of 50 Hz frequency the direction of electromagnetic force is changed influencing the electrode drop (by 180° along the axis OY). The efficiency of impact of electromagnetic force on the removal of electrode drops from the electrode end during surfacing with alternating TMF of 50 Hz frequency is probably less than during surfacing at constant TMF. This fact in our opinion stipulates the less effective increase of α_{melt} of electrodes during surfacing with the impact of constant TMF.

The process of arc surfacing at the reversed polarity using wire under flux with the impact of TMF allows reducing consumption of electric power for surfacing by 20–30 %, i.e. it is a power saving process.

CONCLUSIONS

1. In submerged-arc surfacing the increase of induction of both constant and alternating TMF of 50 Hz frequency in the zone under the electrode end results in growth of a coefficient of melting of wires of ferromagnetic and non-magnetic materials.

2. Maximal relative increase in α_{melt} of wires of 4 and 5 mm diameters during surfacing by impact of constant TMF is 27–30 % at the level of induction of field $B_x = 40\text{--}45$ mT, and for the wires of 3 mm diameter it is 23–25 % at $B_x = 30\text{--}35$ mT. For alternating TMF of 50 Hz frequency the relative increase in α_{melt} is 30, 25 and 20 %, respectively, for diameters 5, 4 and 3 mm.

1. Razmyshlyayev, A.D. (1994) Control of geometric sizes of weld in arc welding and surfacing by action of magnetic fields (Review). *Svarochn. Proizvodstvo*, **9**, 28–31.
2. Akulov, A.I., Kopaev, B.V. (1972) Magnetic control of arc in consumable electrode argon-arc welding. *Avtomatich. Svarka*, **7**, 39–42.
3. Demyantsevich, V.P., Lebedev, G.A., Maksimets, N.A. (1975) Effect of external magnetic field and welding parameters on weld formation. *Svarochn. Proizvodstvo*, **11**, 7–9.
4. Shejkin, M.Z., Varyakhov, N.F. (1969) Application of magnetic oscillations in submerged-arc welding. *Ibid.*, **6**, 24–25.
5. Gagen, Yu.G., Martynyuk, T.A. (1985) Magnetic control of weld formation in automatic submerged-arc welding. *Avtomatich. Svarka*, **11**, 73–74.
6. Razmyshlyayev, A.D. (2000) *Magnetic control of weld formation in arc welding*. Mariupol: PGTU.
7. Iofinov, P.A., Ibragimov, V.S., Dmitrienko, A.K. et al. (1991) Effect of electromagnetic field on melting rate of electrode wire in automatic submerged-arc surfacing. *Svarochn. Proizvodstvo*, **1**, 34–35.
8. Boldyrev, A.M., Birzhev, V.A., Chernykh, A.V. (1989) Increase in efficiency of electrode wire melting during welding in longitudinal magnetic field. *Ibid.*, **4**, 18–19.
9. Razmyshlyayev, A.D., Deli, A.A., Mironova, M.V. (2007) Effect of longitudinal magnetic field on the efficiency of wire melting in submerged-arc surfacing. *The Paton Welding J.*, **6**, 23–27.
10. Razmyshlyayev, A.D., Mironova, M.V. (2009) Calculation of parameters of longitudinal magnetic field providing removal of drop from electrode tip in arc surfacing. *Ibid.*, **7**, 26–29.

TECHNOLOGICAL PECULIARITIES OF CLADDING OF HIGH ALLOYS

I.A. BARTENEV

Karaganda State Technical University, Karaganda, Kazakhstan

Parameters of the technological operations in cladding of alloys of ferrous and non-ferrous metals with a high content of alloying elements are analyzed and generalized. It is shown that the required minimum dilution of the base metal with the high-alloyed deposited one can be achieved only in their separate melting. The most promising technologies for cladding of such alloys are plasma powder cladding and hybrid technologies.

Keywords: *cladding, high alloy, technological peculiarities, melting of filler metal, heating of base metal, penetration of base metal*

Cladding as a technological process for restoration of dimensions of parts and correction of cast defects is known from the end of XIX century [1]. However, a hardfacing, which provides increase of resistance of the parts in several times in comparison with their manufacturing from structural metals, is more efficient. The high alloys and alloys of ferrous and non-ferrous metals with special service properties which can be divided in following groups [2, 3] are used for cladding:

- chromium steels (5–30 % Cr);
- high-manganese steels (11–18 % Mn);
- high-speed steels (2–20 % W, 2–10 % Mo, 5–15 % Co, 3–5 % Cr);
- chrome-nickel austenite steels (12–20 % Cr, 8–25 % Ni);
- high-chromium cast iron (2–5 % C, 18–35 % Cr);
- nickel alloys (15–21 % Cr, 2–5 % Si, 3–30 % Mo, up to 15 % Co);
- cobalt alloys (25–33 % Cr, 3–25 % W, up to 3 % C);
- copper alloys (bronze, brass); carbide compositions (up to 3 % C, 25–33 % Cr, 30–70 % Co, 3–25 % W).

Cladding of the alloys is the greatest difficulty since there is a necessity in technology, modes and materials different from widely used in welding engineering. This is a result of increased susceptibility to crack formation during cladding of the high alloys, necessity in sufficiently accurate representation of required chemical composition of the deposited metal, high sensitivity to crack formation, increased oxidation of the alloying elements and liquation. Widely used methods of arc cladding, in particular for non-ferrous metals, usually do not provide necessary quality and being carried out in three-four layers for obtaining the necessary chemical composition and allowance for machining. The following technological measures were developed and used for elimination of the

negative effect of these factors in cladding of the high alloys:

- thorough surface preparation of the parts for cladding ;
- cladding technologies, providing minimum penetration of the base metal;
- secure protection of a weld pool from oxygen and hydrogen;
- preheating and delayed cooling after cladding;
- influence on initial structure of the deposited metal;
- heat treatment after cladding;
- deposition of intermediate sublayer.

Cladding of the high alloys, in particular, non-ferrous metals requires cleaning of the surface of the parts from oxide films and grease contaminations. Machining using metal cutting tools (cutters, millers and abrasive disks) with further degreasing by organic diluents or treatment by chemically active fluxes is used for this. Such a cleaning provides better spreading and wetting of the surface of part being deposited by liquid filler metal. This is, in particular, important in cladding with minimum and zero penetration of the surface when physics of the process becomes close to a brazing process.

Selection of a technology for cladding in most cases is caused by the necessity to provide accurate content of the alloying elements in the deposited metal from which the service properties of parts depend on. Penetration of the base metal and its dilution with deposited one should be close to zero. The following methods of cladding fulfill this requirement: plasma cladding; induction cladding by pouring of liquid filler metal; electrosag cladding by two electrode strips or using special activating fluxes; hybrid technologies of cladding.

Common physical and technological characteristic for these processes is division of melting of the filler metal and pre-heating of the base metal.

Cladding by means of liquid filler metal [4] was developed in the beginning of the 1940s. In it, the metal molten, for example, in an induction furnace or electric bowl, is poured on the surface of the part being heated up by low-current arc discharge. The efficiency is high at minimum penetration of the part

but additional electric equipment is required for that. This method found limited application for cladding of the small parts by fusible alloys, for example, by babbits for the inserts and bushes of friction bearings. Today this technology is used as a spinning or cladding as well as freezing-on cladding using boride fluxes for cleaning of the part surface from oxide films and its activation [3].

The plasma cladding with powder filler significantly differs from other methods of cladding on type of applied equipment, materials and technological possibilities [5]. Its main advantages are a high quality of formation and obtaining of required chemical composition already in the first layer; minimum penetration and thermal influence on the base metal; fine grained structure of the deposited metal; possibility of cladding of an alloy of any composition using filler powder obtained by liquid metal spraying; secure protection of metal drops and weld pool by inert gas.

The processes of interaction of liquid filler metal with tough base metal are influenced by temperature in a zone of cladding and chemical composition of metals. A depth of penetration is reduced using filler materials with lower melting temperature than in the part. The smaller depth of penetration can be obtained at higher temperature difference. An addition of the surface-active elements, for example, bore and silicon in cobalt-, nickel- and chromium-based alloys can significantly improve spreading of the liquid filler metal and wetting of surface of the part being deposited.

It was determined that melting temperature of the dispersed powder alloys is lower than that of the heavy-melting samples [6]. The reduction of melting temperature of the powder ΔT in comparison with melting temperature T of the solid (heavy-melting) sample can be determined by formula

$$\Delta T = 2T(\sigma_{1,3} - \sigma_{1,2}) / [\sigma_{1,3} - (\sigma_{2,3} + \sigma_{1,2})d],$$

where $\sigma_{1,3}$, $\sigma_{1,2}$ are the coefficients of surface tension of solid metal and melt, respectively; $\sigma_{2,3}$ is the coefficient of interphase tension on the solid metal–melt boundary; d is the diameter (size) of the powder particle.

Therefore, application of powders requires lower heat input in the filler and base metal then into cladding wires and strips of solid section that results in lower overheating and melting of the part surface.

Heating and melting of the base metal by heat of constricted arc is estimated by an effective efficiency which at plasma cladding makes $\eta_s = 0.68-0.72$. Only part of the effective power is used for heating and melting of zone of penetration. It is evaluated by thermal efficiency the values of which are determined experimentally [7] ($\eta_t = 0.32-0.34$). An area of penetration can be determined from formula

$$\eta_t = S_{pen} v_{r,c} \rho H_{melt} / (IU \eta_s),$$

where S_{pen} is the penetration area, cm^2 , equal Bh ; B is the width of penetration zone, cm ; h is the penetration depth, cm ; $v_{r,c}$ is the resultant speed of cladding, cm/s ; $IU \eta_s$ is the effective power of the constricted arc, W , equal q_s ; ρ is the metal density, g/cm^3 ; H_{melt} is the specific enthalpy of molten metal, including latent heat of melting, J/mol .

The largest amount of the particles of metal powder, supplied through the constricted arc, is introduced in the weld pool in form of drops. The biggest fractions of powder are already melted in the weld pool, but they become additional centers of crystallization or «microcooler» under certain modes of cladding and ratios of sizes (mass) of particles of the small and large fractions. This peculiarity of given technology results in refining of the cast microstructure and increase of mechanical properties of the deposited metal (Figure 1). A structural heredity in the powder for deposition–weld pool–deposited metal system [8] is observed.

The minimum sufficient values of penetration of the part surface (not more than 0.5–1.0 mm) is achieved in the plasma-powder cladding at portion of the base metal in the deposited γ_0 in the ranges from 2 to 8 %. Moreover, formation of a joint of deposited metal with the base one can occur similar to brazing, i.e. virtually without melting of surface of the base metal, during cladding of self-fluxing nickel-chromium alloys of Colmonoy type, containing 2–5 % B

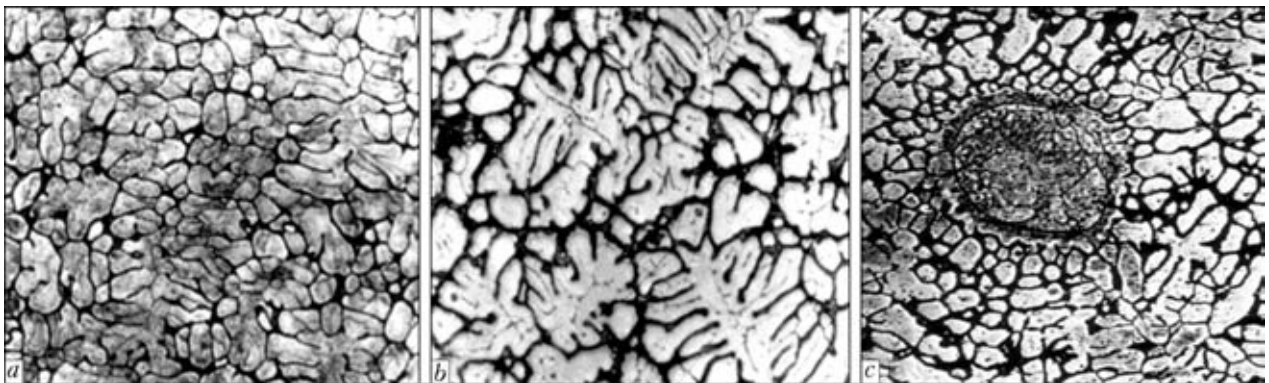


Figure 1. Microstructures ($\times 400$) of deposited high-speed steel 10R6M5 during introduction of the powder of large fraction into the filler powder of small fractions: *a, b* – cladding by mixture with addition of 30 % and 45 % of large fractions, respectively; *c* – non-melted particle of the powder (in the middle) at addition of large fractions

and 2–5 % Si and having melting temperature below than steel. Multiple tests and operation under industrial conditions of the parts of high parameter stop valves, metal-cutting tools (end-milling cutter, cutting taps, disk blades and cutters), parts of extruders, plugs and other parts, deposited with the help of plasma-powder technology, showed high adhesion strength of deposited to base metal.

Current intensity of a transferred arc has the most significant influence on value γ_0 in plasma-powder cladding as well as in all processes of arc cladding. This is, in particular, noticeable at small thickness of the deposited layer. Increase of mass velocity of the powder feed and thickness of the layer widens range of currents at which γ_0 lies in the ranges from 2 to 10 %, that is explained by reduction of direct influence of arc on the base metal.

Increase of consumption of the plasma gas has significant influence on penetration of the base metal. This is related with the level of arc constriction and, respectively, increase of the pressure of arc plasma on metal of the weld pool and penetration capability. Consumption of the transporting gas has similar but less influence. In this technology argon is used as a plasma, shielding and transporting gas.

There is no change of the penetration at reduction or increase of distance from plasmatron to part (arc length) in the plasma-powder cladding in comparison with traditional methods of arc cladding. Stability of transferred arc is preserved, but powder loss increases and shield of metal being deposited becomes worse at distance to the part more than 15 mm.

The mass velocity of powder feed is related with current intensity of the arc and cladding rate. The penetration rises at simultaneous increase of these three parameters of the process. The following formula [5] is proposed for determination of cladding rate:

$$v_c = G_f / \rho \mu B H,$$

where G_f is the mass velocity of powder feed, g/s; $\mu = 0.80$ – 0.85 is the coefficient of bead form at plasma-powder cladding; B , H are the width and height of deposited bead, cm.

The granulated powders of ferrous and non-ferrous metal, applied for plasma-powder cladding, are notable for variety of compositions and can be manufactured by spraying of any alloy, first of all alloys based on iron, nickel, copper and cobalt. Composition of the deposited metal in the first layer corresponds with chemical composition of the filler powder due to technological peculiarities of the plasma-powder cladding. At excellent formation of the deposited beads in most cases this allows using a single-layer cladding and significantly reducing allowances for further machining of the deposited part.

The fluxes for high-temperature brazing and alloys with melting temperature below than that of structural steels are used as a charge in induction cladding

[9]. Heating in the high-frequency field firstly melts the flux and then filler materials is melted and spread over the activated surface. The flux consists of borax, boric anhydride and silico-calcium and cleans surface of the part from oxide film. The process of induction cladding similar in this case to brazing and the possibility of dilution of the base metal with the deposited high alloy of Sormait type is eliminated by difference in the melting temperatures. The plough shares manufactured on this technology successfully operate under conditions of intensive abrasive wear.

Technology of the horizontal electroslag cladding by two strips, developed by Austrian company «Boehler» and PWI, is used for manufacture of the bimetal plates (low-carbon steel + stainless steel) [10]. Stable electroslag process takes place using fluoride low-silicon fluxes of AN-26P and 48-OF-10 types and weld pool level rises in 20–30 mm over the surface of the base metal in a gap between the strips. This allows reducing portion of the base metal in the deposited one up to 5–8 %. Smaller value of γ_0 can be obtained in electroslag cladding of copper on steel using fluoride and boride fluxes containing CaF_2 , NaF , KF , $\text{Na}_2\text{B}_4\text{O}_7$, B_2O_3 which activate the surface of the part and melt the filler metal [11]. The crack formation in steel on the fusion line and propping action of liquid copper, entering in these cracks (Rehbinder effect), is eliminated at that. The latter effect takes place in simple arc cladding with significant penetration. The plate electrodes and consumable nozzles in vertical position are used during this process at temperatures below melting temperature of low-carbon steel (1200–1350 °C).

The intergranular cracks usually propagating normal to the fusion line can be formed in the base metal during cladding of copper alloys on some steels. Application of a sublayer from chrome-nickel ferrite-austenite steel with content of not less than 40 % of ferrite phase in the structure completely eliminates possibility of formation of such cracks at further cladding of copper-based alloys on such a sublayer. Sometimes the necessity in sublayer can be caused by other reasons. For example, high thermal stresses, provoking failure as a result of thermal fatigue after effect of specific amount of cycles, appear during operation of the deposited part under conditions of thermal loadings due to differences in linear expansion coefficients of the base and deposited metals.

A method of cladding using a composite filler material, being developed in the Karaganda State Technical University, can be also referred to this group. Small penetration of the surface is observed only on the edges of the deposited bead of 23 mm width and 6.5 mm height (Figure 2, *a*) at distinguished fusion line in the middle part of the bead section. Hardness of the deposited metal (high alloy manganese steel) makes HRC 44–52 in the first layer. The microstructure contains quite fine dendrites growing from the surface of the base metal with high content of austenite and martensite (Figure 2, *b*).

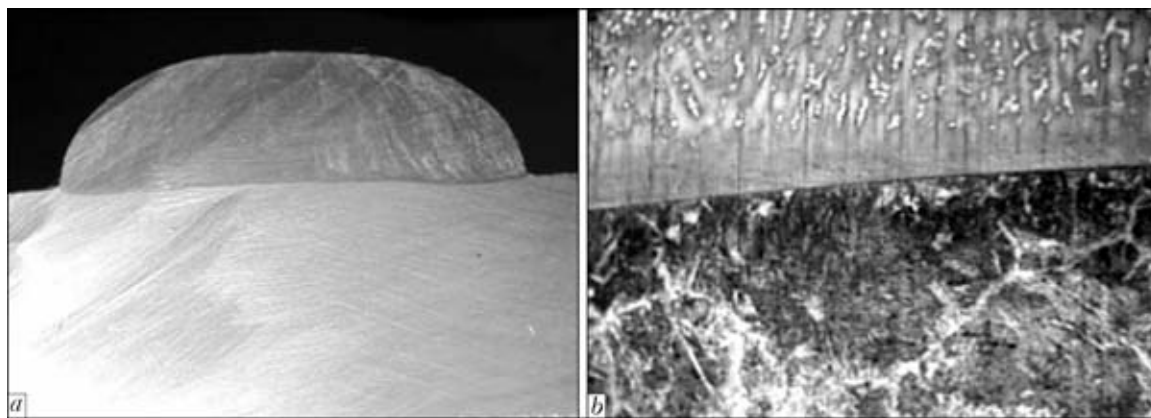


Figure 2. Macrosection of the deposited sample (a) and microstructure ($\times 400$) of high-manganese steel (on the top) deposited on St3 steel using combined filler metal

The heat treatment in the form of tempering is carried out in most cases after cladding of high alloys. A high tempering at 600–700 °C for 3–24 h is used for nickel-chromium alloys of NKh15SR2 type for redistribution of internal stresses in the dissimilar alloy joints. Short heat treatment in a form of two-, three-times repeated tempering at 560 °C is applied to high-speed steels after plasma-powder cladding of simple shape metal-cutting tools (disk cutters, cutters). Tempering reduces internal stresses in the high-speed steel, quenching in air during cladding, as well as increases secondary hardness up to *HRC* 63–64 for tungsten-molybdenum steels and up to *HRC* 66–67 for cobalt steels. Heat treatment of the high-speed steels is carried out at a complete cycle, annealing + quenching + + tempering, for such steels during cladding of workpieces of multiedge cutter.

CONCLUSIONS

1. Cladding of high alloys with minimum penetration of the base metal can be realized technologically and justified economically.

2. Separate melting of the filler metal and heating of the base metal are necessary for obtaining minimum dilution of the base and deposited metals.

3. The plasma-powder cladding is the most preferable for high alloys allowing easily regulating pene-

tration and depositing wide range of chemical compositions of ferrous- and non-ferrous based alloys with the help of powders, obtained by the liquid metal spraying.

4. Tempering is often used for reduction of the residual stresses in high alloy deposited metal.

- (1982) Scientific-technical inventions and projects. In: *Select. works of N.N. Benardos*. Kiev: Naukova Dumka.
- Frumin, I.I. (1961) *Automatic electric arc surfacing*. Kharkov: Metallurgizdat.
- Ryabtsev, I.A. (2004) *Cladding of machine parts and mechanisms*. Kiev: Ekotekhnologiya.
- Nikitin, V.P. (1956) Investigations of new methods for increase in welding productivity and quality based on principle of separate control. In: *Problems of arc and resistance electric welding*. Kiev: Mashgiz.
- Gladky, P.V., Pereplyotchikov, E.F., Ryabtsev, I.A. (2007) *Plasma cladding*. Kiev: Ekotekhnologiya.
- Patskevich, I.R., Deev, G.F. (1974) *Surface phenomena in welding processes*. Moscow: Metallurgiya.
- Sidorov, A.I. (1987) *Recovery of machine parts by spraying and cladding*. Moscow: Mashinostroenie.
- Ryabtsev, I.A., Pereplyotchikov, E.F., Mits, I.V. et al. (2007) Effect of initial structure and particle size composition of powder on structure of metal 10R6M5 deposited by the plasma-powder cladding method. *The Paton Welding J.*, **10**, 18–22.
- Tkachev, V.N., Fishtejn, B.M., Kazintsev, N.V. et al. (1970) *Induction cladding of hard alloys*. Moscow: Mashinostroenie.
- Frumin, I.I., Kalensky, V.K., Panchishin, Yu.A. et al. (1977) Development of the process and analysis of some technological specifics of electroslag cladding with strips. In: *Theoretical and technological principles of surfacing*. Kiev: PWI.
- Lychko, I.I. (1969) *Electroslag cladding of copper and its alloys on steel*. Kiev: UkrNIINTI.

CHAMBERS FOR EXPLOSION WELDING OF METALS (REVIEW)

P.S. SHLENSKY, L.D. DOBRUSHIN, Yu.I. FADEENKO and S.D. VENTSEV
E.O. Paton Electric Welding Institute, NASU, Kiev, Ukraine

Existing protection equipment and explosion chambers for explosion treatment of metal are analysed. The focus is on metal chambers for explosion welding. Advantages and drawbacks of different designs of the chambers and prospects for their upgrading are outlined.

Keywords: *explosion welding, explosion chamber, tubular explosion chamber, explosive*

Explosion welding (EW) has been applied to advantage for about half a century in different industries. The volume of products manufactured by using this technology is growing every year. The range of products manufactured by EW is also continually growing. Reportedly, today in the world there are over 20 organisations working in the EW field, and more than 40 organisations applying other explosion technologies [1]. The continually growing demand causes increase in the need for the EW equipment.

The EW process can be performed in open grounds, for which the necessary conditions are availability of large sites and remoteness from inhabited localities. As this is inseparably linked with substantial costs of transportation and increase of production prices, the favoured variant is the use of workshop explosion areas. The adverse by-factors in EW are air shock waves, noise and pollution of the environment with toxic explosion products. Therefore, the efforts on development of various devices and explosion chambers for protection from the damaging factors of explosion were initiated simultaneously with the emergence of EW.

Different methods are employed to localise the damaging factors of explosion, the simplest being filling (tamping) the external explosive charges [2] with inert materials. Reduction of the intensity of shock waves in case of using tamping is caused by consumption of part of the energy of a charge for crushing and scattering of the tamping material. The key drawbacks of this method are increased pollution of the environment with the explosion products and need to make tamping for each explosive charge.

Water curtains can be used to reduce the intensity of shock waves. For example, Company «DMC Nitro Metal» (Sweden) uses a water curtain formed in air by spraying water with an additional low-capacity explosive charge blown up with some lead [3]. This method is less labour-consuming than tamping, but it has the same drawbacks.

The phenomenon of intensive damping of shock waves in foams [4], which are the 3–5 % water solution of a surface active material, was discovered in the course of work conducted by the E.O. Paton Electric Welding Institute in 1973. The foam absorbs toxic gases and dust particles, damps noises, but it does not solve the problem of decreasing seismic disturbances and protection from splinters.

Of interest are devices used to damp shock waves in mines. As to the method used to reduce the shock waves, they are subdivided into solid, perforated and disintegrating. Solid barriers damp the waves completely, whereas perforated and disintegrating – partially. The solid barriers include steel doors and concrete flat arches, which damp the waves due to their reflection from the arch faces and subsequent interaction of the resulting reflected waves [5]. The perforated barriers have holes and labyrinths for the air flow, the shock wave damping factor achieved in this case ranging from 1.1 to 2.9, depending on the perforation degree [6]. An example of the perforated barrier is a screen made from steel or hemp ropes with wooden posts or conveyer belt strips interweaved into it to raise the efficiency of damping of the shock waves.

Used mine works, mines, tunnels of other subsurface structures that served their time have found application for arrangement of sites for explosion treatment of metals. The advantage of such sites is that performing the work in them does not depend on the season, time of day or weather conditions. Temperature, humidity of air and its composition remain constant in a subsurface ground, which permits optimising the technology and producing items of the improved quality. Natural vaults of the subsurface ground protect the industrial and civil structures in the neighbourhood of the ground from the effects of the shock waves and reduce the level of noise pollution.

Despite the positive experience of using mine works for explosion treatment of metals, it should be noted that they are usually situated in the mining regions, rather than in the developed engineering regions. This causes difficulties related to transportation of raw stock, explosives and other required materials

to large distances. Arrangement of subsurface grounds involves difficulties with shipments within the site and problems of the sufficient strength of the vaults. Another difficult problem is ventilation of the interior after explosion and prevention of increased humidity.

One of such grounds is situated in subsurface stone pits in the state of Pennsylvania (USA), and is employed by the DMC Company. The plates assembled for welding and put on a massive platform are fed to the explosion tunnel chamber by railway lines fitted with a reliable damper. After explosion and purging, the platform with a clad piece is rolled out from the tunnel chamber [7].

Building of the explosion chambers and equipment allowed the metal treatment processes to be performed in a workshop. Initially, the attempts were made to build concrete explosion chambers. They remained intact somewhere and are still in operation. Such chambers are cumbersome and look like a thick-walled round building with a dome-shaped roof. Construction of such a chamber requires high material costs, while the permissible value of an explosive charge is low [7]. Therefore, now the concrete chambers are abandoned, and metal explosion chambers are built instead. The latter can be located both in grounds and in workshops.

Despite a wide variety of the above protection means, the metal explosion chambers are the best choice for mass production of small-size items.

One of the first Ukrainian explosion chambers was a vacuum chamber fabricated and employed at the Kharkov Aviation Institute [8]. The chamber was intended for sheet-metal forming by using charges with up to 2 kg of explosive. Physically, it had the form of a cylindrical shell with a 3 m diameter and 2.5 m high cap and a support, on which it was possible to mount a mandrel with a diameter of up to 2 m. The chamber had no loading hatch, and access to the mandrel was provided by removing the shell with the help of a telpher.

At present, explosion forming is carried out by using different types of the explosion equipment. Each type of the equipment has its own technological pe-

culiarities, advantages and drawbacks, which depend on the operations performed (drawing, expansion, sizing). The work performed by the Kharkov Aviation Institute, generalisation of the experience accumulated by the CIS factories that apply explosion treatment of metals, and analysis of potentialities of each type of the equipment as to dimensions of workpieces, power consumption, service properties, classes of workpieces, price and productivity made it possible to work out requirements [9] to all types of the equipment:

- operating reliability, strength and durability;
- minimal capital expenditures for their construction;
- possibility of using them to form pieces with a wide variety of dimensions;
- convenience and simplicity in operation.

Main types of the hydraulic explosion equipment include hydraulic explosion pools, armour pits, armour chambers and vacuum chambers. The pools are the basic equipment for hydraulic explosion treatment. They are meant for accommodation of a transmitting medium (water) and performance of an explosion safe for the attending personnel. The pool is a steel cylindrical or conical water-filled shell, which is strengthened by reinforced concrete. The die with a billet and an explosive charge fixed on it is placed at the centre of the pool on a bottom steel plate resting on a concrete anvil block. The anvil block and walls of the pool are insulated by a hydraulic seal located between them.

As proved by practice, the armour pits with concrete walls have short service life, as concrete quickly crumbles out under the explosion load effect. Sometimes the use is made of the structures wherein the armour pit walls are made from concrete protected by metal plates from the effect of the shock waves. Wooden armour pit have walls made in the form of two cribs of logs with a diameter of 15–20 cm. In operation, the armour pits should be carefully ventilated from gaseous explosion products [7].

A large scope of theoretical and experimental works on strength design and calculation of shells, hatches, supports and other facilities was completed by the Technological Design Institute of Hydro-Pulse Techniques of RAS SB (KTI GIT) [10]. Explosion chamber KVG-16 for treatment of extended pieces has a horizontal cylindrical shell (1.6 m diameter, 0.09 m thick and 8 m long) designed for blowing up of a charge with a capacity of up to 16 kg of explosive (Figure 1). The chamber has a hatch with two lids, i.e. the internal (load-bearing) lid that takes up the main load during explosion, and the external (sealing) lid. The chamber houses a work table (support) made from metal plates with rubber gaskets, the important drawback of which is a short service life of the upper plate that withstands a limited number of explosions. The special manipulator is used to load the chamber.



Figure 1. Explosion chamber KVG-16 with pulled out work table

It pushes a workpiece with the charge into the explosion chamber. The external lid is opened by using a hydraulic cylinder, and the internal one is opened and closed by the manipulator rod. The chamber is fitted with an emergency hatch. Such chambers are applied at the Novosibirsk Switch Factory.

Semi-automatic chamber VK-10 made on the basis of the experience accumulated by Scientific Production Association «ANITIM» (Barnaul, RF) can serve as an example of the modern spherical explosion chamber for explosion treatment of metal (Figure 2) [11]. The chamber 280 t in weight is designed for 20 kg of explosive. The chamber is 10.5 m in diameter, and its casing wall thickness is 20 mm.

Unique chamber 13YaZ mounted on a special foundation (Figure 3) is a high-capacity spherical explosion chamber. It functions at the Moscow Regional Shared-Use Explosion Center of the Russian Academy of Sciences (SUEC) [12]. The chamber is an ideal sphere 12 m in diameter (the difference in diameters at several points is no more than 3 mm). The casing of the chamber is made from armour steel 100 mm thick. Its weight is about 500 t, and weight of its foundation is 320 t. The chamber has two loading hatches, i.e. the top one with a diameter of 600 mm, and the bottom one with a diameter of 800 mm. It is designed for blowing up of 1000 kg of explosive, and it successfully passed the tests. However, the chamber is intended for research purposes to study explosions in fuel gas mixtures and is of little use for industrial purposes.

Some chambers have structures with multilayer shells. For instance, a two-layer cylindrical chamber with a capacity of 110 m³, consisting of two metal cylinders with a wall thickness of 50 mm, the 350 mm thick gap between which is filled up with steel shot, is in operation at SUEC. The chamber is designed for blowing up of 50 kg of explosive.

The chamber intended for explosion welding of pipes is characterised by the special loading and sealing methods [13]. The ends of its horizontal cylindrical shell have coaxial holes for loading of the pipes to be welded and explosive charges inside it. The gap between the pipes and shell is sealed with a water curtain.

Explosion protection chambers (anti-diversionary units) have found acceptance along with the conventional explosion chambers of the research and industrial application. As a rule, these chambers are of a rectangular shape, can operate in the standby mode, and are not re-used after blowing up of a limiting weight of explosive [10]. Such chambers are unsuitable for explosion treatment of metal.

In the 1970s, the E.O. Paton Electric Welding Institute developed a fundamentally new design of a high-capacity explosion chamber designed for the explosive charges of up to 200 kg. The casing of the chamber is made from fragments of tubes plugged from the outside, the axes of which intersect at the



Figure 2. Semi-automatic explosion chamber VK-10

chamber centre. Strength and high lag effect of the tubular casing are provided by the presence of a sufficient number of rigid connections between the tubes, and by filling the inter-tube space with sand. The main advantages of this structure are a high technological effectiveness, thus allowing it to be manufactured from mass-produced gas distribution tubes, and reparability.

Two high-capacity (for 200 kg of explosive) tubular explosion chambers (TEC) were built. The first was made at Research and Engineering Centre «Explosion Treatment of Materials» of the E.O. Paton Electric Welding Institute (Glevakha, Kiev Region) (Figure 4), and the second — at Design Bureau «Yuzhnoye» (Dnepropetrovsk).

The drawback of the TEC design is a long time of operations of loading and unloading of billets, which makes these units insufficiently effective for commercial application. In this connection, in 2009–2010 Research and Engineering Centre «Explosion Treatment of Materials» developed and mounted TEC with a semi-automatic mechanism for feeding and unloading of billets (Figure 5). This chamber is an upgraded scaled (1:5) model of TEC and designed for blowing



Figure 3. SUEC unique spherical explosion chamber 13YaZ

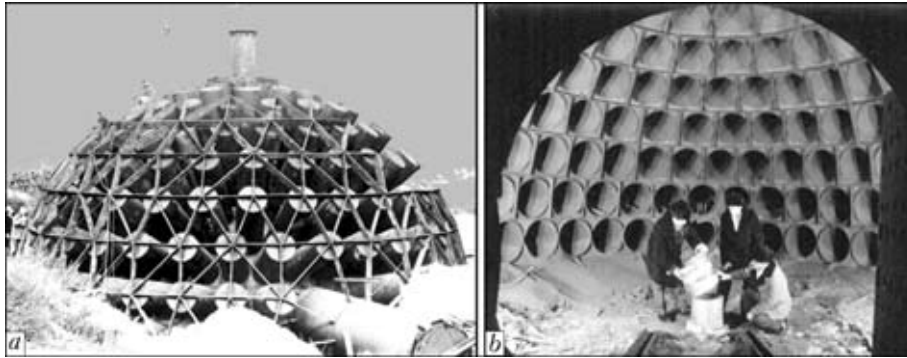


Figure 4. Tubular explosion chamber for 200 kg of explosive (Glevakha): *a* — view during construction; *b* — inside view

up of up to 2.4 kg of explosive. According to the principle of scale modelling, the M 1:5 chamber corresponds to a chamber for 300 kg of explosive in M 1:1.

The scaled model of TEC is a three-stage welded structure with an inside diameter of 2 m. The main (middle) stage consists of 283 sections of steel tubes with a diameter of 140 mm, length of 600 mm and wall thickness of 4.5 mm. The external stage is composed of bottoms 8 mm thick, plugging tubes and steel braces with a diameter of 16 mm, which connect tubes to each other (so-called «bundles», looking like hand-sets). The internal stage consists of the hemispheric sectors 8 mm thick, which connect inlets of the tubes and form a perforated internal hemispheric shell. Weight of the chamber casing is 3.6 t. Therefore, the ratio of the metal weight in tons to the permissible weight of explosive in kilograms is 1.5.

Now the phase of development of a general-application explosion chamber can be considered completed. The main types of such chambers (spherical, cylindrical, tubular) and peculiarities of gas-dynamic processes and dynamics of structures in them have been identified, this providing the scientific basis for design engineering [10]. What is lacking for completeness is statistics of damages and failures, which would

allow formulating the procedure for evaluation of reliability and durability of an explosion chamber under the regular operation conditions. The first attempt to develop such a procedure was made in study [11]. However, it is based on the statistical data generated from operation of welded structures, and not from tests of the explosion chambers.

The next phase of development is to build single-purpose explosion chambers as an element of equipment for large-scale manufacture of standard products (in explosion forming this phase began already in the last century). The following problems will remain topical for single-purpose chambers:

- improvement of systems for automatic loading and unloading of billets and ventilation of the interior of an explosion chamber to reduce the time interval between explosions; and
- lowering of the level of noise and seismic effect.

One of the specific features of explosion welding in chambers is the use of flat explosive charges, the size of which is commensurable with the size of an explosion chamber. This excludes the possibility of using of the spot charge and spherical/cylindrical symmetry simplifications, which are very convenient for theoretical analysis. It is well-known that a spherical explosion chamber should have a minimal weight for the specified weight of a maximum permissible explosive charge. For cylindrical symmetry this indicator is a bit higher. And for large flat charges it grows several times [10], which was also proved by our measurements in the chamber. Therefore, an explosion chamber for explosion welding should have specific design peculiarities that make it different from conventional chambers. The problem of designing of such chambers is far from being solved as yet.

Another peculiarity is the use of explosives with inert fillers (sand, most often). This allows reducing the weight of an explosive and level of noise, but hampers ventilation of the interior of the chamber and increases emission of environmentally harmful impurities into the atmosphere.

Finally, explosion welding is characterised by increased requirements to a material and design of the support. It should feature a good absorption of dynamic impact energy and have an ability of being



Figure 5. General view of semi-automatic tubular explosion chamber

deformed uniformly, as much as possible, over the entire surface area to minimise residual distortions of large-size flat pieces. At present, metal shot is considered to be the best material for supports. It provides a lower level of residual distortions compared to other materials. However, further decrease of residual distortions is still a topical problem.

Another pressing problem is the possibility of evacuation of explosion chambers. It is reported that evacuation improves the quality of explosion welded joints. At the same time, it makes design of the explosion chambers more complicated and more expensive, and reduces their productivity.

In the future, application of special workshop automated explosion chambers will lead to increase in output of thin-sheet bimetal for its subsequent utilisation to manufacture elements of machines and devices, as well as bimetal of any combination and thickness, including for further rolling.

1. Banker, J.G. (2009) Industrial applications of explosion welding (Review). *The Paton Welding J.*, **11**, 42–46.
2. (1992) *Unified safety regulations in explosion operations*. Kiev: Normativ.
3. Bogrovsky, Ya., Fruchek, M., Korzun, M. (1976) Some problems related to increase in explosion effects. In: *Proc. of 3rd Int. Symp. on Application of Explosion Energy for Fabrication of Metallic Materials with New Properties by Welding, Cladding, Hardening and Explosion Compacting of Powders* (Marianskie Lazni, 19–22 Oct., 1976), 515–522.
4. Kudinov, V.M., Palamarchuk, V.I., Gelfond, B.E. (1977) Damping of shock waves by foams. In: *Application of explosion energy in welding technique*. Kiev: PWI.
5. Gurin, A.A. (1978) *Control of shock waves in explosion operations*. Moscow: Nedra.
6. (1974) *SN 453–73: Recommendations on designing of shelters located in mine working*. Moscow.
7. Krupin, A.V., Soloviov, V.Ya., Popov, G.S. et al. (1991) *Explosion treatment of metals*. Moscow: Metallurgiya.
8. Bazhin, I.I., Stukalov, N.G., Chebanov, Yu.I. (1970) Experience of designing of vacuum chambers in units of the workshop type. *Impulsnaya Obrab. Metallov Davleniem*, Issue 1, 84–87.
9. Krivtsov, V.S., Borisevich, V.K. (2007) State-of-the-art and prospects of application of pulse power sources for technological processes of materials treatment. *Aviats.-Kosmich. Tekhnika i Tekhnologiya*, **47**(11), 10–17.
10. Demchuk, A.F., Isakov, V.P. (2006) *Metallic explosion chambers*. Krasnoyarsk: RIO KrasGU.
11. Nikolaenko, P.A. (2010) *Stress-strain state and strengthening of metallic explosion chambers: Syn. of Thesis for Cand. of Techn. Sci. Degree*. Moscow.
12. (2009) Moscow Regional Shared-Use Explosion Center of the Russian Academy of Sciences (SUEC). *The Paton Welding J.*, **11**, 77.
13. Willian, F., Howel, G. *Explosive welding device*. Pat. 3848794 USA.

From the history of welding

TO 130th ANNIVERSARY OF THE FIRST METHOD OF ARC ELECTRIC WELDING

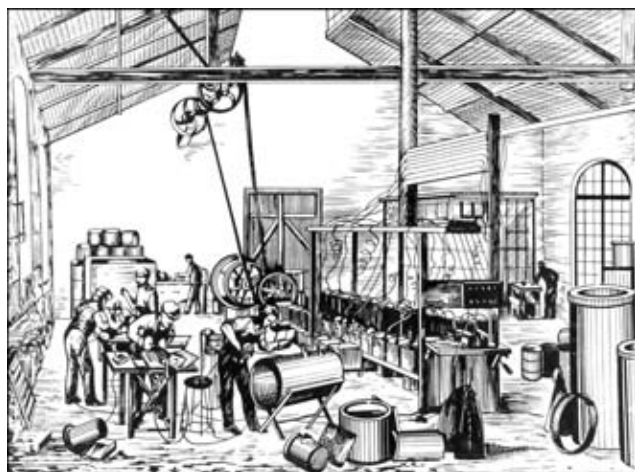
In 1881 the electrical engineers, who came to Paris to attend the International Electrical Engineering Exhibition, watched Nikolas de Benardos, colleague of P.N. Yablochkov, the famous inventor of «Russian light», performing brazing-welding of different exponents by heating parts using electric arc in the laboratory of N.I. Kabat. In a facsimile list Benardos noted that projects and inventions from Nos. 21 to 39 (1877–1881) were made in St. Petersburg; 40 to 42 – in Zakaspijsky region, where the company of Yablochkov implemented the electricity, and 48 to 54 – in Paris. No.46 stated «Electric brazing of metals, electrogefest». The considerable part of this list contains inventions in the field of electric engineering: corrugated batteries, electric arc lamp, candlestick for the candle of Yablochkov with automatic switch of a current, battery of powder of crystal lead, commutator for filament lamps, etc.

The life and activity of the inventor of the first method of a new type of joints attracted attention after 50 years when the arc welding turned into the leading technology of manufacturing the critical metal structures due to efforts of many inventors, scientists, rationalizers.

Nikolay N. Benardos was born in July 26 (August 7), 1842, in the village Benardosovka (now village Mostovoe of Bratsk district of Nikolaev region, Ukraine) in the family, coming of military servants of Greek origin.

Being a child he learned at home in Benardosovka. He learned not only reading, writing and different languages, but also forgery and joinery at the splendid grandfather's workshop. He entered medical faculty of Kiev University, then he was transferred to Moscow Petrovsko-Razumovskaya Agricultural Academy.

In 1869 he left to register his mother's heritage (a land in 12 km from town Lukh of Kostroma province, Russia) and stayed there. He built a house, workshops, greenhouse, also helped in building school and drug-



Print «The first welding workshop «Electrogefest» at the works Creuzot (1890, France)

store. Being elected to the Zemstvo Assembly (elective district council in pre-revolutionary Russia) of Yurievets uyezd (district) he struggled for free education and medical care. Then he was put to prison for about a year. In newspapers he discussed problems of aeronautics, medicine, agriculture, claimed for different inventions and suddenly went bankrupt. In 1877 he moved to St. Petersburg and took a great interest in electric engineering.

Most probably that the first method of arc welding was created by Nikolay Benardos in St. Petersburg, where the laboratories and industrial facilities of the Electric Lighting Company «P.N. Yablochkov the Inventor and Co» were sufficiently equipped for manufacturing batteries with corrugated plates suitable for welding, controllers of welding current, water rheostats, holders, etc. He brought to Paris a ready-made equipment and mastered technology. However, he started patenting his invention only in 1885 and within three years he was granted patents of many European countries and the USA. The reason for delay was paying a great fee and need in funds for realization (implementation) of invention. If the service within a short term (1–3 years) was not established, the patent would be abated. That is why most inventors were unhurried to register their developments.

In 1884 the mansion «Privolnoe» with all premises in Lukha, mortgaged in a hypothecated bank, was sold to pay for the debts. The rest of money Benardos used for patenting in Russia (including also electric arc welding). The patenting abroad was financed by a merchant S.O. Olshevsky, who became a co-owner of the patents.

The solemn procession of «Electrogefest» was described in many books and articles. However some adventurers took a possession over the patents of Benardos and his model workshop of welding works, the first in the world created by him and the society «Electrogefest» (on operation and implementation of electric welding and other inventions) in 1885. The owners of the society did not wish to spend money to improve welding and Nikolay Benardos continued improving the equipment, torches, devices and welded

joints for his own money. The possibilities of welding as an independent operation in modeling are disclosed in the patent of Benardos titled as «microcasting» or «metallic modeling». To enhance quality of weld metal he applied magnetic control, flux-cored wire, shielding gas and other. Hoping to receive a governmental order he developed a project of repair of the Tsar Bell (Moscow Kremlin) and a rise to the bell-tower.

Since the beginning of 1883 Benardos worked in London and other cities of Great Britain, improving equipment and process of welding. Already in the late 1880s the equipment and technology for arc welding were implemented in different fields of industry in France, Spain, Great Britain, Germany, the USA and other countries.

At the end of 1890s the health of inventor became worse, he passed a long treatment in Moscow, lived with his son and then decided to settle in Kiev province in the village Byshev near Fastov. Being on the summit of glory the famous inventor left without a penny. Sometimes the seriously ill Nikolay Benardos could not afford his daily bread, but as soon as he got money he spent them on different materials and started working on the new invention. In 1902 the house and household premises were set on fire by some peasants from neighborhood. All the drawings, documents, mockups were burnt. After the fire he moved to Fastov where he worked at the boiler works and locomotive depot. In September 8 (21), 1905, Benardos died. Nobody knows about the place of his burial. Neither magazines nor newspapers informed about the death of the author of more than two hundred inventions and projects in the field of electrical engineering, electric technologies, agriculture, military affairs, transport, aeronautics, household, building and medicine.

Basing on the documents prepared by the E.O. Paton Electric Welding Institute, UNESCO included the historic event — «100-anniversary of invention of welding by Benardos» to the «Calendar of memorable dates in 1981» on the representation of Ukrainian SSR.

On May 18–21, 1981 the solemn meeting and scientific conference were held in Kiev. In Fastov the monument was unveiled and in Pereyaslav-Khmelniysky the museum was opened. The similar events were held on June 11–13, 1981 in Ivanovo and Lugh. The information about Benardos in a form of a post stamp and special envelopes was enlisted to descriptions of philatelic catalogues of the world. The movie about Benardos was many times demonstrated by the Central TV. Many scientists supported the idea of holding the conferences «Benardos readings» every two years in Ivanovo, Kiev and Nikolaev in turn. The scientific magazines of many European countries published articles about the history of inventing the electric welding. And in 1985 in Great Britain the large International Conference took place devoted to the hundred anniversary of granting the first patent in the world on electric welding to Benardos.

Prof. A.N. Kornienko, PWI

INTERNATIONAL SCIENTIFIC-PRACTICAL SEMINAR IN KIEV

International Scientific-Practical Seminar «Application of Flash Butt and Combined Flash Butt + Arc Welding of Large-Diameter Pipes» was held on 13–14 April 2011 at the E.O. Paton Electric Welding Institute. The purpose of the Seminar was to discuss results of cooperation between the E.O. Paton Electric Welding Institute (Ukraine), Company «KZU Group Engineering Ltd.» (Bulgaria), Closed Joint Stock Company «Pskovelektrosvar», Open Joint Stock Company «Gazprom» and the Bauman Moscow State Technical University (Russia) with the assistance of scientists of the Ghent University (Belgium). «Automaticheskaya Svarka» journal acted as an information partner of the Seminar.

The Seminar was attended by about twenty specialists in welding, non-destructive testing, materials science, design and calculation of welded structures. The Seminar was held in a format of presentations and subsequent exchange of opinions of the participants on each of the presentations.

Opening the Seminar, Prof. S.I. Kuchuk-Yatsenko, Academician of the National Academy of Sciences of Ukraine, noted an intensive construction of a new generation of pipelines intended for increased pressures, taking place in the last decade. The pipelines are made from thick-walled high-strength steel pipes. Construction of such pipelines is characterised by a substantial increase in requirements to the quality of welded joints, as well as labour intensiveness. In this connection, improvement of the available technologies and development of the new ones for automatic position butt welding of pipes are among the hottest areas in current research. The successful experience of using flash butt welding for construction of main pipelines in the 1980s is indicative of the enormous potential of this welding method, which has been underutilised in the last one and a half–two decades.

The Conference included discussion of the presentations made in three areas: «Flash Butt Welding Technology and Equipment», «Methods for Non-Destructive Testing of Welded Joints on Pipelines», and «Current Approaches to Evaluation of Mechanical Properties of Circumferential Joints on Pipelines».

Lively discussions took place on almost all of the presentations, this evidencing a considerable interest of participants of the Seminar in scientific and practical problems of application of flash butt welding for construction of modern pipeline systems.

Increase of working pressures in large-diameter pipelines and utilisation of new high-strength steel grades required improvement of service characteristics

of the welded joints, development of new technological approaches and building of a new generation of equipment for welding of pipes.

The presentation made by Yu.V. Shvets, staff scientist of the E.O. Paton Electric Welding Institute, was dedicated to upgrading of the technology for flash butt welding of thick-walled pipes. As shown by analysis of the results of tests of over 1000 welded specimens, the use of the developed modes of flash butt welding and subsequent local induction heat treatment provides sound welded joints on large-diameter pipes. Mechanical properties of the welded joints, including impact toughness at low temperatures, meet requirements of American standard API 1104, Norwegian standard DNV OS F101 and Russian standard STO Gazprom 2-2.2-358–2009.

The issues of building of the fundamentally new equipment for flash butt welding of main gas and oil pipelines (including off-shore gas pipelines) were covered in the paper presented by V.I. Khomenko and D.M. Gudkin, specialists of «Pskovelektrosvar». It was noted that the Plant, in collaboration with the E.O. Paton Electric Welding Institute, «Gazprom» and «Gazprom VNIIGAZ», and the Bauman Moscow State Technical University, is currently addressing the problems of both upgrading of the earlier produced flash butt welding machines and development of the fundamentally new systems for welding, heat treatment and non-destructive testing of the welded joints. Much work has been completed in the last years, allowing the baseline models of a new generation of welding and auxiliary equipment to be designed for flash butt welding of large-diameter pipes. Results of one of the developments of the Plant were demon-



Working fragment of the Seminar



Success of cooperation is based on united efforts

strated in a video showing operation of a new system for welding of 1220 mm diameter pipes.

V.G. Krivenko, Director of Engineering Centre «Pressure Welding», presented the data on building of mobile pipe welding systems, allowing the entire package of welding and auxiliary operations to be performed under semi-stationary and field conditions. Such systems for flash butt welding of rails have been successfully functioning for many years in many countries all over the world. Peculiarities of the new systems for welding of small- and medium-diameter pipes, fitted with the new-generation welding machines, were presented. These machines are characterised by the use of modern electric and hydraulic drives, as well as computerised systems for control and monitoring of the welding process parameters.

The papers presented by V.I. Kyrian and Yu.V. Shvets, scientists of the E.O. Paton Electric Welding Institute, dedicated to investigation of impact toughness properties of the base metal of modern pipe steels and flash butt welded joints caused active discussions among participants of the Seminar. Modern pipe steels are known to have marked mechanical, structural and chemical heterogeneity, as well as different values of impact toughness of the base material tested in different directions (along and across the rolling direction). As shown on the basis of analysis of a substantial volume of experimental data, evaluation of impact toughness of the welded joints by the sharp notch procedure yields inadequate information on operating reliability of the welded joints.

Presented were the investigation results on evaluation of impact toughness of the flash butt welded joints, including by using a fundamentally new procedure of three notches (3V). Compared to the standard Charpy method, this procedure allows a more precise evaluation of impact toughness of the welded joints with a pronounced mechanical heterogeneity. Participants of the Seminar supported the opinion on the necessity to activate the work on preparation of a standard regulating application of the 3V procedure

to evaluate tough-plastic properties of the flash butt welded joint.

Results of the work on investigation of combined welding of pipelines were presented in a paper by B.I. Kazymov (E.O. Paton Electric Welding Institute). It is a known fact that making of the root weld in position butt arc welding of pipes is traditionally a serious technical problem. The idea of combined welding consists in using flash butt welding for making the joint on the internal part of the pipe sections and subsequent filling up of the groove by arc welding. As shown in the paper, this technology holds high promise for construction of pipelines with a wall thickness of more than 20 mm.

Results of cooperative investigations of the E.O. Paton Electric Welding Institute and «Pskovelek-trosvar» are indicative of high mechanical properties of the combined welded joints. The set of values of mechanical properties of the combined welded joints meets requirements of both international (API 1104) and Russian standards. To define the application field for the combined flash butt + arc welding technology (for steels of different strength grades and manufacturing technologies), it seems reasonable to continue investigations on evaluation of quality of the combined welded joints in cooperation with the Ghent University and «Gazprom VNIIGAZ».

Participants of the Seminar expressed high interest in the opinion of the specialist of the Ghent University Dr. Rudi M. Denys on all of the discussed issues. The main idea of the paper presented by Dr. R.M. Denys consisted in the necessity to apply an integrated approach to ensuring reliability of the welded joints on pipelines, including the requirement to allow for the specific values of mechanical properties of modern pipe steels, values of strength, ductility and toughness of metal within the welded joint zone, as well as the level of residual welding stresses.

The issues of non-destructive testing of the welded joints on pipelines were considered in the papers by M.V. Grigoriev (Bauman Moscow State Technical University) and I.V. Zyakhov (E.O. Paton Electric Welding Institute). Investigations of the possibility of detection and identification of different types of defects in the joints made by flash butt and combined welding showed that the ultrasonic inspection methods provide revealing of all inadmissible defects of flash butt welding. The expediency of using computer-aided ultrasonic inspection was proved by the R&D efforts made by the Bauman Moscow State Technical University. Available is the computer-aided ultrasonic inspection equipment meeting requirements of «Gazprom». It was suggested that the work should be initiated to develop a special document — guidelines for computer-aided ultrasonic inspection of flash butt welded joints.

Summarising the results of the Seminar, Prof. S.I. Kuchuk-Yatsenko noted that the experience of long-



time operation of the flash butt welded joints on pipes under the Extreme North conditions in Russia in the 1980s proved that this welding method provides high reliability of the circumferential joints on different-diameter pipes made from steels of the X50–X70 strength grades. Realisation of the potential of flash butt welding in construction of new pipeline systems depends on the joint efforts of scientists, designers and production workers. No doubt this potential will be implemented within the next few years.

Summing up, participants of the Seminar noted its topicality and practicality for further development of the welding science, approaches to evaluation of serv-

ice properties of the welded joints, improvement of the welding technologies and equipment, as well as of the technologies for postweld treatment of the joints and methods for non-destructive testing of the welded joints. The resulting document of the Seminar, i.e. Memorandum on Application of Flash Butt Welding and Combined Flash Butt + Arc Welding of Large-Diameter Pipes, defined the primary challenges for the organisations — participants of the Seminar, the addressing of which will require their joint efforts.

Dr. I.V. Zyakhov, PWI

NEW BOOK

(2011) **Pressure Butt Welding of High-Strength Steels and Alloys:** Coll. of papers. — Kiev: E.O. Paton Electric Welding Institute of the NAS of Ukraine. — 120 pp., soft cover, 200×297 format.

The collection consists of papers published in «The Paton Welding Journal» in the period from 2005 to 2010 on the problems of flash-butt welding and other pressure welding processes and includes the following sections:

- flash-butt welding of railway rails and frogs
- technology and equipment for press welding of pipes
- butt welding of shaped sections
- butt welding of high-strength difficult-to-weld alloys and bimetal joints.

The authors of papers are pressure welding scientists and specialists known in Ukraine and abroad. The collection is designed for scientific staff, engineers, technologists and designers, lecturers and post-graduates, dealing with pressure welding of steels, aluminium and titanium alloys, intermetallics and other materials.



Kindly send the orders for the book to the Editorial Board of «The Paton Welding Journal»

Phone/fax: (38044) 200-82-77, 200-54-84, e-mail: jurnal@paton.kiev.ua

The book is distributed in the printed form (delivery by registered postal packet) and in electronic form in *.pdf format

(sending by e-mail with payment based on the act of work performed)

SUBSCRIPTION FOR «THE PATON WELDING JOURNAL»

If You are interested in making subscription directly via Editorial Board, fill, please, the coupon and send application by fax or e-mail.

The cost of annual subscription via Editorial Board is \$324.

Telephones and faxes of Editorial Board of «The Paton Welding Journal»:

Tel.: (38044) 200 82 77, 200 81 45

Fax: (38044) 200 82 77, 200 81 45.

«The Paton Welding Journal» can be also subscribed worldwide from catalogues of subscription agency EBSO.

SUBSCRIPTION COUPON	
Address for journal delivery	
Term of subscription since	20 till 20
Name, initials	
Affiliation	
Position	
Tel., Fax, E-mail	



ADVERTISEMENT IN «THE PATON WELDING JOURNAL»

External cover, fully-colored:

First page of cover
(190×190 mm) – \$700
Second page of cover
(200×290 mm) – \$550
Third page of cover
(200×290 mm) – \$500
Fourth page of cover
(200×290 mm) – \$600

Internal cover, fully-colored:

First page of cover
(200×290 mm) – \$350
Second page of cover
(200×290 mm) – \$350
Third page of cover
(200×290 mm) – \$350
Fourth page of cover
(200×290 mm) – \$350

Internal insert:

Fully-colored (200×290 mm) – \$300
Fully-colored (double page A3)
(400×290 mm) – \$500
Fully-colored (200×145 mm) – \$150
Black-and-white (170×250 mm) – \$80
Black-and-white (170×125 mm) – \$50
Black-and-white (80×80 mm) – \$15

- Article in the form of advertising is 50 % of the cost of advertising area
- When the sum of advertising contracts exceeds \$1000, a flexible system of discounts is envisaged

Technical requirement for the advertising materials:

- Size of journal after cutting is 200×290 mm
- In advertising layouts, the texts, logotypes and other elements should be located 5 mm from the module edge to prevent the loss of a part of information

All files in format IBM PC:

- Corell Draw, version up to 10.0
- Adobe Photoshop, version up to 7.0
- Quark, version up to 5.0
- Representations in format TIFF, color model CMYK, resolution 300 dpi
- Files should be added with a printed copy (makeups in WORD for are not accepted)